AMERICAN UNIVERSITY OF BEIRUT

MULTIPLE PARAMETERS OPTIMIZATION AND CONSTRUCTION PROCEDURE FOR 3D PRINTED REINFORCED CONCRETE FRAME ELEMENTS

by
ABDALLAH WASSIM ABOU YASSIN

A thesis
submitted in partial fulfillment of the requirements
for the degree of Master of Engineering
to the Department of Civil and Environmental Engineering
of the Faculty of Engineering and Architecture
at the American University of Beirut

Beirut, Lebanon
January 2019

AMERICAN UNIVERSITY OF BEIRUT

MULTIPLE PARAMETERS OPTIMIZATION AND CONSTRUCTION PROCEDURE FOR 3D PRINTED REINFORCED CONCRETE FRAME ELEMENTS

by

ABDALLAH WASSIM ABOU YASSIN

Approved by:

[ ]

Dr. Farook Hamzeh, Assistant Professor — Advisor
Civil and Environmental Engineering
American University of Beirut

[ ]

Dr.George Saad, Associate Professor — Member of Committee
Civil and Environmental Engineering
American University of Beirut

[ ]

Dr. Hiam Khoury, Associate Professor — Member of Committee
Civil and Environmental Engineering
American University of Beirut

[ ]

Dr. Joseph Assad, Associate Professor — Member of Committee
Civil and Environmental Engineering
Notre Dame University

Date of thesis/dissertation defense: [January 4, 2019]

AMERICAN UNIVERSITY OF BEIRUT

THESIS, DISSERTATION, PROJECT RELEASE FORM

Student Name:	Abou Yassin	Abdallah	Wassim
	Last	First	Middle

● Master's Thesis ○ Master's Project ○ Doctoral Dissertation

☐ I authorize the American University of Beirut to: (a) reproduce hard or electronic copies of my thesis, dissertation, or project; (b) include such copies in the archives and digital repositories of the University; and (c) make freely available such copies to third parties for research or educational purposes.

☑ I authorize the American University of Beirut, to: (a) reproduce hard or electronic copies of it; (b) include such copies in the archives and digital repositories of the University; and (c) make freely available such copies to third parties for research or educational purposes after:

☑ **One ---- year from the date of submission of my thesis, dissertation, or project.**
Two ---- years from the date of submission of my thesis, dissertation, or project.
Three ---- years from the date of submission of my thesis, dissertation, or project.

Abdallah Wassim Yassin February 4, 2019

Signature Date

ACKNOWLEDGEMENTS

To whom has helped me free my imagination and think autonomously and critically of everything around me. To whom has always received me with a cheerful smile and an incessant attentiveness listening with awe to what I have to say. To the considerate and courteous friend who always treated me like a peer. To my academic supervisor, my supportive mentor, and my big brother which I owe plenty. Dr. Farook Hamzeh, thank you for being who you are, and for helping me reach my potential. I couldn't have had a better instructor even if I wanted to, and for that I am truly and deeply grateful.

I'd also like to thank my committee members Dr. George Saad, Dr. Joseph Assaad and Dr. Hiam Khoury for being very genuine and helpful with many matters that I have looked over. Your guidance and support have added much value to my research.

To the calm and thoughtful manager of CEE laboratories, Mr. Helmi El-Khatib, all my respect and appreciation for your immediate help in many situations, and your day-to-day involvement in all lab issues that befell on me and could have troubled my progress. I couldn't have finished my thesis on time if it weren't for you.

To the energetic, fun, caring, adorable, and helpful Lab Engineer of CEE laboratories, Ms. Dima Al Hassanieh, you have helped me in countless situations. I might not be able to count them all here, but if it wasn't for your help, together with Imad El Chiti, on my first disastrous day in the lab, I wouldn't have made it this far. Thank you for every precious minute of your time.

Further extending my gratitude, I would like to thank Mr. AbdelRahman El-Sheikh, Mr. Bashir Asyala, and Mr. Jamil for their help in the structural engineering laboratory with many tips and best practice knowledge while working in the labs.

To my dearest friends and lab companions who we shared the wonderful experience of mopping the lab floor countless times (after several hours of actually doing useful stuff), Mazen Helwi and Hala Zahr thank you for being with me through the many downs, and eventually the ups.

To all who I have discussed many concepts related to my work and who eagerly helped me brainstorm ideas, Imad El Chiti, Fatima Al Sakka, Zuheir Abdallah, Nadim Aaesha, Hussein Saad, Mohammad Ali, your collective support fine-tuned my study dramatically.

To all my friends in the construction management, structures, materials, and geotechnical labs, Hasnaa Al Hussein, Ghali Al Samad, Mazen Helwi (yes, again), Fatima Al Sakka, Diana Salhab, Yara Daoud, Bahaa Tayba, Malek Ghanem, Ruba Rizk, Christelle Baset, Ahmad Labban, Rayan Mrad, Paul Maamari, Amir Al Arab, Mohamad El Ahmad, Reem Jaber. Thank you for every pizza night, every smile, every hand shake, and every existential-crisis-during-thesis-writing conversation we had. Your cheerful attitude and sense of humor made the whole experience of life at AUB one worth living. Many of us will part ways after we leave AUB, but our shared memories will live within our minds for very long. I wish you all a prosperous and successful life.

To the amazing mechanical engineering team helping and promptly fixing any problems in the machines we use, Dr. Nasseem, Chris, Marwan, Yves and Ali, thank you for your valuable efforts.

Further, I would like to thank my very patient and generous supervisors at my current job, Dr. Yehya Temsah and Mr. Johnny Chami. If it wasn't for your unequivocal trust in me, your understanding of my situation while writing my thesis, and your continuous support, I wouldn't have made it this far.

To every staff, janitor, labor and security guard who did their daily chores, I am very grateful for your effort in keeping our workplace a clean, safe, and comfortable space that would help students focus only on their studies.

Last but foremost, I would like to express my deepest gratitude to my parents and siblings. Wassim and Fatima, you have raised me to be the free, autonomous, and independent person I am today. Your accumulated effort throughout the years have reared a son that is proud of you as much as you are proud of him. Thank you for your continuous support and love.

AN ABSTRACT OF THE THESIS OF

AbdAllah Wassim Abou Yassin for Master of Engineering
Major: Construction Management

Title: Multiple Parameter Optimization and Construction Procedure for 3D Printed Reinforced Concrete Frame Elements

Concrete 3D printing is seen to revolutionize the construction industry as it promises a solution for problems that have plagued the construction industry in the last decades, such as productivity loss, material waste, process inefficiencies, limitations on geometric complexity due to the rigidity of tools used, and low innovation levels. However, this technology is still in its infancy and suffers from many shortcomings itself.

One obvious limitation for the industrialization of concrete 3D printing around the globe is the lack of a practical and efficient procedure to reinforce 3D printed concrete elements. Although some research has been published on procedures to reinforce 3D printed concrete, each proposed method still has its flaws that would still favor using traditional methods for construction.

Given the inherent deficiencies in the existing system, and the lack of a suitable method to reinforce 3D printed concrete, a new procedure is proposed in this study that makes use of a predetermined behavior of fresh material properties to optimized the nozzle speed (process parameter) as the machine prints, in order to manufacture concrete 3D printed samples that can be reinforced with traditional longitudinal and transversal steel bars. The hardened properties and structural performance of the 3D printed samples is tested, analyzed, and compared with traditionally cast samples to validate the viability of the proposed procedure. The method used in this study was mainly laboratory experimentation, testing, and measurement of the mechanical properties of 3D printed concrete.

Results show that a properly executed 3D printed plain concrete element might yield compressive and flexural strengths similar or higher than that of regularly cast concrete depending on the direction of loading, whereas reinforced concrete 3D printed beams yielded a strength slightly lower than that of regularly cast beams. Cracking patterns are observed to initiate similarly in 3D printed and regular samples, yet and due to the layered nature of the printing process, cracks tend to propagate through the interface joining two filaments causing a drop in the capacity of the section.

A key finding of the study show that when designing for shear in 3D printed reinforced concrete beams, the possibility of losing strength due to a failure in the filament interface should be taken into account, which would necessitate a reduction in the section's concrete shear capacity.

CONTENTS

Appendix

ILLUSTRATIONS

TABLES

CHAPTER I

INTRODUCTION

Evolution has shaped every aspect of our world, and technology has been the most significant factor in our evolution which propelled us from primitive creatures with primal tools living in undeveloped societies, to where we are today (Schick & Toth, 1994).

Throughout history, technology has evolved as well and its growth has been observed to follow a specific trend. Narayanan (2001) defines 4 stages for technology evolution, taking the form of an S-Curve as shown in Figure 1. Stages of Evolution, S-Curve. As technology evolves from stage 1 to stage 4, its state of evolution changes from emergence to rapid development, declining improvement then reaching its maturity in stage 4. Transition from stage 1 to stage 2 is only possible when enough knowledge and expertise is accumulated from stage 1 to actuate the rapid growth later.

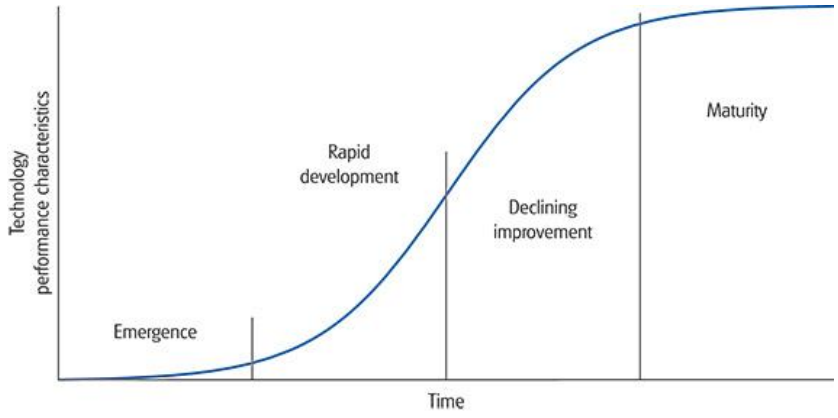

Figure 1. Stages of Evolution, S-Curve

Stage 2 is characterized by the rapid development of the performance this technology exhibits and is usually lead by high-tech companies, whereas stage 3 focuses on the ease of use and convenience of this technology by end customers. This stage is

usually lead by product companies. Stage 4 is where this technology plateaus. Stage 4 allows for the technological progression to occur; where new technologies emerge from old technologies (Narayanan, 2001).

Structural concrete is a technology that revolutionized how civil engineers build different types of structures. Although structural concrete is a relatively new technology, its wide adoption is due to the fact that it has many advantages over traditional building materials such as steel, timber and rocks. It has been used in a wide range of structures such as buildings, tunnels, bridges, water tanks, and dams.

As a technology, concrete evolution doesn't differ much from other technologies. It follows the same trend described earlier. The first modern record of concrete was in the early 1760, when John Smeaton used it in building the walls of a river lock. For 75 years after Smeaton's first usage of concrete, exploration of concrete as a material was recorded by several researchers such as J. Parker, Louis Vicat, Joseph Aspdin and Dancois Marte Le Brun. The first use of reinforcement was recorded in 1854 when Joseph Louis Lambot used reinforcement in a small rowboat. For the next 48 years, several patents were granted for using different types of reinforcement in structural concrete members mainly to W. B. Wilkinson, Francois Coignet, and Joseph Monier. In addition, reinforced concrete buildings were built mainly by W. E. Ward and E. L. Ransome. Testing on RC elements started in 1877 by Thaddeus Hyatt who tested 50 beams for flexure. Tests on concrete were performed for 86 years before ACI published its first specifications on the use of ultimate strength design of reinforced concrete. (Hassoun & Al-Manaseer, 2012). Advanced concrete material technologies later diffused from the original concrete material to enhance its performance. Light weight concrete

(1924), high strength concrete (1930), heat resisting and refractory concrete (1936), fiber reinforced concrete (1960) are examples of such technologies (Newman & Choo, 2003).

As well as investigating concrete material properties and structural integrity, concrete construction processes were investigated. Using formwork as a technology for concrete molding grew in parallel with concrete construction growth. In 1925, N. C. Hollis obtained a patent for movable forms (Hollis, 1925). Other types of formwork were later patented in from 1960s to 1980s such as horizontal slipforming, vertical slipforming, jump forming and cantilever forming, leave in place forms, and others (Concrete Construction Staff, 1980). Other methods for building concrete structures diffused from the original method such as precast concrete (Amirikian, 1946), pre-stressed and post-tensioned concrete (Nawy, 2011), and modular construction (Lawson, Ogden, & Goodier, 2014) were later explored.

With concrete technology reaching its plateau, and in a step for natural evolution progression, a need for customization was surfing up, hence alternative construction methods using robotics and computer technologies coupled with additive manufacturing techniques were explored (Howard, Levitt, Paulson, Pohl, & Tatum, 1989; Paulson Jr, 1985).

Additive manufacturing is a relatively new technology that is believed to revolutionize how products and buildings are realized. Although first attempts of utilizing the technology dates back to 1960s, its first commercial use was in 1987 with stereolithography from 3D systems (Wohlers & Gornet, 2014). Ten years later, the first attempt of using additive manufacturing in construction was reported by Joseph Penga.

Penga (1997) argued that automation attempts in construction were not increasing productivity as in manufacturing sectors. The reason is that robots were

developed to duplicate human labor without changing the process. Upon that, Penga developed a new process that takes CAD layers and transforms them to motion of an end-effector (nozzle) to deposit a layer by layer sand and cement filament, that react together to produce an extremely brittle material, forming shapes and patterns which could not be realized by regular concrete casting. However, this research was not further continued. The year after, B. Khoshnevis invented a new additive fabrication technology called contour crafting (CC). This process uses a computer controlled nozzle mounted on a 3-axis gantry system to extrude wet concrete layers and build them above each other. Trowels were also used to smoothen the printed surfaces. His process was further refined by studying the orifice shape on the printed layers (Kwon, Bukkapatnam, Khoshnevis, & Saito, 2002), studying its application in the automation of constructing an entire building (Khoshnevis, 2004), and optimizing the toolpath operation plan for either a single nozzle or multiple nozzles operation simultaneously (Zhang & Khoshnevis, 2013). Other processes for concrete 3D printing emerged later such as D-Shape concrete 3D printing (Dini, Chiarugi, & Nannini, 2008), Cable suspended contour crafting systems (Bosscher, Williams, Bryson, & Castro-Lacouture, 2007; Williams II, Xin, & Bosscher, 2008), Concrete 3D Printing (Gosselin et al., 2016; Lim et al., 2009; Lim et al., 2012), and swarm 3D printing robots (Hunt, Mitzalis, Alhinai, Hooper, & Kovac, 2014; Oxman, Duro‐Royo, Keating, Peters, & Tsai, 2014; van der Zee, de Ruiter, & Meijs, 2017). Each one of the mentioned processes is characterized by certain attributes that makes it more practical for a particular usage. Of these criteria are the printing speed (productivity), printing resolution (quality), on-site applicability (practicality), freeform capability (flexibility), level of autonomation (innovation), and social impact (sustainability).

Material properties were also thoroughly studied. Well established concrete mixes had to be redesigned to suit this new process. Traditionally, hardened properties of concrete were of main interest to us. However, in 3D printed concrete, both fresh and hardened concrete properties are equally important. Fresh concrete properties of importance in 3D printing process and especially in contour crafting are: extrudability, workability, buildability and open time (Le, Austin, Lim, Buswell, Gibb et al., 2012). Hardened properties of interest in 3D printed concrete are: density and void measurement, compressive strength, flexural strength, bond strength, and drying shrinkage (Le, Austin, Lim, Buswell, Law et al., 2012). To control both fresh and hard concrete properties, admixtures that tune concrete properties should be added. Both fine-grounded admixtures such as fly ash, silica fume and blast furnace slag as well as chemical admixtures such as super plasticizer, accelerator, retarder and viscosity modifying agents were thoroughly discussed. Tests procedures on measuring the fresh property characteristics were also described (Ma & Wang, 2017).

After developing well defined processes and optimized design mixes, 3D printing took another step in its evolution process to witness the manufacturing of real scale buildings by companies in several locations worldwide. A graphical representation of C3DP projects were summarized by Langenberg (2015) as shown in Figure 2. The projects ranged from residential buildings and villas to offices, hotels and bridges (Bos, Wolfs, Ahmed, & Salet, 2016; Clarke, 2017). With this diffusion from academic research to the industry, additional factors need to be taken into consideration. Most importantly is the structural integrity of 3D printed elements.

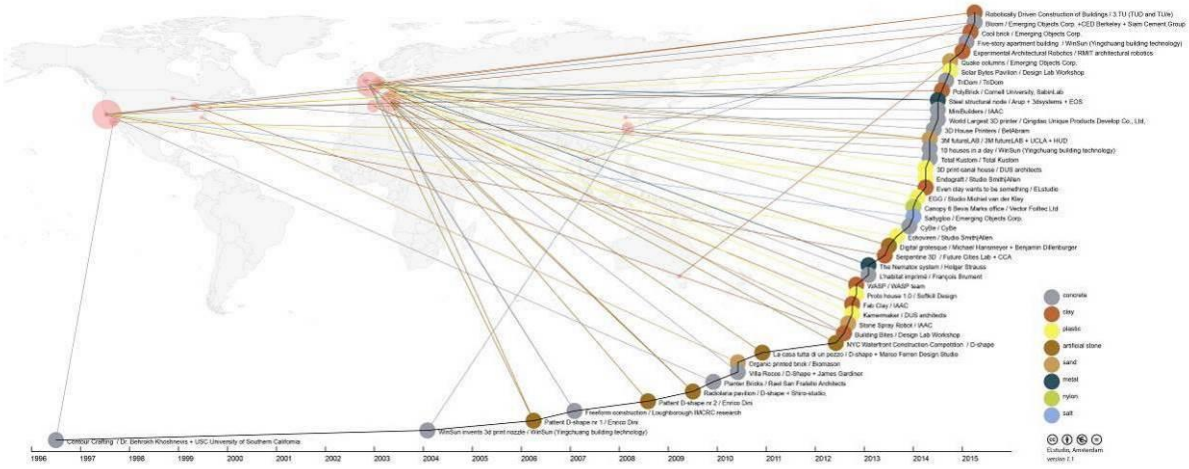

Figure 2. Infographic mapping 20 years of 3D printing in architecture (Langenberg, 2015)

Structural integrity means that a building can withstand the loads acting on it without excessive deformation or failure. This integrity is mainly ensured by the continuity of both concrete and steel in structural elements. While concrete is very strong in compression, its tensile strength is very low, hence steel reinforcement is added to provide flexural strength. To provide flexural strength in concrete, several studies on automating the reinforcement placement in 3D printed concrete were suggested. It started with Khoshnevis in 2006 where he extruded steel coils with the extruded concrete layers (Khoshnevis, Hwang, Yao, & Yeh, 2006). Other attempts of reinforcement were recorded later. Printing false-work concrete, placing a steel cage inside the mold and finally casting concrete inside was suggested (Wu, Wang, & Wang, 2016). Post-tensioning was also applied in the cyclist bridge 3D printed by (TU/e) in Netherlands (Clarke, 2017). Another attempt for printing reinforced concrete was presented by the Chinese contractor HuaShang where he first erected steel bars, then used a printing head composed of two nozzle that prints concrete from both sides, solving the issue of printing concrete on already erected reinforcement. In-process printing of fibers was also studied taking into consideration the type and length of fibers printed, and the directionality effect on the

mechanical properties of the printed specimen (Farina et al., 2016; Hambach & Volkmer, 2017; Panda, Paul, & Tan, 2017). “Mesh Mould” used an automated robotic wire bending and welding tool for creating steel meshes for doubly curved concrete walls. Finally, cable reinforcement entrained in concrete extruded filaments were explored by researchers at Eindhoven University of Technology (Salet, Bos, Wolfs, & Ahmed, 2018).

Another important factor that is necessary for the design of reinforced concrete members is the isotropic behavior of concrete, where code design provisions take into consideration that the mechanical properties of concrete are the same regardless the direction of the load applied. In 3D printed concrete, this is not the case. Additively manufactured concrete has been proven, in many studies, to possess anisotropic behavior. Le et. al (2012) conducted experimental analysis on the hardened mechanical properties of high strength 3D printed concrete. Their results showed that a 30% reduction in compressive strength is possible depending on the print path and the direction of loading. A similar reduction was observed in the tensile bond strength between layers. However, the flexural strength showed higher values than the molded specimen. Other contributions to this area of study provided similar results of anisotropy in 3D printed concrete (Hambach & Volkmer, 2017; Marchment, Xia, Dodd, Sanjayan, & Nematollahi, 2017; Panda et al., 2017; Zareiyan & Khoshnevis, 2017b).

For the wide spread adoption of 3D printed concrete as a technology used in the construction industry, structural integrity as well its interrelation with all other components should be thoroughly explored. From the brief introduction given above, it is shown that the first three components (technology, process and materials) have been thoroughly studied. However, the main reason hindering the widespread of this technology in the construction industry is the presence of ambiguities relating to the

different mechanical properties and material behaviors of concrete 3D printed structural elements as well as the ease of placing reinforcement with least human intervention.

CHAPTER 2

LITERATURE REVIEW

2.1. Additive Manufacturing Evolution

Additive manufacturing (AM) is an innovative way to manufacture 3D objects from 2D drawings. The layered manufacturing procedure differs from the traditional procedures by how the intended shapes are realized. Traditionally, large bulks of materials were fed into the manufacturing system and parts were created by removing materials from the bulk until the final shape is realized. This would result in material and energy waste. Design is also constrained with the ability of the machines to produce the required shapes. Additive manufacturing makes efficient use of materials and energy by only depositing materials where needed. In addition, any design shape can be manufactured regardless the complexity in design (Huang, Liu, Mokasdar, & Hou, 2013).

The first additive manufacturing machine was invented by Carl Deckard and Joe Beaman in 1986 at the University of Texas. They described their invention as revolutionary as it used to manufacture plastic parts additively using stereolithography (SLA); a technique that consists of solidifying a resin using ultraviolet light on a micro level to build a 3D object layer by layer (Lipson & Kurman, 2013). Other additive manufacturing techniques emerged later on mainly Selective Laser Sintering (SLS), Fused Deposition Modeling (FDM), Electron Beam Melting (EBM), Laminated Object Manufacturing (LOM) and many other techniques (Wong & Hernandez, 2012).

Since then, additive manufacturing evolved considerably, and the use of additive manufacturing diffused into many sectors such as aerospace (Joshi & Sheikh, 2015), automotive (Conner et al., 2014), medical and healthcare (Khaled, Burley, Alexander, &

Roberts, 2014; Murphy & Atala, 2014; Rengier et al., 2010), education (Canessa, Fonda, Zennaro, & Deadline, 2013), engineering (Duballet, Gosselin, & Roux, 2015; Gosselin et al., 2016) and construction (Bos et al., 2016; Labonnote, Rønnquist, Manum, & Rüther, 2016; Wu et al., 2016).

2.2. Diffusion of Additive Manufacturing into Construction

The diffusion of additive manufacturing into the construction industry was first recorded by Joseph Penga (1997). In his study, Penga used a process that starts by drawing the intended shape on a computer aided-design (CAD) software. Then the shape is sliced into layers and translated into motion controlling the navigation of the end effector. The effector then deposits materials in a layered manner forming a 3D object. The deposited material used by Penga was a sand a Portland cement mixture. Spraying mist of liquid water was used to bind deposited layers to each other. The manufactured structures included internal cavities in concrete that could not have been molded as regular concrete casting. Tests to assess the mechanical properties of the manufactured elements were performed and anisotropy in the manufactured concrete was found inherent. With this technique, the author estimated that an average two story house of a 7.5m height and 200m2 area would take 2 months to construct if the machine was operated 24 hours per day continuously (Pegna, 1997).

The process described above yielded good mechanical properties of the manufactured elements. However, the time it would take to print a relatively small house was not that much appealing, and the results were not enough for the construction industry to shift their investments into this technology, yet it provided a start point for further research and development.

2.3. Concrete Additive Manufacturing Processes

In addition to Penga's study described above, other processes that aim to automate construction emerged. The procedure once known as additive manufacturing now has several name tags based on the process used. Three main processes for 3D printing concrete were mostly discussed and developed and their development will be described below:

2.3.1. Contour Crafting

The concept of contour crafting (CC) was first publicized in 1998, when Behrokh Khoshnevis published an article that introduced this technology as "Innovative Rapid Prototyping Process Makes Large Sized, Smooth Surfaced Complex Shapes in a Wide Variety of Materials". This new process uses computer control and robotics to automate the formation of free-form smooth surfaces quickly and accurately (Khoshnevis & Dutton, 1998). After his introduction to the original concept in 1998, Khoshnevis extended his research in this topic and studied several components of CC. In 2002, a study that addressed the effect of orifice shape in CC on the printed filaments. Several parameters were varied and optimization based on the results was performed. His study concluded that the square shaped orifice provided the best printing quality (Kwon et al., 2002). Two years later, Khoshnevis revealed his vision of completely automating the construction process using CC. In essence, a nozzle will be mounted on a gantry system and can move in x, y and z directions. The nozzle will be used to extrude the paste used for printing. In addition, several arms could be installed on the gantry system to handle several tasks at the same time. The original concept is shown in Figure 3 below.

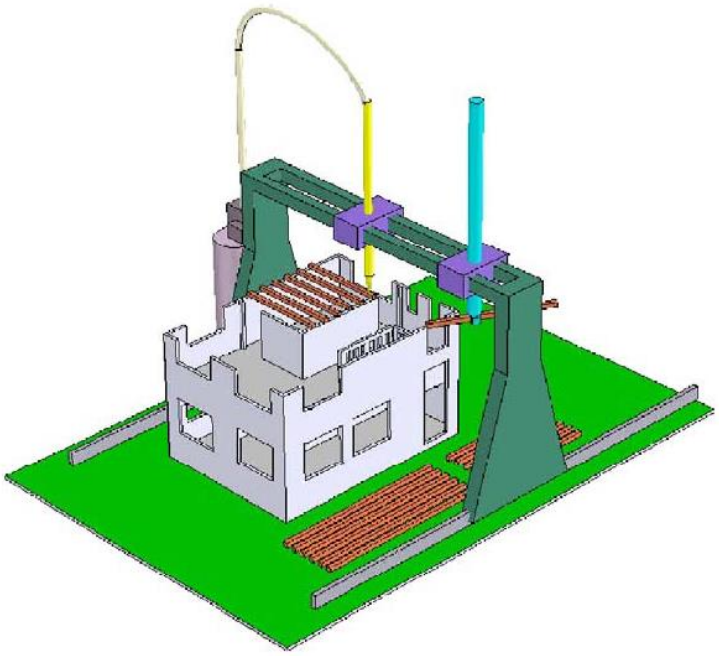

Figure 3. The original concept of CC as presented by Khoshnevis (Khoshnevis, 2004)

Applications and advantages of this system include: 1) Design and construction of exotic architectural buildings, 2) The use of multiple materials in construction, 3) Automating utility conduits installation, 4) Surface preparation for paint application, 5) Insertion of smart materials such as strain sensors into the constructed elements, 6) Automating tasks such as reinforcement installation, tiling of floors and walls, plumbing and electrical fixtures and painting (Khoshnevis, 2004). Extraterrestrial application of CC was also explored (Khoshnevis et al., 2005).

After establishing the basic concepts, experimental and numerical analysis were conducted to further optimize the process. The studies mainly targeted buildability and toolpath optimization using multiple nozzles (Di Carlo, Khoshnevis, & Chen, 2013; Zhang & Khoshnevis, 2013).

Although many other concrete 3D printing processes were later realized, CC has been the most popular system due to its high printing speed and flexibility, which are two

important factors for the scalability of this technology and adoption in real building construction. For that purpose, we will be using CC in this research to meet our objectives stated in.

2.3.2. Concrete Printing

Although very similar in concept to CC, concrete printing differs in two main areas from the latter. Concrete printing is mainly used for off-site production of architectural shapes, while CC's main purpose it to be used on-site and automate the construction of an entire building in one run. Moreover, concrete printing uses a small nozzle diameter (9mm-20mm) which allows for greater geometric control of the printed elements. A drawback for accuracy however, is the time it takes to print the entire shape (Lim et al., 2012).

Researchers at Loughborough University have used this process to print several shapes and reported high quality and accuracy in the printed elements. In addition, they have demonstrated a strategy to reinforce the printed elements by leaving voids in printed elements and inserting steel bars then grouting (Lim et al., 2012). The printed element and reinforcement are shown in Figure 4.

Figure 4. Printed element and reinforcement locations (Lim et al., 2012)

2.3.3. D-Shape

Among all 3D printing techniques, D-shape printing is the process that builds the most exotic shaped structures. The process is an off-site technique that is composed of a gantry frame capable to move in both horizontal and vertical directions. An array of nozzles are mounted on the moving frame. The nozzles build the layers by spraying powdered cement on a support bed then binding the cement layers by spraying water vapor after placing layers. A layer of sand is deposited after each layer of concrete to support the built structure (Jakupovic, 2016).

Figure 5. Sample projects built using D-shape (Dini, 2010)

This technique was invented by Enrico Dini where he started researching on the topic between 2005 and 2007. In addition to his research, Dini experimented with the process and built several real scale prototypes (Dini, 2010). A sample of his work is demonstrated in Figure 5.

2.3.4. Other Concrete Printing Processes

The abovementioned concrete printing processes were the ones most commonly used and cited in the literature. However, other innovative processes worthy to mention were also explored. A brief description of each process will is presented below:

- Cable-suspended robotic CC: This process uses tendons driven by motors to manipulate the end effector which extrudes concrete. The system can be mantled on a

mobile platform which is highly customizable depending on the size of the building. This process is characterized by better portability, lower cost and unbound built area (unlike traditional CC where the build area is bound by the size of the frame supporting the end effectors) (Bosscher et al., 2007).

- 3D printing with robot swarm: The main advantage of this process is the use of small, autonomous printing robots that are spatially coordinated to print a structure. The robots can be small vehicles or drones carrying a print head and the printing materials (Hunt et al., 2014; van der Zee et al., 2017).

- Printing with industrial robots: This approach is similar to the original CC process except that industrial 6-axis robotic arms are used to deposit the extruded material (typically concrete) from the nozzle. Another core difference in this process is that the additives are only mixed with the mortar right before deposition occurs. The detailed process and the benefits of this process are discussed in the paper published by Gosselin et al. in 2016 (Gosselin et al., 2016).

2.4. Projects Built Using 3D Printers Worldwide

In addition to the academic effort spent on researching new processes to 3D print concrete, the industry had some contribution in the evolution of 3D printing as well. In the following section, some 3D printed projects that were built worldwide will be briefly discussed and the state of evolution of 3D printing will be assessed upon that.

2.4.1. Winsun

Winsun is a Chinese construction company that has been a worldwide leader in 3D printing buildings. Although it is thought that they have taken the IP rights from CC without the permission of its inventor, Behrokh Khoshnevis (Krassenstein, 2015), the projects they have accomplished using this technology are outstanding. Some projects

completed by Winsun are: 1) the ten 3D printed houses each measuring 200 m2 each costing around $4800, 2) 3D printed villa measuring 1100 m2, 3) two 3D printed courtyards measuring 130 m^2 and 80 m^2 each and 4) a six story 3D printed building (Tess, 2016). The projects listed are shown in Figure 6.

Figure 6. Winsun 3D printed project samples. (1) Ten printed houses, (2) 3D printed villa, (3) 3D printed courtyard, (4) 6 story 3D printed building.

2.4.2. HuaShang Tengda

The Chinese construction company HuaShang is a leading company in 3D printing concrete structures. The process they use is completely developed in house. Although their process is not fully automated, where labors erect the steel bars and the plumbing system prior to printing, their approach is much better that their counterpart, Winsun which used precast 3D printed walls then assembled them on-site. Thy key factor of success for their innovative approach is the use of a novel 3D printing nozzle. The nozzle is designed to deposit concrete from both sides of an element, encasing rebar, plumbing systems and other utilities with concrete. The 2 story building of 400 m^2 area was designed, then built only in 45 days, to withstand an earthquake as strong as 8 on the Richter Scale (Scott, 2016). Figure 7 shows parts of the innovative process used to print the two story building. A video showing the process of printing used by HuaShang Tengda can be found on their official website (HuaShang Luhai, 2016).

Figure 7. HueShang 3D printed house. (1) Nozzle encasing erected pipes with concrete, (2) structure finished showing the rough surface finish, (3) 3D printed reinforced concrete 2 story house, (4) nozzle encasing erected reinforcement in walls.

2.4.3. Apis Cor

This Russian based company uses a mobile print machine that can cover a print area up to 132 m2. Setting up the machine on-site would only take 30 minutes with 2 people operating it. Horizontal and vertical reinforcement is embedded in the printed walls to provide structural integrity (apis cor, 2017).

A prototype of their work is presented in Figure 8. The total cost of the materials used in this home summed up at $10,134 and was completed in only 24 hours (Garfield, 2017).

Figure 8. Apis Cor printed home. (1) In process of printing, (2) Apis Cor printed home covered with insulating material and paint.

2.4.4. Eindhoven University of Technology & BIM Infra

After 3 months of printing around 800 layers of concrete, the printed blocks were pre-stressed then assembled on-site, in collaboration between Eindhoven University of Technology and BAM Infra. The 3D printed cyclist bridge spans 8 meters long and measures 3.5 meters in width (Figure 9). A five tons load was applied for testing the bridge and the latter complied with all safety measures (Irving, 2017).

Figure 9. 3D printed Cyclist Bridge. (1) Cross section of the bridge showing pre-stressed strands, (2) assembling the 3D printed bridge on-site by BAM Infra

2.4.5. Philippines Hotel

The owner of this hotel, Lewis Yakich teamed up with Andrey Rudenko to build the world's first 3D printed hotel suite. The hotel is a 130m2 structure with all plumbing, wiring and reinforcement installed into it. The total time spent to design and build the hotel was about 100 hours (Wang, 2015).

Figure 10. 3D printed hotel in Philippines

2.4.6. Dubai Office Building

The built office building was part of Dubai's 3D printing strategy aiming to print 25 percent of their buildings in 2030. The project was led by Sheikh Mohammed bin Rashid Al Maktoum, vice president and prime minister of the United Arab Emirates and ruler of Dubai. The process started by offsite printing of the parts, then parts were transported to the site location and assembled in the designated location. Labor costs were reduced by more than 50 percent on this project, as stated by the government of Dubai (Molitch-Hou, 2016).

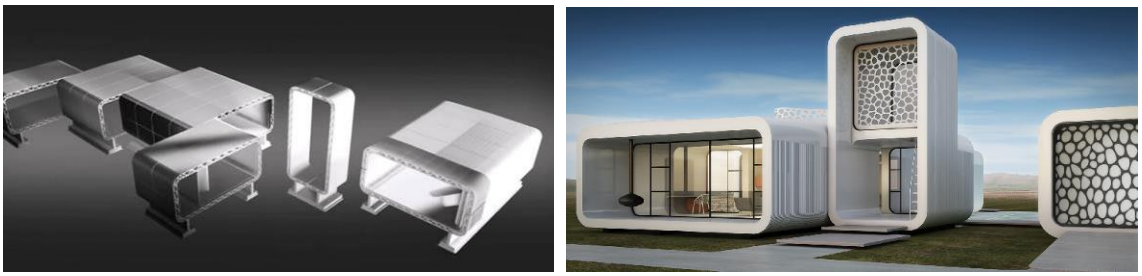

Figure 11. Dubai 3D printed office building

2.5. Different Interacting Components in Concrete 3D Printing

Many studies have acknowledged the interdependency between the different components of a 3D printing system and their effect on the final product. A comprehensive review will be provided to demonstrate the complexity in the interdependency between these different components and to shed light on the importance of both, the methodology used to realize a particular product, and the initial goal that drives the desired methodology. However, before conducting this review, some basic terms need to be established for a clear discussion. The terms relate to the different components of a concrete 3D printing system and are listed below:

2.5.1. Technology

3D printing is a technology driven process. It is a collection of many individual components to form a complex functioning system. When considering technology in 3D concrete printing, for this study, the individual components that form the system will be under study. Components can be either software, hardware, machines or equipment used in the system. Some of the technology components are listed below:

- Software and hardware: Motion and nozzle control system, material deposition control system, sensors, CAD/BIM software, geometry slicing software, G-code software, 3D printing simulation software and topology optimization software. In addition a software that could integrate BIM into CC was introduced as the Planning and Operations Control Software for Automated Construction (POCSAC) (Davtalab, Kazemian, & Khoshnevis, 2018).
- Machines and equipment: Gantry frame system, industrial robots, mobile platform for robot, mixer pump, nozzle, trowels, pumping hose, and material storage tanks.

2.5.2. Process

On a macro level, the different 3D printing processes were described in the section " Concrete Additive Manufacturing Processes" above. However, what mainly defines each process is the difference in the parameters related to the technology components. For example, all printing processes use a nozzle to deposit the extruded material, yet each nozzle cross section dimensions would differ based on the intended use, and of course with the change in the diameter, motion speed would change as well. Another example is the difference between the CC approach and the 3DP approach where both are mounted on a gantry frame and extrude fresh concrete, yet the CC is meant to fully automate the construction process whereas 3D printing is for off-site manufacturing of individual components, hence the main difference is the size of the gantry frame used in each approach along with the sizing of all other components and equipment that would suit the difference in scale.

Based upon that, the term "process" will mean the different 3D printing approaches (CC, 3D printing and D-shape) as well as the different parameters that define and control those approaches. Main parameters that describe the machine and equipment properties are: 1) print speed, accuracy, print path, rotational speed and angle, acceleration, material deposition offset, pump pressure, hose length, storage tanks capacity, frame dimensions along both horizontal and vertical directions, robotic arm length and robot speed, structure support system, element-to-element assembly system, and rebar installation system.

2.5.3. Materials

Perhaps the most critical components of the 3D printing system are the ones related to the materials used. When discussing materials in 3D printing concrete, four main aspects would be of the greatest importance. The latter are listed below:

- Raw Materials: These may include an array of materials used in the mix design mainly including cement, sand, fine aggregates, water, mineral admixtures (Silica fume, Fly ash, Blast furnace slag, Limestone filler, and Nano-silica) and chemical admixtures (Superplasticizers. Accelerators, Retarders, and Viscosity modifying agents). A detailed description of both mineral and chemical admixtures functions in a design mix as well tests on 3D printed concrete can be found in (Ma & Wang, 2017).

- Mix design: The proportions of raw materials used to optimize the designed mix for the intended use.

- Fresh properties of concrete: Those include mainly the extrudability, workability, open time, buildability, thixotropy and adhesion.

- Hardened properties of concrete: Including mainly tensile, shear and flexural strength, compressive strength, bond strength and friction, density and void ratio, and shrinkage properties.

2.5.4. Structural Integrity

Concrete elements need to be reinforced with steel bars to resist loads inducing flexure in the structure. For this study, the term structural integrity will be inclusive of many factors such as the axial, flexural and shear capacities of the 3D reinforced concrete printed elements (3DRCP), type and shape of the printed element, energy dissipation capacity, ductility, Interaction between steel, concrete and grout (if grout present), and code compliance.

2.5.5. Interrelations between different 3D printing components

With the main components of a 3D concrete printing system defined, a detailed review of the different interdependencies between the components will be conducted. The review will emphasize on the importance of each component in a 3D printing system and the complex nature of the interrelation between these components on the quality of the final printed structural element. Some of the interrelations found in the literature are listed below:

1. Studying the interaction started by studying the effect on the nozzle shape on the surface quality of the printed elements. Two nozzle shapes; square and elliptical, were studied and the main parameters of the study were the extrudate velocity (Ve), the linear speed of the nozzle relative to the deposited extrudate (Vr), and the deposition height (h). Optimization of the parameters and the materials used was carried out to achieve the desired surface quality. The results showed that the square nozzle yielded better surface smoothness than the elliptical shaped nozzle and the results were verified numerically using finite element modeling (FEM) (Kwon et al., 2002). This study showed an interaction between the technology, process, and material parameters.

2. Changing the printing process from the conventional CC to the cable suspended CC led to the study of additional factors such as the kinematics of the system. In addition the maximum tension in cables was calculated and compared with the allowable values (Bosscher et al., 2007).

3. Several constraints were identified in (Lim et al., 2009), mainly:

- Size of the printed element/ structure is restricted by the machine size.
- Printing speed makes the printing process slower than conventional casting but the elimination of tools and formwork would reduce the whole process.

- The complexity of the design, slicing, and the nozzle diameter can greatly increase the G-code file size.
- The print resolution is affected by the particle size and the deposition rate.

4. A comparison between the four main 3D concrete printing methods; Penga, CC, Concrete Printing, D-Shape, was carried out and summarized in a table. The main parameters that were compared are: 1) Process (3D printing or extrusion), 2) Use of mold, 3) Build material, 4) Binder, 5) Nozzle diameter, 6) Nozzle number, 7) Layer thickness, 8) Reinforcement, 9) Mechanical properties, 10) Print size, 11) Pre/ Post processing. In addition the mechanical properties were found dependent on the printing process. Moreover, the correlation between pump and machine speed as well as the flow rate of a particular nozzle diameter were studied (Lim et al., 2012).

5. A "dilemma" was explained by Le et al. (2012), where they stated that the need for a certain workability is required for consistent flow requires a long open time. While the latter also help develop better interlayer bond strength, the buildability is compromised (Le et al., 2012).

6. Fabrication loads on lower fresh concrete layers imposed from the CC layered technique were varied with the rate at which concrete gains strength over time and a safe fabrication limit was determined by taking into consideration that the strength should not fall below the stepped loading function (Di Carlo et al., 2013).

7. In a study to optimize the print path in a given building, the author suggested either using a single gantry system with multiple nozzles or multiple gantry systems depending on the building area and complexity (Zhang & Khoshnevis, 2013).

8. Mix design goals were shown to be conflicting with each other as shown by Malaeb et al. (2015). For example a high compressive strength would mean low water

to cement ratio. However, a low W/C ratio would decrease workability. In the same manner, flowability for concrete to flow in the system, yet the mix needs to be buildable to sustain its own weight and the weight of subsequent layers. Finally, the extruded concrete should set quickly, yet it needs to maintain a certain setting time to allow for a stronger bond between concrete layers.

9. The nozzle design was also governed by the mix design obtained based on the required buildability and to prevent segregation.

10. The results of their experiments were presented in three graphs. The first compares flowability to buildability upon using different design mixes. Second, open time was assessed upon the variation in the retarder dosage. The third graph shows the effect of retarder dosage on workability (Malaeb et al., 2015).

11. Standard cylinders were printed with different toolpaths, and the compressive strength test showed that the failure mode is dependent on the print path (Duballet et al., 2015).

12. A process that uses a rather innovative approach to 3D print double curved walls containing mesh made of steel reinforcement was explored. The author acknowledged the importance of the interdependency between the concrete design mix, the mesh typology and the process of fabricating the mesh and pumping concrete inside of it (Hack, Lauer, Gramazio, & Kohler, 2015).

13. In a review paper published by (Labonnote et al., 2016), several interdependencies were identified and are listed below:

- Concrete used in 3D printing has a high level of abrasiveness, which might affect the maintenance schedule of the used pump.

- The equipment used in a certain 3D printing process may change based on the scale of the printed structure. For large-scale construction, large volumes of materials need to be stored which have been a major challenge in the development of additive manufacturing processes.

- Depending on the 3DCP process used, well established concrete mixes will become obsolete and will require re-designing due to the difference in the process parameters.

- The type and size of the building may govern the use of a certain process. For example building a skyscraper might be more feasible if using the swarm approach than the CC approach.

- Advances in topology optimization programs, in addition to a precise print resolution will enable the manufacturing of structural elements with lighter weights.

- Depending on the geographic location of the printed element and the materials available, the used materials might change, which will affect the entire printing setup.

14. In an attempt to enhance the bond strength, it was suggested to press the nozzle slightly into the filament. This was believed to enhance interlayer adhesion and subsequently the structural properties of the printed concrete (Bos et al., 2016). However, this would compromise the dimensional integrity and accuracy of the print geometry (Panda, Paul, Mohamed, Tay, & Tan, 2018). More importantly, the authors acknowledged the interdependence between design, material, process, and product. They stated that all the latter components should be taken into consideration when designing a print strategy (Bos et al., 2016). The latter is presented in Figure 12 below.

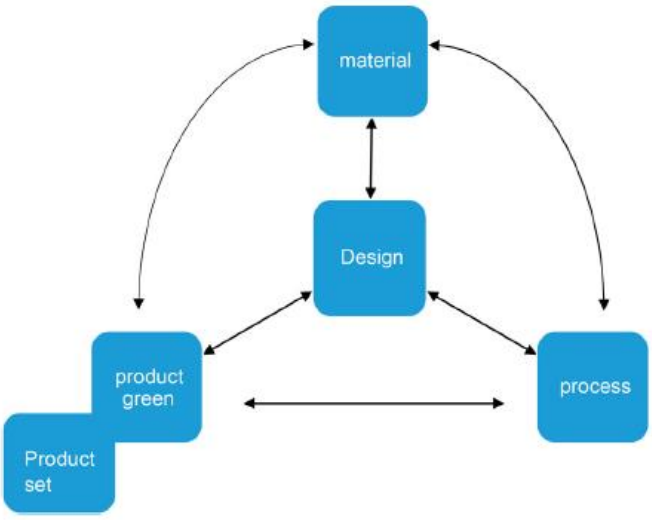

Figure 12. Interrelation between design, process, material and final product (Bos et al., 2016)

15. A comprehensive review paper on the materials and tests used in 3D concrete printing detected an interdependence between the material properties as well. To meet requirements of the fresh properties of 3D printed concrete, a significant increase in the cement content is required, which might lead to the increase of heat of hydration leading to shrinkage in concrete (Ma & Wang, 2017).

16. The paper "Classification of building systems for concrete 3D printing" introduced an additional direction for varying the types of process used in a 3D printing process. For a holistic classification, five parameters were defined and used, which are: "object scale x_o, extrusion scale x_e, printing environment e, printing support s, and assembly parameter a" (Duballet, Baverel, & Dirrenberger, 2017).

17. Another paper by (Ma, Wang, & Ju, 2017) studied the interdependency of the material design parameters with the printer design parameters and suggested a procedure in a flowchart to optimize the mix design for cementitious mixtures used in construction scale 3D printing. The flowchart described is shown in Figure 14.

18. At Eindhoven University of Technology (TU/e), multiple parameters of the main components of the 3D printing system were found dependent on each other, and in a step to fully control the final shape required, the relationships between the different interacting parameters needs to be well understood. System parameters were categorized according to parameters into four levels (Salet et al., 2018):

- Predefined system parameters: At this level, the basic parameters for the concrete, 3D printer and geometry are set and from these parameters, trial and error starts to start the optimization process.
- Informed system parameters: This level explores the interdependency between the most important system parameters. Main parameters are shown in Figure 13.
- Analyzed system parameters: At this level, the behavior and properties of the printed concrete are also added to the chain of interdependencies interacting with the process parameters. Behaviors and properties include the stability of concrete during printing, interface strength, time dependent stress-strain relationships, and finite element analysis (FEA) of the fresh and hard properties of the printed concrete.
- Optimized system parameters: This is the most advanced and complex level of parameter system control. It functions by utilizing algorithms to find the best printing protocol and system parameters. Shapes of 3D printed elements can also be determined using topology optimization algorithms and the print strategies are set based on the boundary conditions.

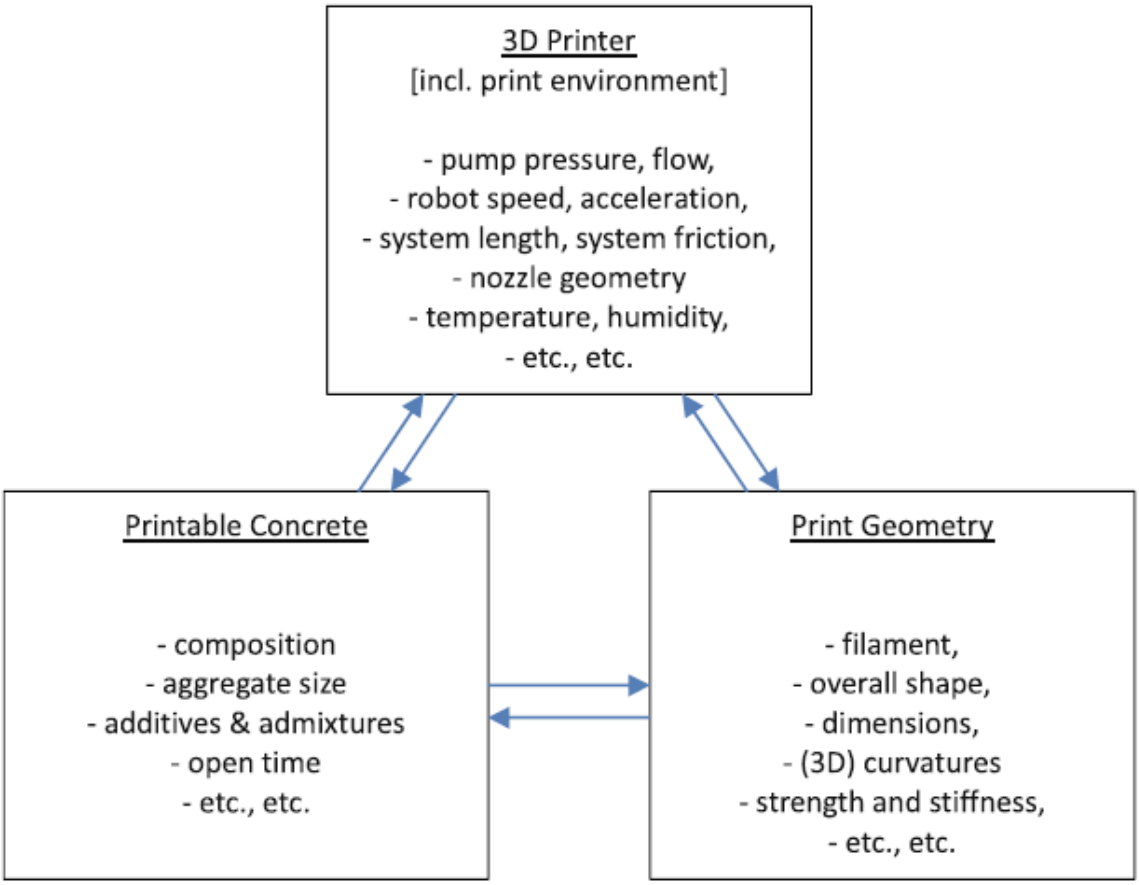

Figure 13. Interdependency between different system parameters of the 3D printing system at TU/e (Salet et al., 2018)

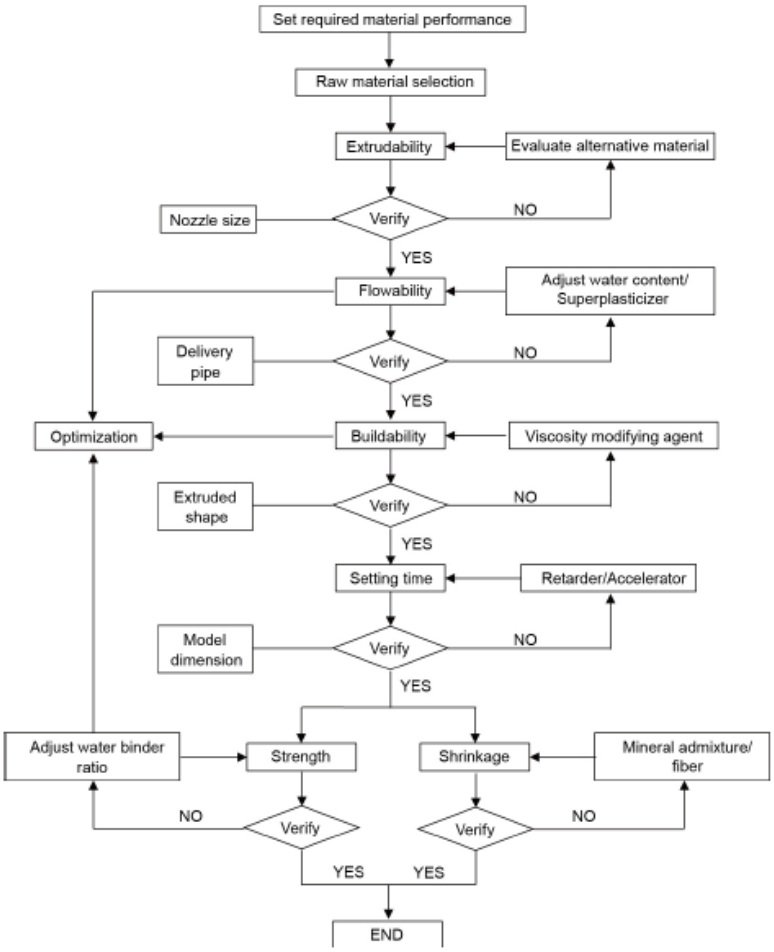

Figure 14. Flowchart showing the 3D printing mix preparation procedure (Ma et al., 2017)

2.6. Structural Integrity of 3D Printed Concrete

After analyzing literature that relates to assessing the mechanical properties of 3D printed concrete, and that related the structural integrity of 3DPC, two main areas of deficiency were detected. First, all 3D printed concrete appear to possess anisotropic properties. In addition, not a single method demonstrated that it can be used to effectively and autonomously reinforce 3D printed concrete without drawbacks. The highlights of the literature is summarized below.

2.6.1. Anisotropy

Hardened properties of 3D printed concrete specimen were tested both poor and good printing concrete. Poor printing showed a decrease in the mechanical properties which indicates higher anisotropy than the good printed concrete and the mold cast specimen. Test cubes were tested for compressive in three directions and it was concluded that a properly executed printing process will yield almost same results as the mold cast specimen. However, if loading in the plane of the printed layers, a small reduction will be introduced due to shear induced between layers due to any flaws between layers. An oblique printing path would further reduce the compressive strength by around 30% than the control. Results of the flexural strength showed higher anisotropy, as the flexural strength in 3D printed specimen were higher by up to 45% than the mold cast specimen when tension was aligned to the extruded filaments and less by 36% when the load caused tension between layers (Le et al., 2012).

Due to the strong interdependency between anisotropy and the interlayer adhesion between layers, interlocking between layers were studied and was found to significantly increase the bond strength by up to 26% using splitting tests. The study showed that as the tongue length of the interlock increase, the bond strength increases, yet to a certain limit (Zareiyan & Khoshnevis, 2017a). However, the effect of increasing the tongue width on the bond strength was not studied.

Another study that investigated the effect of delay time on the mechanical properties of the printed specimen assured that anisotropy in compressive and flexural strengths is observed irrespective of the delay time (Marchment et al., 2017).

2.6.2. Reinforcing 3D printed concrete elements

Three main methods were mentioned in the literature to reinforce 3D printed concrete. While some are more practical than others, all demonstrate problems that need to be solved before they can be practically used in structural engineering design practices and construction methodologies.

2.6.2.1. Mesh Mould Metal

First method was presented by mesh mould where a robotic wire bending and welding manipulator was developed to construct a mesh typology that can later be used as formwork that could sustain concrete pumped into it. The concrete mix should have special requirements mainly low slump and water to cement ratio and good workability to trowel the outer surface when done pouring. This version of the process had some drawbacks such as the challenge in optimizing the mesh density with concrete slump and workability, as well as surface finish quality (Hack et al., 2015). In addition, if very thin wires are used, flexural strength may not be adequately provided, nor will code provisions for reinforcing concrete walls be met. An updated version of their process enhanced the structural integrity of reinforced concrete walls where vertical and horizontal reinforcement were robotically assembled then concrete was poured into the mesh structure (Gramazio Kohler Research, ETH Zurich, 2017). Figure 15 shows the complex mesh typology and the concrete after poured into the double curved wall.

Figure 15. Mesh Mould reinforcement typology and concrete infill

2.6.2.2. WASP Project

The second attempt to reinforce 3D printed concrete elements was the beam project in Italy by researchers at the University of Naples Federico. The project aimed to build affordable 3D printed houses. They started by printing separate parts of the beam and joined them with steel bars joined externally (Molitch-Hou, 2015). Three years later, (Asprone, Auricchio, Menna, & Mercuri, 2018) published a paper that studied the earlier proposed reinforcement methodology experimentally and analytically. Results showed that the major failure locations were near interface between different concrete segments and between concrete and the embedded anchor bolt. Deflection was also reported with high values without steel yielding. Drawbacks of this method are mainly steel corrosion, fire-resistance, and environmental degradation.

2.6.2.3. Eindhoven University of Technology

The third method was presented by researchers at Eindhoven University of Technology (TU/e). Their innovative approach to reinforce 3D printed concrete was accomplished by embedding high strength steel cables into each printed filament. The cable diameters was small enough to provide the needed flexibility for the cable to be layers between concrete layers and in curved parts. 3 point bending test showed that the cables provide strength equivalent to steel bars. However, bond strength was found to be the problem and most failures were either bond slip between steel cables and concrete if properly reinforced, or cable breakage if the section is under-reinforced.

2.7. Concrete 3D Printing: A Structural Engineer's Perspective

Studying the structural integrity of 3D printed concrete has been considered from the very beginning of this technology. The subject was triggered when Khoshnevis as he tried to embed coils in the extruded 3D printed filaments (Khoshnevis et al., 2006). However, no studies were performed to assess the performance of the method proposed. Several studies that assess the structural integrity of 3D printed concrete followed, all of which were discussed thoroughly. Despite all the efforts done up to date to provide structurally sound 3D printed elements and buildings, there is yet a gap that needs to be filled before the technology can be considered a reliable construction technology, and before we witness the wide spread of C3DP in the construction industry. The reason for that is due to the complex nature of the system as a whole and the interdependencies between the different 3D printing components. The latter has been dwelled upon in the section *"Interrelations between different 3D printing components"* above. This gap is further widened when looking at C3DP technology from a structural engineer's perspective. An elaboration of this thought is clarified in the next section. It has to be noted that the following sections are a reflection of thoughts and a prediction of the future trends in concrete 3D printing from a structural engineer's point of view, hence the lack of referencing in the text.

2.7.1. Concrete 3D Printing From a Structural Engineer's Lens

Two geometric trends can be observed in 3D printed concrete, either 3D printing of complex architectural shapes that are characterized by individualization and contextualization or printing commercial homes at low costs using cheap materials. Either ways, both trends will eventually require embedding reinforcement in the printed elements to provide flexural and shear strength. Although 3D printing promises full

automation of the construction process, it seems that we are far away from achieving that. With the goal of automation in mind, researchers have mainly explored processes that can be used to print entire buildings while focusing less on how that can actually be achieved while embedding reinforcement into the 3D printed structural elements. Although several approaches have explored single elements printing off-site, not much has been done to both optimize the onsite printing process with reinforcement embedment. Although our ultimate goal is to print concrete buildings in one run, with full automation, we need to breakdown the whole structural system into parts and study an optimized way to print each part alone, then figure out a way to assemble/connect the parts together while printing. As mentioned earlier, each component in a C3DP system is related to all other components, and in order to study the entire system while keeping in mind to provide both longitudinal and transversal steel reinforcement, an additional layer of complexity will be added to the process.

When breaking down elements and studying each structural element alone, it can be noticed that when printing each element, a different printing setup is required. The main structural elements that compose a reinforced concrete building are: columns, walls, beams, slabs, and foundations. An overview of the considerations to be taken while printing each element is listed below:

2.7.1.1. 3D Printing Reinforced Concrete Columns (3DPRCC):

An RC column's main function is to carry the gravity (dead and live) loads from slabs and beams and transfer them down to the foundations. In addition, column might carry moments induced from either unbalanced conditions, or rigid connections with beams and top slabs or most likely from lateral loads such as wind or earthquake load. Hence, a 3DPRCC should have axial, shear and flexural nominal capacities, higher than

the forces applied on it. Moreover, a 3DPRCC should also satisfy the cover requirements as per the concrete design codes. Hence, three main considerations need to be taken into account when printing a 3DPRCC: First, the nozzle must be designed to a size that can both ensure an appropriate cover (typically 4cm), and ensure accurate deposition of the printed layers. A nozzle of diameter/width 4cm might compromise the accuracy of the print and restrict the size at which columns are printed (only columns with multiples of 4cm can be printed; assuming no elasto-plastic deformations occur in the 3D printed concrete filament after deposition). Buildability problems might also arise when enlarging the filament size. Thus a nozzle diameter/width of 2cm is seen to the most appropriate size for 3D printing columns. Further adjustments might later be suggested depending on the size of the columns that are to be printed. A second consideration that needs to be taken is the process by which reinforcement is going to be embedded into the concrete column. This is a major consideration because it will affect every aspect of the printing process. For example, if the outer concrete layer is to be printed then a prefabricated steel cage is placed into the concrete mold and concrete is poured into the mold, no further considerations are required for print path design. However, this would not be considered innovative nor automated as there is a high level of human intervention. Another approach suggested in this study is to print the entire concrete column while leaving voids where longitudinal reinforcement are to be placed. Stirrups are also placed in between layers, depending on the layer's height, in a way that complies with the designed stirrups spacing. With that in mind, a complex design of the print path in the cross section is expected, and different print paths might be designed each layer to avoid the formation of weak joints along the height of the column. In addition, rebar layout (spacing between bars, number of bars, and distribution of bars in the cross section) must be optimized to provide a

smooth print path that can be executed with the nozzle used. The third consideration is the direction of the print plane with respect to the applied load. In concrete columns, the main load that governs the section size is the axial force applied. Hence, it is preferable to set the print plane perpendicular to the direction of loading as it will yield the highest axial force. However, this will cause a deficiency when the column is subjected to a lateral load since the applied moment as well as the shear forces will be parallel to the print plane. An alternative can be suggested, which is to print the column along its full length (as if printing a beam), then both the flexural and shear capacities provided by the concrete will be enhanced, yet at the cost of losing some of its axial capacity and a more critical crack propagation and failure mode. In addition, the column would not be as easily reinforced and the degree of automation would be lower as it would have to be lifted and assembled in its placed after printing.

Additional considerations need to be taken into account as well such as the connectivity between the foundations and the printed column and the connectivity between columns and beams or slabs as well as the connectivity between columns and other columns when building multiple stories. Alignment of reinforcement in the voids so that added grout can encase the bars equally (or with minimum distance) might also be a challenge.

2.7.1.2. 3D Printing Reinforced Concrete Walls (3DPRCW):

A wall's usage in a structure can be classified into either a load bearing wall, a lateral load resisting system of walls, or a retaining wall. Load bearing wall function is similar to a column's function. Shear walls lateral loads resisting system provides stiffness to the structure and takes in-plane lateral forces. A retaining wall's main function is to carry the lateral loads imposed by soil loads. Out-of-plane loads are typically applied

on these types of walls. Due to anisotropy in 3D printed concrete, a wall's function will determine its print path design and filaments orientation. If the wall is designed as a shear wall, it would yield better results if the print plane is parallel to the direction of the loading and the printed filaments are oriented in the long direction of the wall. However, retaining walls would yield better results if the print path is directed with the wall height. All this assumes that the nozzle used is relatively small with respect to the wall thickness. However, if a fork nozzle is used (as presented by HuaShang), and reinforcement were preassembled, the effect anisotropy would be negligible in both shear walls and retaining walls. However, the degree of automation would be less. Another consideration in 3D printed concrete walls is if the wall outer concrete layers are to be printed as falsework, the lower one third of the falsework should have developed a strength enough to carry the load imposed when concrete is poured into the middle part. Horizontal tie reinforcement can be placed between layers to provide this lateral strength as well.

Innovative approaches such as the one introduced by meshmold need to be explored well and its on-site applicability should be verified as well.

2.7.1.3. 3D Printing Reinforced Concrete Beams (3DPRCB):

Printing beams with full automation can be a challenge for the construction industry. This is due to the nature of this element's function and the material it is made of. Concrete is known for its low flexural strength, and its strength is almost negligible when concrete is fresh. Hence, concrete cannot even support its own strength if printed as a cantilever. The same is true for slabs as well. For that, beams need to be printed on a supporting bed and wait till is gains strength to remove the bed.

As for the filament direction, it is best if filaments are along the length of the beam as shown by (Le et al., 2012). The reason is that, with an adequate bond between

layers, the filaments length is in the direction of tension stresses caused by flexural forces. Printing a beam as a column would cause a significant loss in strength since the loading will cause the bond to facture and the cracks will propagate rapidly in the section causing it to crack. Reinforcement can be either provided by embedding cables within the printing process, or by placing steel bars on the length of the beams after each layer is done. Post-tensioning would also be an option if the printed beam was designed to have holes for tendons later insertion.

The nozzle diameter will greatly depend on the dimensions of the beam. For beams, the nozzle can be of greater widths (depending on the reinforcement method applied). However, the height is limited to a certain value to take into consideration the cover requirements. An issue that needs to be solved is how to print the beam with stirrups embedded.

2.7.1.4. 3D Printing Reinforced Concrete Slabs (3DPRCS):

Slabs are probably the biggest challenge in concrete 3D printing. In our vision to automate the entire construction process, slabs seem a constraint since until now there is not a practical way to 3D print concrete slabs. On-site and off-site 3D printing of concrete slabs have not yet been explored as well, neither have there been a comprehensive study to assemble 3DPRCS. Nozzle size can be of large widths yet of a maximum limit in height, due to reinforcement placement requirements. Reinforcement can be laid down after the first layer of concrete is placed, then additional layers are placed as per the design. The top layer of reinforcement is placed then the final layer of concrete is printed. A crane would lift the slab and place it in the designated location.

2.7.1.5. 3D Printing Reinforced Concrete Foundations (3DPRCF):

In foundation design, concrete 3D printed bearing elements would highly depend on the anisotropy and bond strength of the printed shapes. The bidirectional moment induced from the axial force transmitted from the column above would cause stresses that might cause cracks in the foundations. Additional considerations need to be considered to prevent minerals and water to propagate into the foundation and steel bars.

2.7.2. Further C3DP Research Areas for Structural Engineers

In addition to the abovementioned considerations, and in order for 3D printing to be widely adopted in the construction industry, other areas of research and application need to be explored. An overview of each area will be summarized below:

2.7.2.1. Hybrid Construction

When design is complete and the building needs to be prepared for printing, it is preferred if a simulation would be done taking into consideration several alternative of what needs to be 3D printed, what can be cast in place, and what should be assembled. The simulation results should be used for decision making and optimization. The capacity and flexibility of the 3D printing system available will be two main factors affecting the simulation model and the corresponding results. Ideally, the printing process would be fully automated. However, practically there will be tradeoffs, where a hybrid construction method that utilizes both the traditional construction methods and the 3D printing process is used due to better applicability. For example, foundations might be cast in place due to complexities in laying down steel cage and due to the nature of the terrain and the soil in foundation works. However columns and walls might be easier and more economic if manufactured additively on-site and in-place. Slabs and beams might be either printed or manufactured on-site or off-site. Then using a crane, horizontal load bearing elements can

be assembled in their corresponding location. A mechanism for assembling beams and slabs should be pre-planned and exact locations of hooks, slots, corbels or any other connecting element should be provided.

What must be made clear is that we are far away from full automation of constructing a whole building in one run, and a hybrid construction would seem to be the starting point of concrete 3D construction. The effect of this hybrid construction on the structural analysis and design should be well studied and accounted for, as new factors need to be taken into consideration.

2.7.2.2. Structural Optimization

After a detailed analysis of the buildings 3D printed around the world, it was observed that in most buildings, reinforced concrete shear walls and partition walls are printed entirely on-site and in-place. Other studies showed that printing concrete walls can save both time and money. If that is the case, then it might be feasible to utilize the 3D printed concrete partition walls in the lateral load resisting system. If that was successfully implemented, the printed structural systems would have a lateral stiffness capable of resisting severe earthquakes forces. That would solve the problem of building tall buildings using the 3D printing technology.

Equations that can accurately calculate the mechanical properties should be derived, yet a lot of experimental and numerical studies need to be performed to derive reliable results.

After establishing a strong base of knowledge of the behavior of 3D printed concrete elements and deriving the corresponding equations, as well as defining standards, codes and specifications for 3D printed concrete materials and procedures, commercial programs that can perform complex analysis and design optimization of 3D

printed concrete structures can be customized to aid structural engineers with more reliably design such structures.

In addition, topology optimization programs would play an important role in structural optimization of architecturally complex shapes.

CHAPTER 3

RESEARCH CONTRIBUTION

3.1. Problem Definition and Research Significance

Concrete 3D printing will only be commercialized when all four basic components (shown in Figure 16) of this new technology evolve together from the first stage which is the emergence stage to the second stage which is the rapid development stage as described in Figure 1. Currently, extensive research has been conducted on technologies, processes and materials as shown in the literature. However, for the transition to stage 2, procedures to provide structural integrity for different types of 3D printed elements should be further investigated. That can be mainly achieved by: 1- figuring out how 3D printed elements can perform best depending on how they are manufactured, and 2- by finding a way to automate placement of longitudinal and transversal reinforcement in the 3D printed concrete elements based on their intended usage.

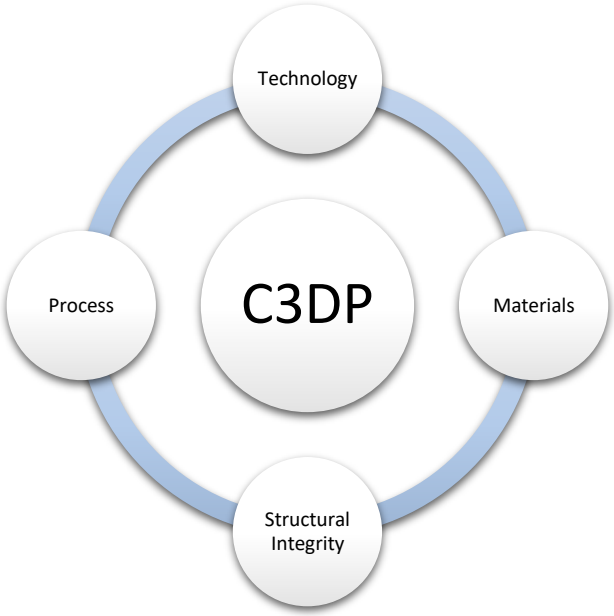

Figure 16. Concrete 3D printing (C3DP) interacting components

For this research, a new methodology for reinforcing 3D printing concrete will be proposed. This methodology enables an automated process for creating reinforced concrete beams and columns. The effect of manufacturing 3D printed samples on the mechanical properties and the behavior of the samples will be assessed.

The research results could provide a benchmark for further research on this particular topic. Next steps would be to conduct extensive experimental and numerical tests to establish rules that would quantify the structural capacity of the printed elements and the effect of anisotropy on the final printed element. Parameters such as cohesion, contact surface and loading direction will be main variables in such equations. After establishing well defined procedures for assessing the structural performance of concrete printed structural elements, a feedback mechanism will occur between all four components and this loop would further optimize each component until standardized procedures can be followed and the design and fabrication procedures can be drafted into building codes.

3.2. Problem Statement

Based on the above discussion, and in accordance with the scope of this research, three problem statements that are strongly interdependent could be verbalized:

1. Lack of data on a proper 3D printing mix design and data related to the interdependence between the mix design constituents and the process parameters, for the machine at the American University of Beirut.
2. No research has explored the axial and flexural performance of 3D printed rectangular sections with grout filling prefabricated holes.

3. Despite all trials to reinforce 3D printed concrete elements, none of the trials have proposed an automated 3D printing process for concrete columns and beams reinforced with continuous steel bars.

3.3. Research Objectives

Considering the problems stated above, three main objectives can be formulated for the purpose of this study.

1. Optimize mix design constituents and process parameters to enable printing multilayered predesigned concrete samples with the required filament dimensions.

2. Compare the axial and flexural strength as well as the failure mode of 3D printed samples with control samples.

3. Study the behavior of 3D printed reinforced concrete beams and validating the effectiveness of printing with voids, then inserting reinforcement and grouting to reinforce 3D printed samples.

3.4. Research Questions

Answers for the following questions will be provided at the end of this research study:

1. How much superplasticizer and retarder should be used, and at which rate and nozzle offset to ensure a printable, workable and buildable concrete mix with uniformly printed filaments.

2. Will the 3D printed concrete samples manufactured using the proposed method have comparable axial and flexural strength as the normally cast samples?

3. How will the shear capacity and failure mode of the 3D printed beam with rebar and grout be affected if compared to a monolithically cast beam with regular reinforcement?

CHAPTER 4

METHODOLOGY

The experimental work in this research will be divided into three phases. In phase one, chemical additive percentages will be varied with different nozzle speeds, and their effect on the filament width will be plotted and analyzed. The results of this phase will be the foundation for later experimental phases as a clear understanding of the mix behavior with time will be available.

In phase two, plain concrete samples will be tested for both axial and flexural capacities. The objective of this phase will be to compare the different printed specimens with the control specimen and determine the effect of 3D printing on the axial and flexural strength of plain concrete samples.

The third and last experimental phase aims to provide a new method to reinforce 3D printed concrete beams and columns. This will be carried out by designing a print path that would manufacture a voided square 3D printed concrete sample. Reinforcement and grouting will be later inserted into the voids and the samples will be tested for ultimate shear capacity. The results will be compared with normally cast samples to understand the difference in ultimate shear capacities and failure modes between normally cast and 3D printed reinforced concrete beams.

Prior to laying down a detailed methodology, a need to explain the dynamic procedure of constraint resolution and management arises, due to the immense contribution of the latter in shaping the adopted methodology.

4.1. Constraint Resolution

In a typical 3D printing system, many factors interact together to deliver the final desired outcome. However, for a factor to be labeled as a constraint, it should be rigid in nature; that is not easily adjusted to suit the desired need. After a couple of trial and error mixes, six constraints were identified in our current 3D printing system which are: 1) nozzle diameter, and 2) pumping rate, 3) number of consecutive 3D printed concrete filaments in the cross section which will govern the cross section dimensions, 4) axial capacity of the machines in the structural laboratory of the American University of Beirut, 5) maximum clear span for specimen testing of the machines in the structural laboratory, 6) maximum capacity of the mixer drum size,. An explanation of how the above constraints could drive the methodology design is illustrated next.

Upon initial trials with a 4cm nozzle diameter, the filament width obtained was 6cm to 8cm in width, on a nozzle offset 3cm, a pumping rate of 6L/min, and nozzle speed of 8000mm/min. The above result did not satisfy the required filament width which is 4cm (filament width value was chosen to ensure a sufficient cover for reinforcement that will be later embedded in prefabricated voids). Trails were carried out by either increasing the pumping rate from 6L/min to 12L/min, or by incrementally increasing the speed from 7000mm/min to 16,000mm/min. When the pumping speed was increased, and due to the highly viscous nature of the concrete mix, the fast rotation of the drum blades would expose the drum-to-hose concrete entry point to air, which in turn enters the hose and a discontinuous flow of concrete would be obtained. Hence the only option was to pump on 6L/min speed. When the nozzle speed was incrementally increased, the filament width got narrower, yet reaching a point where concrete filaments would break apart due to high speed. Another drawback of high speed is if the designed print path has a 90 degree angle,

the machine would have to decelerate so that it would change direction. This deceleration would cause a noticeable variation between filament width in straight segments and near corners. The above constrains led us to reduce the nozzle diameter from 4cm to 2cm.

With the nozzle diameter set, the desired 4cm filament width could be obtained by varying mix design constituents and process parameters (nozzle speed and nozzle height offset). The filament width however, imposed another constrain which is the cross section dimensions. With a set filament width and a print pattern designed to avoid concrete to concrete layer overlaps within the same layer, limited print path patterns can be designed to manufacture the desired outcome. In order to design a print path taking into consideration void locations, at least 6 filaments need to be printed on the same plane (2 for covers on each side, 2 for voids on each side assumed symmetrical, and 2 for inner filling). This would limit our smallest section size to 24cm x 24cm (6 filaments x 4cm/filament). With this sample size, other considerations need to be taken into account. The first issue that would come to mind is whether the drum maximum capacity would be sufficient to print the desired samples. A 24cm x 24cm sample with 48cm in height would consume around 28L of concrete to manufacture. This however, does not mean that an exact amount of 28L should be used to print the desired sample, since two other components in the system should always have a certain amount of concrete in them to ensure a continuous extrusion of the paste; the hose and the drum. The hose has a length of 4m and an inner diameter of 4cm, hence a volume of 5L. The drum-to-hose concrete entry point should also be covered with around 5L of concrete at all times to avoid air intrusion into the hose and to maintain a steady flow. Hence the minimum amount would sum up at 38L which is right below the maximum capacity of 40L. If only a single incremental increase in the specimen size is desired, that is to 36cm x 36cm and a height

of 36cm, the volume of the desired sample would require 46.6L of concrete which is unattainable with the current drum capacity. Assuming no buildability issues arise when constructing a 24cm x 24cm x 48cm sample, careful considerations need to be taken to accommodate for the load and length capacities of the current machines in the structural and construction lab at the American University of Beirut (AUB). Three machines are available at the structural and construction lab of AUB, each of which having different length and load capacities. The latter are listed in table 1.

Table 1. Machine capacities in the structural and construction laboratory at AUB

Machine	Axial loading capacity (Tons)	Axial loading Length capacity (m)
FORM+TEST	300	0.3
MTS	100	2
Tinius Olsen	200	0.75

A 24cm x 24cm sample with a compressive strength above 34.7 MPa would exceed the compressive capacity of both the MTS and the Tinius Olsen leaving us with no choice but to perform compressive testing on the FORM+TEST machine with samples of scale 1:1. Four-point bending testing can be performed of the MTS for samples exceeding 1:1 ratios. Results of the above discussions will later shape the test matrix design in the second and the third phases of the experimental procedure.

4.2. Experimental Procedure, Phase 1:

4.2.1. Test Matrix Design

In this phase of the experiment, three factors were varied to better understand and optimize the mix design and process parameters. A better understanding of the behavior of the mix, when certain factors are varied, would give us an idea of when to use what parameters when printing complex shapes. This understanding would immensely affect the quality of the printed samples. The test matrix hence, targeted two mix design parameters; high range water reducer (HRWR) percentage and retarder percentage, and one process parameter; the nozzle speed. Three speeds were tested with three varying percentages of HRWR summing up to 9 tests. In an additional test, HRWR and speed were fixed and a 0.2% retarder dosage was added to the mix. The output is a plot of the variation of filament width with time.

Table 2. Variable mix test matrix design

Test Notation	Speed (mm/sec)	HRWR %	Retarder %
6000-VC1.50-RT0.0		1.5	0
6000-VC1.55-RT0.0	100	1.55	0
6000-VC1.60-RT0.0		1.6	0
7000-VC1.50-RT0.0		1.5	0
7000-VC1.55-RT0.0	116.67	1.55	0
7000-VC1.60-RT0.0		1.6	0
8000-VC1.50-RT0.0		1.5	0
8000-VC1.55-RT0.0	133.34	1.55	0
8000-VC1.60-RT0.0		1.6	0
6000-VC1.60-RT0.2	100	1.6	0.2

Accordingly, the tests are identified by a three part notation system. The first term indicates the speed of the nozzle adopted to print the concrete filaments. The second and the third part indicate the chemical admixture and percentage used. VC denotes for Viscocrete 20 HE, while SR denotes for Sika Retarder. Table 2 summarizes the tests which were performed.

4.2.2. 3D-Printing System and Pattern Preparation

The 3D printing system is composed of three main components: 1) computer hardware and software, 2) gantry frame machine and, 3) the mixer-pump. These components interact interdependently to manufacture the desired samples, and if any component breaks down, the system seizes to work. The three components are shown in figure 17.

Figure 17. Components of the 3D printing system. (1) Computer hardware and software, (2) Gantry frame system, (3) Mixer-pump

To print the desired geometries, a drafting software (Autodesk AutoCAD) was used to draw the required shape and a 3D-print preparation software was used to create G-code print paths. The machine used is a gantry frame system that moves in x, y and z direction with a nozzle of diameter 20mm attached to the extruder. The printing space was limited to the frame dimensions which is 1.4m × 1.2m × 0.75m. A mixer pump was used to mix the constituents and to transfer the cement paste to the nozzle.

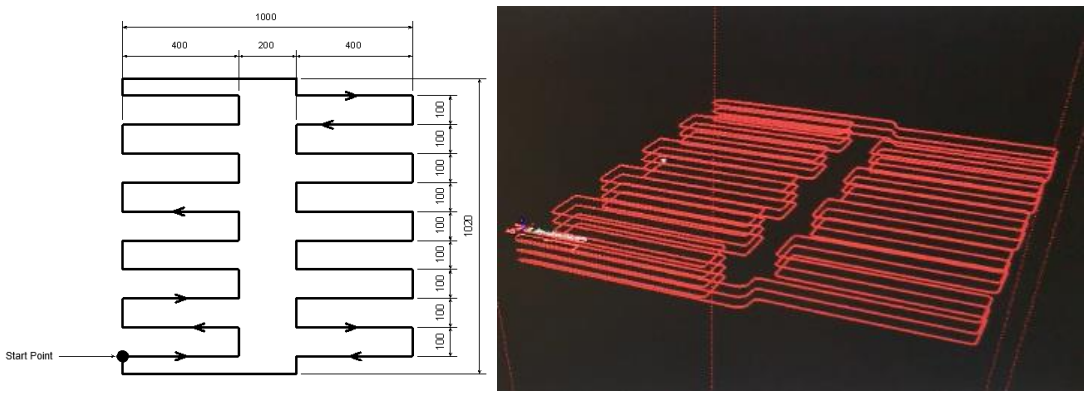

Figure 18. Designed print path for phase 1 of the experimental methodology

The print path was designed to draw twenty lines on a single plane, each line 40cm in length (figure 18). The time required to fill a single plane is between 1.6 to 1.875 minutes depending on the nozzle speed. However, a 40L mix can ensure a continuous flow of concrete for at least 5 minutes. Thus a single plane would not be sufficient to carry out the full experiment. To tackle this issue, several sets of Styrofoam sheets were used as removable printing beds. When a single Styrofoam sheet is filled with concrete filaments, the Styrofoam sheet is removed clearing the way for new concrete to be printed. The layout of the Styrofoam and the printed concrete layers are shown in figure 19.

Figure 19. Layout of three layers of Styrofoam on the printing bed and printed concrete filaments

Materials are weighed and prepared prior to mixing and all materials are placed within reach to the mixer pump. 10% of the water is first added to the mixer, and while rotation on speed 1, sand and cement are added gradually. 80% of the water content is added simultaneously with sand and cement. After adding all mix constituents, the last 10% of the water mixed with a weighed amount of superplasticizer are added to the drum. This process takes 3-5 minutes to complete. After all constituents are added, the mixer is

set to speed 2 and is mixed for two minutes, then allowed to rest for one minute and then mixed for one more minute on speed 2. The mix would then be ready for pumping.

A computer program that is linked to the mixer-pump would give the command to start pumping, then two seconds later (delay for the hose to fill with concrete and ensure continuous flow) the designed print path would run as planned. When the code is finished, 3D printed filaments would be printed on pre-labeled Styrofoam sheets and each filament width is measured for later plots.

4.2.3. Materials and Mix Proportions

After several mix trials were tested by slightly increasing HRWR percentage from 1% up to 2%, an acceptable range of the admixture was found to be between 1.5% and 1.6%. Hence, and in alignment with the objectives of phase 1 of the experimental methodology, three mixes were designed, each mix with an incremental increase of HRWR percentage of 0.05%. One additional mix was added to the methodology to study the effect of retarder on the mix. Specifications of each of the mix constituents are listed below:

- Binder material: Portland cement type 1.
- Fine Aggregates: Natural sand. The gradation curve is shown in figure 20 and the percent fines (Percentage of silt and clay in sand) is 21%.

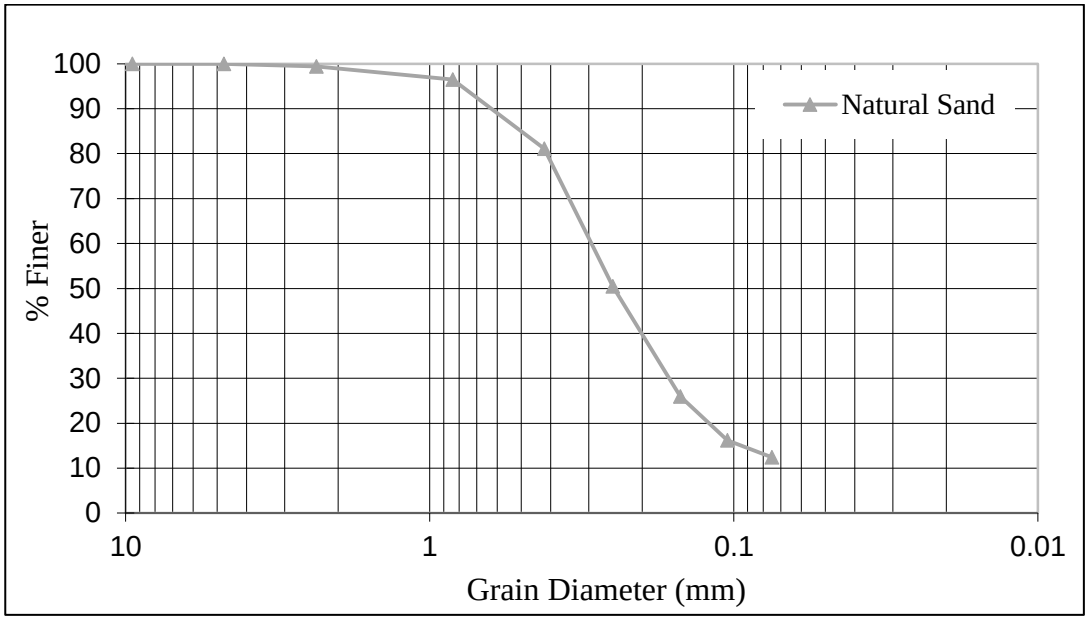

Figure 20. Gradation curve of sand used for all mixes

- High range water reducer (HRWR): Viscocrete 20 HE was used in all mixes. The latter is a Polycarboxylate Ethers (PCE) based superplasticizer (third generation SP) that complies with ASTM C494-86 standards. The data sheets of Viscocrete 20 HE is attached in appendix A.

- Retarder: Sika® Retarder was used for this study. The retarder used is a modified Phosphates based retarder that complies with ASTM C 494-81 standards. The data sheets of Sika® Retarder is attached in appendix B.

Constituents of mixes one to nine are found in table 3, while those of mix ten are found in table 4. 40 L mixes were prepared for all the latter mixes.

Table 3. Mix constituents of tests 1 to 9

Materials	Weight (Kg)		
Cement	24.6		
Sand	56		
Water	10.691	10.679	10.666
SP%	1.50%	1.55%	1.60%
SP Weight	0.369	0.381	0.394

Table 4. Mix constituents of test 10

Materials	Weight (Kg)
Cement	24.6
Sand	56
Water	10.617
SP %	1.60%
SP Weight	0.394
Retarder %	0.2%
Retarder Weight	0.049

4.3. Experimental Procedure, Phase 2:

4.3.1. Test Matrix Design

In this phase of the experiment, plain concrete elements are tested for compressive and flexural capacities. Their capacities and failure modes are compared with the control (normally cast) samples. Hence, four different specimen types are presented and summarized in table 5. The test matrix was designed in consideration of the constraints explained earlier.

Type C samples are regular cast in place specimen used as control samples, whereas type P samples are 3D printed samples. Two aspect ratios were manufactured, samples with a ratio of 1:1 will be tested for compressive strength, while samples with aspect ratio 1:2 will be tested for flexural strength. PH and PV samples are samples of the same aspect ratio but the direction of loading differs; PH loaded perpendicular to the layers plane and PV loaded parallel to the layers plane. Three additional standard cylindrical samples were manufactured for testing according to ASTM C39 standard. The latter are denoted as Cc.

Table 5. Test samples matrix – Phase 2

Specimen Type	Construction Method	Cross-Section Geometry (cm)	Aspect Ratio (1:x)	Number of Samples
Cc	Cast in mold	15×30	2	3
C:1		24 × 24	1	3
C:2			2	3
PH:1	3D Printed	24 × 24	1	2
PV:1			1	2
P:2			2	3

4.3.2. Cast in Place Control Specimen Preparation

For the control specimens C:1 and C:2, three samples of each size were prepared for testing. Material mixing was performed on different mixers due to the difference in sample sizes and mixer capacities. C:1 and Cc samples of volume equal to 13.824L and

5.2L had their mix constituents blended in a 20L maximum capacity mixer shown in figure 21.

Figure 21. 20 L maximum capacity mixer

The samples were molded and cast in a controlled environment at a temperature ranging between 22°C and 25°C. A nonstandard testing shape was adopted in this study to compare to 3D printed samples of the same size (which are constrained to certain sizes based on the nozzle diameter). Mold greasing and casting are shown in figure 22.

Figure 22. Molds greasing and specimens casting for C:1 samples

A similar procedure was followed for samples C:2 yet the 40L mixer-pump was used because the volume of the samples exceeds the volume of the 20L mixer. Sample preparation before casting and the mixer-pump are shown in figure 23.

Figure 23. Mold preparation and mixer-pump used for casting C:2 specimens

4.3.3. 3D-Printing System and Specimen Preparation

The print path was designed to manufacture samples additively, layer after layer. A layer height of 3cm was used and a speed of 6 L/min yielded best 3D printed filaments. The print paths were designed according to three constraints: 1) The nozzle is continuously depositing concrete; 2) No layer overlaps occur while printing in a given layer; 3) A certain area of the cross section will not be printed and a void forms in that area for later insertion of rebar and grouting. The print path design is shown in figure 24.

Materials are weighed and prepared prior to mixing and all materials are placed within reach to the mixer pump. 10% of the water is first added to the mixer, and while rotation on speed 1, sand and cement are added gradually. 80% of the water content is added simultaneously with sand and cement. After adding all mix constituents, the last

10% of the water mixed with a weighed amount of superplasticizer are added to the drum. This process takes 3-5 minutes to complete. After all constituents are added, the mixer is set to speed 2 and is mixed for two minutes, then allowed to rest for one minute and then mixed for one more minute on speed 2. The mix would then be ready for pumping.

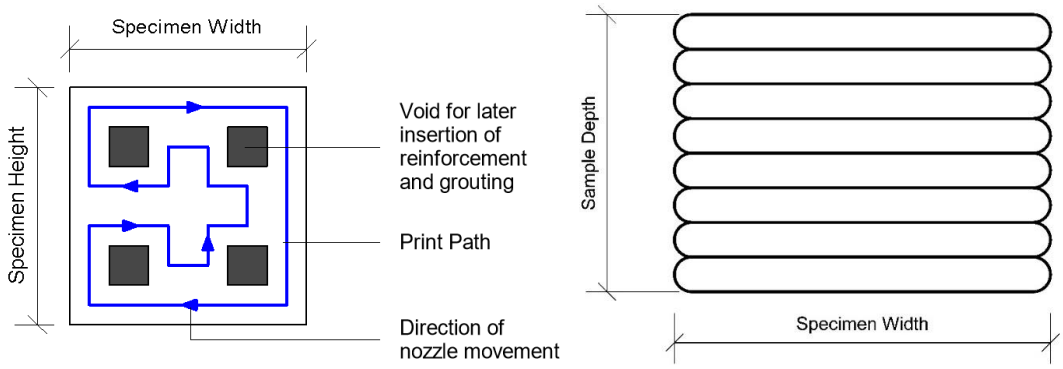

Figure 24. 1) Cross section showing the different variables in a 3D printed concrete column. 2) Elevation view of a printed specimen

A computer program that is linked to the mixer-pump would give the command to start pumping, then 2 seconds later (delay for the hose to fill with concrete and ensure continuous flow) the designed print path would run as planned. When the code is finished, a 3D printed sample would be manufactured as shown in figure 25.

Figure 25. 3D printed sample under study

Upon completion, samples are left to harden for 24 hours before moved to the curing room. Samples are moist-cured for 7 days, then removed to dry for 1 day.

Due to the limited amount of concrete available per one run, the possibility of printing any more than one 24cm x 24cm x 48cm sample is unattainable. With a filament height of 3cm, sixteen layers are required to build the required sample. However, several trials showed that whenever more than 13 layers of fresh concrete are stacked up in a time span not exceeding 3 minutes, the elasto-plastic stresses in the bottom layers exceed the capacity of the fresh concrete causing the entire sample to collapse (figure 26). Hence, an alternative method had to be considered to print any sample with an aspect ratio above 1:1.

Two possible solutions were suggested, either 1) print a portion of the sample, wait for concrete to gain some strength, then extrude the rest of the layers above the hardened concrete, or 2) print two separate half samples, then bond them together after they harden.

Figure 26. Failure of sample upon reaching 13 layers within a 3 minutes time-lapse.

The first solution, although less disturbing to the automated process, has its constraints and drawbacks. For example, by the time the concrete hardens and new concrete is being added, the mix would have lost its workability and the filaments would not have the same dimensions as the ones below, assuming that concrete does not harden

in the hose. A major drawback to this process, which is vital to rejecting it, is the bond strength between old and new layers of concrete. Since any sample exceeding aspect ratio 1:1 will be tested for flexure, it is detrimental to voluntarily create a cold joint in mid span of the sample. Hence we resigned to solution two.

ACI 503.1-92 is the standard specification for bonding hardened concrete, steel, wood, brick and other materials to hardened concrete with a multi-component epoxy adhesive. This document gives detailed procedures to bond hardened concrete to hardened concrete including surface preparation procedures, and epoxy specifications. The document will be attached in appendix C, yet a detailed procedure of the performed work will be described next.

First, concrete sample surfaces were prepared using mechanical abrasion (figure 27). Then, concrete surfaces were inspected for any loose concrete and the latter were removed. Last, concrete surfaces were cleaned with water to remove dust and were allowed to dry sufficiently.

Figure 27. Surface preparation of samples

ASTM C881 specifies the standard specifications for epoxy-Resin-Base bonding systems for concrete. From this document, the epoxy needed to bond hardened concrete samples was identified. The specs were as following:

- Type IV - For use in load bearing applications for bonding hardened concrete to hardened concrete and other materials and as a binder for epoxy mortars and concretes.
- Grade 3—Non-sagging consistency.
- Class C—For use above 15°C [60°F] the highest allowable temperature to be defined by the manufacturer of the product.

With the following specs in hand, a materials supplier company was contacted and a product whose specs are matching the required specs were provided. The data sheet for the product is available in appendix D.

Epoxy was applied to the prepared surfaces after completely drying as shown in figure 28. Three samples each composed of two 3D printed concrete samples were prepared while taking careful measures to keep the holes aligned to each other for later grouting.

Figure 28. Application of Epoxy to the prepared concrete surface

After preparing three samples of both P:1 and P:2 sample types, and allowing epoxy to harden for 24 hours in P:2 samples, self-compacting concrete with high fluidity (same mix design used for 3D printing yet with a 2% super plasticizer percentage) was used to fill the voids in the samples. Since at this stage of the experimental work, a comparison between 3D printed concrete plain elements and normally cast specimen was to be conducted, there was no need to insert rebar in the voids. Samples were cured for 28 days after this point in order for the SCC concrete to gain its 28 days compressive strength. The prepared samples P:1 and P:2 are shown in figure 29.

Figure 29. Samples P:1 and P:2 after grouting voids

4.3.4. Materials and Mix Proportions

Due to the comparative nature of this study, a compressive strength target was not set. Instead, focus was devoted for optimizing a mix that would meet the required fresh properties of concrete, mainly extrudability, workability, and buildability. Open time and subsequently bond strength are important parameters, yet nothing was done to specifically enhance them since the time between two consecutive layers merely exceeded 12 seconds. To ensure that the hard properties (compressive and flexural strength) of both

the control and the 3D printed samples are the same, the same mix design will be used in both cases. Two mix sizes were used, a 25L mix for printing samples P:1 and a 40L mix for samples P:2. Tables 6 and 7 show the constituents of each mix.

Table 6. 25L Mortar Mix Constituents

25L Mix			
	Mass (Kg)	Specific Gravity (SG)	Volume (L)
Cement	15.375	3.15	4.88
Water	6.674	1	6.674
Sand	35	2.65	13.2
HRWR (1.55%)	0.238	1.09	0.259
Total			25

Table 4. 40L Mortar Mix Constituents

40L Mix			
	Mass (Kg)	Specific Gravity (SG)	Volume (L)
Cement	24.6	3.15	7.81
Water	10.679	1	10.679
Sand	56	2.65	21.13
HRWR (1.55%)	0.381	1.09	0.415
Total			40

4.3.5. Test Setup and Procedure

Specimen of types C:1 and P:1 had their 28 days compressive strength evaluated by axial compression test on a press of 300 Ton nominal capacity machine and up to the failure of the specimen. The specimen were capped with sulphide on the upper end to ensure contact surface is parallel for uniform distribution of stresses in concrete. The relation between stress and strain is measured in specimens using linear-variable differential transducers (LVDTs) fixed at the bottom steel plate of the testing machine.

Specimen of types C:2 and P:2 had their flexural capacities evaluated by flexural testing using the four point loading on the MTS machine. The specimen have a span length equivalent to two times its depth and were subjected to concentrated loads at one third and two thirds of its span until failure. The layout of the specimen and the loading

point locations are shown in figure 30. An LVDT placed at mid span was used to measure the stress strain relationship in the specimen under study.

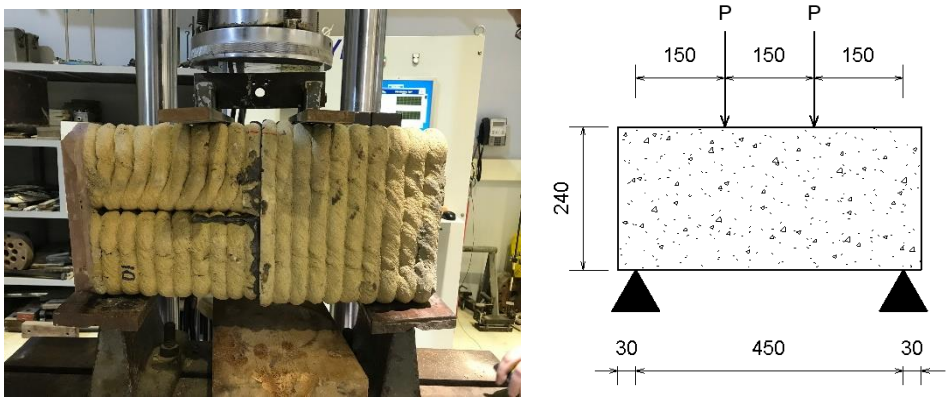

Figure 30. Flexural test experimental setup

4.4. Experimental Procedure, Phase 3:

4.4.1. Test Matrix Design

Two different specimen types are presented and summarized in Table 7. The test matrix was designed considering the constraints discussed earlier in this chapter. Two beam types were designed: Type C:4 is a regular cast in place beam whereas types P:4 is a concrete 3D printed beam. Both samples will be tested for ultimate capacity on the MTS machine and the ultimate capacity and failure modes will be compared for assessing the viability of reinforcing beams as proposed.

Table 7. Test samples matrix – Phase 3

Beam Code	Construction Method	Cross-Section Geometry (cm)	Length (cm)	f'_c (MPa)	Bottom Reinf.	Top Reinf.	Shear Reinf.	Nb of Samples
C:4	Cast in place	24	96	50	2T14	2T14	T8@10	3
P:4	3D Printed		98					3

4.4.2. Specimen Design

Design of the beam's longitudinal and transversal reinforcement area was performed using ACI 318. Thus, the minimum required area of steel in the beam cross

section should be greater than $\frac{1}{4}\frac{\sqrt{f'c}}{fy} * bw * d$ of the beam's gross section area. Transversal reinforcement minimum requirements were also met by providing shear reinforcement greater than the minimum which is $\frac{1}{16}\frac{\sqrt{f'c}}{fyt} * bw * s$. Figure 31 shows the reinforcement layout in sections and elevations for the designed beam. 2Ø14 were used for longitudinal bars in top and bottom layers. Transversal reinforcement of diameter 8mm at a spacing of 9cm was used in all specimen at the full length of the beam. The nominal moment capacity of the designed section was found to be 32.63 KN.m, theoretically failing at load P equal to 115.19 KN. It should be noted here that the beam is by ACI 318 standards a deep beam, and its design should be carried out using the strut-tie method. Hence, the beam capacity was determined using the latter method, yet no noticeable difference was observed. Stirrups were distributed in a way to ensure a shear failure would occur before the flexural failure would. Shear capacity was calculated based on stirrup distribution and was found to have a capacity of 96.32 KN. Hence the beam should theoretically fail by shear.

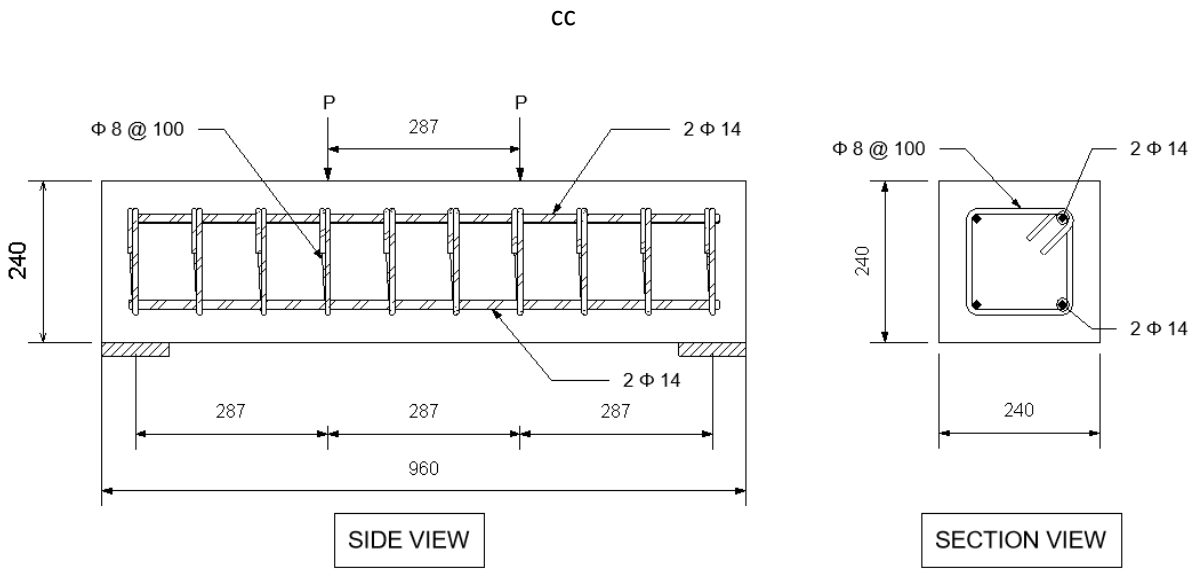

Figure 31. Reinforcement layout for the manufactured beams

4.4.3. Control Specimen Preparation

For the control specimen C:4, three samples were prepared for testing. Material mixing was performed on two batches due to the limited drum capacity. The 24cm x 24cm x 96cm samples are 55L in volume, whereas the maximum drum capacity is 40L. Thus two mixes were prepared for each sample; a 40L mix and another 25L mix. A 10 minute gap time between pouring the first and the second mix is present due to the second mix preparation time. A small dosage of retarder (0.2%) was used along with a mechanical vibrator to ensure cohesion between the two mixes.

The formwork, made of marine plywood were manufactured to have inner dimensions of 24cm x 24cm and a depth of 96cm. A view of the formwork preparation and greasing are shown in figure 32.

Figure 32. C:4 samples molds greasing and preparation

Three steel cages of the same type were prepared based on the structural design requirements and the tested mode of failure. Both bottom and top rebar ensure a 4cm cover to stirrups of diameter 8mm. Two bottom and two top reinforcement of 14mm diameter were used as longitudinal reinforcement. The steel cage is hanged 3cm from the top and ensuring an even cover from all sides. Views of the steel cages are shown in figure 33 and figure 34.

Figure 33. Steel cages preparation

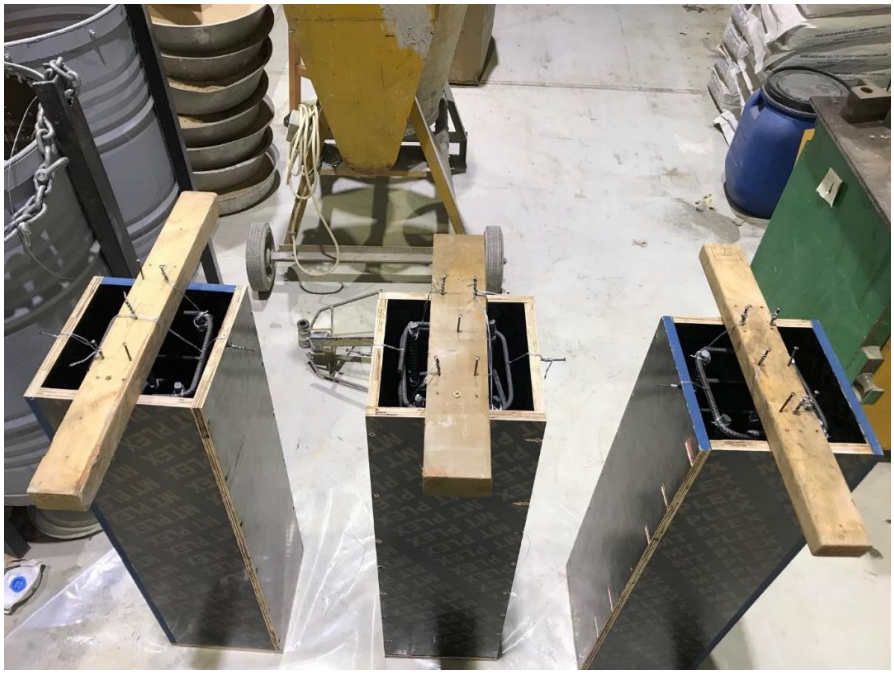

Figure 34. C:4 Samples ready for casting

All six mixes (three 40L mixes and three 25L mixes) were prepared prior to any concreting work as shown in figure 35-1. All mixes were poured in the AUB structural and construction lab at the same day. The time between two consecutive mixes ranged between 10 and 15 minutes. Surface smoothing was performed at the end of each mix with a hand trowel after removing the wires anchoring the steel cage.

Figure 35. Material preparation and C:4 specimens casting

4.4.4. 3D Printed Specimen Preparation

In this phase of the experiment, the layer height (nozzle offset) was changed to 2.5cm to further reduce the possibility of having filaments distorted due to an excessive offset between the printing bed and the nozzle. The print path was designed according to the same constraints as before and the print path is the same as the one used in the previous experimental phase.

Due to the high similarity in executing this phase and the previous phase of the experiment, only the differences will be outlined, mainly in reinforcement procedures.

Both stirrups and main bars were cut to the desired lengths; 100 cm bar per one stirrup and 90 cm bar per one longitudinal rebar. Stirrups were bent to the desired shape using the steel bending machine in the lab as shown in figure 36.

Figure 36. Fabrication of steel bars and stirrups

Then stirrups were inserted into predefined layers while concrete is being extruded right before the nozzle transitions between two different vertical layers. Stirrups

are correctly aligned to the pattern holes to leave space for later insertion of vertical reinforcement (figure 37).

All twelve individual parts of the three P:4 samples were 3D printed and cured for 7 days before surface preparation took place. Then, epoxy was applied to the prepared surfaces and was allowed to harden for 24 hours. It is worth noting that in order to ensure holes were aligned when glued with epoxy, a T14 rebar was inserted into the hole until epoxy dried out. Epoxy coating and assembly of the four samples are shown in figure 38.

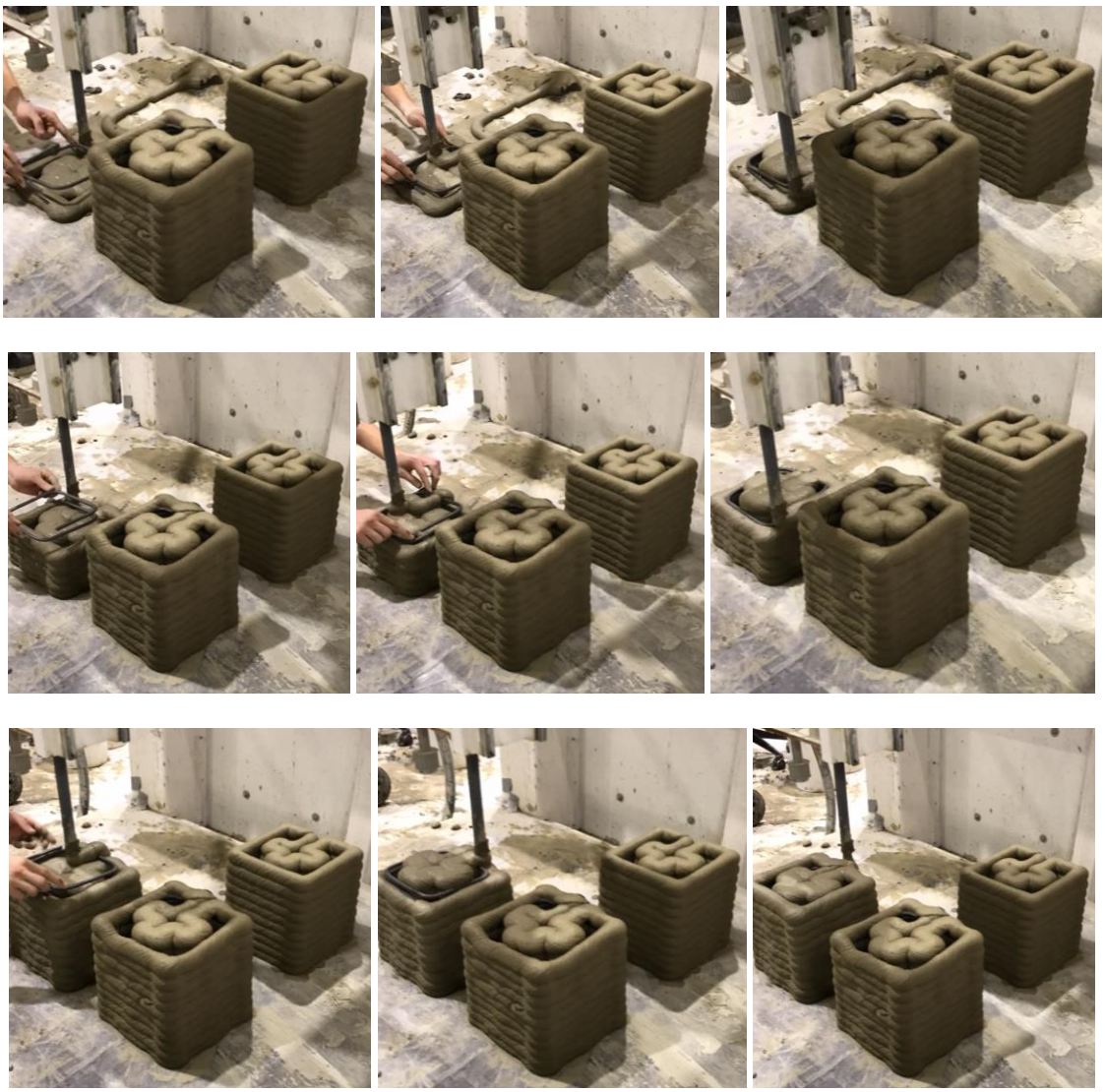

Figure 37. Placing stirrups into 3D printed specimen

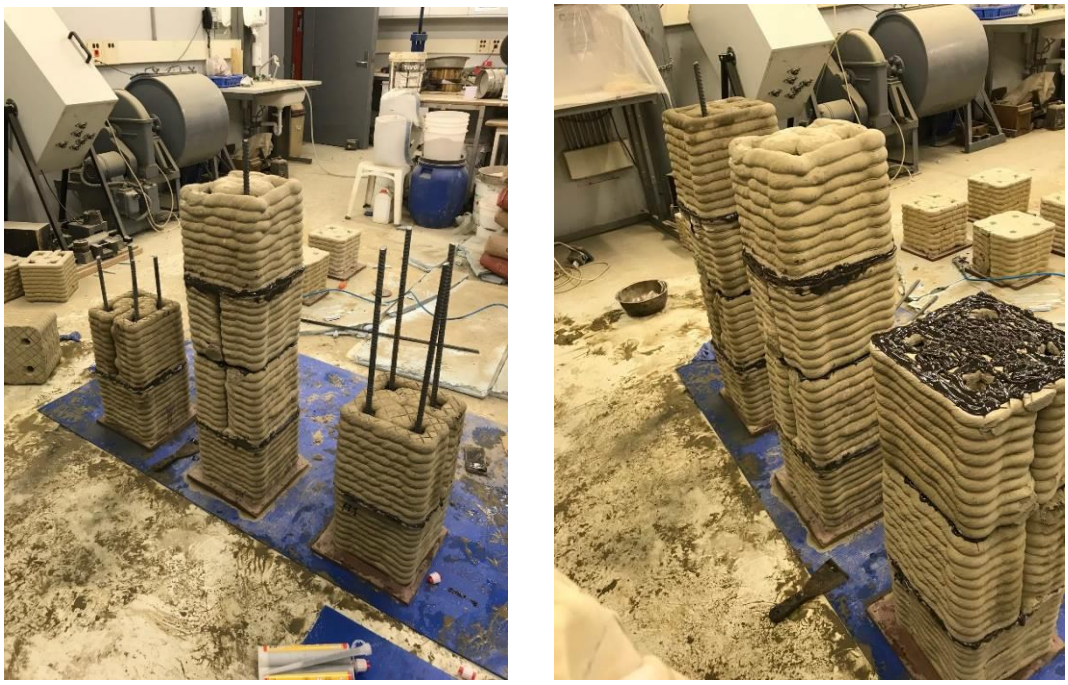

Figure 38. Epoxy surface coating and specimen assembly

Epoxy was left to gain strength and dry out for 24 hours, after which three separate 7L mixes of SCC were prepared, and voids were filled with the flowable concrete. After voids were completely filled with SCC and no air was left, a 90cm T14 rebar was inserted into each mortar filled void. Samples after rebar insertion and grout are shown in figure 39.

Figure 39. P:4 specimens after grouting and reinforcement insertion

4.4.5. Materials and Mix Proportions

The materials used in this phase of the methodology is built upon the trials from the two previous phases. An additional 0.2% retarded was added to both mixes to anticipate any unwanted loss of workability.

Table 8. 40L Mortar Mix Constituents

40L Mix			
	Mass (Kg)	Specific Gravity (SG)	Volume (L)
Cement	24.6	3.15	7.81
Water	10.630	1	10.630
Sand	56	2.65	21.13
HRWR (1.55%)	0.381	1.09	0.415
Retarder (0.2%)	0.049	1	0.049
Total			40

Three steel bars used were tested for yielding and ultimate capacities for each diameter used. All information obtained from the tests are shown in figure 40 and figure 41.

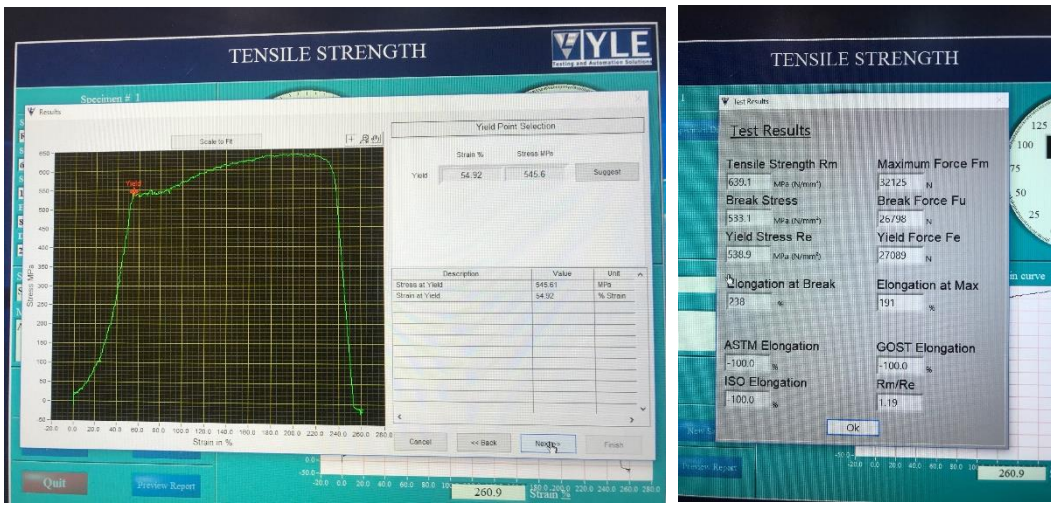

Figure 40. Results from steel bar tensile testing for T8 bars

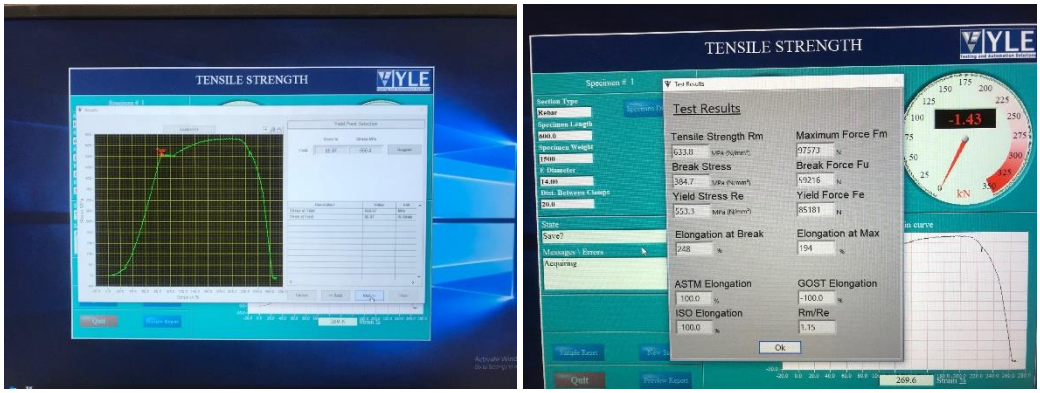

Figure 41. Results from steel bar tensile testing for T14 bars

4.4.6. Curing of the Specimens

For the cast in place specimen, the mold was removed 24 hours after casting. When forms are removed, curing using white burlap-polystyrene sheets was applied after spraying concrete surfaces with water. As for the printed elements, curing will started four hours after the element is completely printed. Curing was continually applied for the first seven days after removing the forms or printing. Then, the samples were left in the lab in a controlled environment with a temperature ranging between 23°C and 26°C and humidity ranging between 50% and 65% until the testing day.

4.4.7. Test Setup and Procedure

The reinforced concrete control and 3D printed beams had their flexural strength evaluated using the MTS machine. The span between the centerline of the supports was taken to be equal to 85cm. Two concentrated loads were applied continuously at a distance from the supports equivalent to one third and two thirds of the span at intervals of 28.67cm. The concentrated loads were applied in increments of 0.02mm/second until failure. Both vertical deflection and crack widths were calculated, the former with an LVDT placed at mid-span, and the latter with a crack comparator.

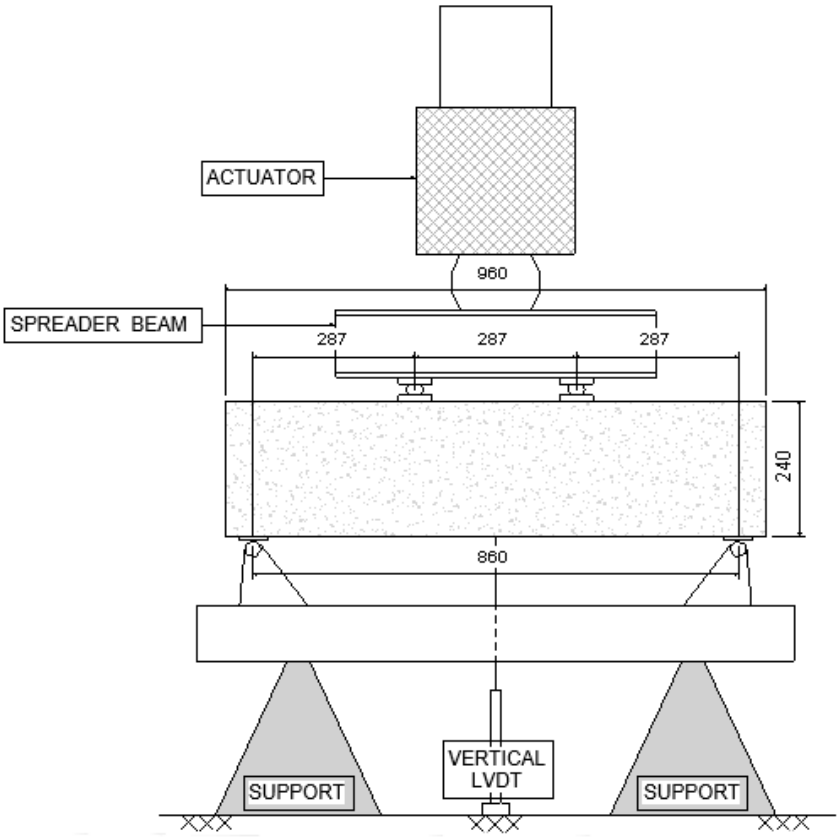

Figure 42. Schematic view of P:4 and C:4 specimens test setup.

Figure 43. Test setup for P:4 samples

Figure 44. Test setup for C:4 samples

CHAPTER 5

RESULTS AND DISCUSSIONS

5.1. Phase 1 Experimental Results

Results of the first experimental phase are presented in the following section. The printed filament width variation with time is plotted on four different graphs, three of which compare results of mixes with the same HRWR percentage, and another graph compares a mix with or without retarder.

For a constant SP dosage, generally and as expected, the filament width would decrease as time increases, which implies that the workability of the mix is decreasing with time. However, when using a superplasticizer dosage of 1.50%, an abnormal behavior of the mix was observed. At all three tested speeds, the workability started at an initial high filament width value, and decreased in width as time passed until reaching a point at which filament width starts increasing again. In contrary to what was expected, the minimum filament width was not obtained at the finish time of the test, but at the lower bound of the intermediate-filament-width fluctuation phase. As for the filament width values when using a 1.50% SP, a lower speed yielded a wider initial and final filament width whereas a faster speed yielded a thinner filament width. Three main points are of interest to us when using a 1.50% SP ratio, the initial filament width reading (FW_I), the lowest filament width reading (FW_L), and the filament width reading when the test finishes (FW_F). The first point readings of three different speeds recorded filament widths of values 4.1cm, 3.5cm, and 3.2cm for speeds 100mm/sec (V_1), 116.67mm/sec (V_2), and 133.34mm/sec (V_3) respectively. The lowest filament width readings were 3.3cm, 2.7cm, and 1.9cm for speeds V_1, V_2, and V_3 simultaneously. At the end of the three tests with

1.50% SP, the values obtained were 3.5cm, 3.1cm, and 2.4cm for speeds for speeds V_1, V_2, and V_3 simultaneously. The graphical plot of the previous results are shown in figure 45 and the tabular results are shown in table 9.

Table 9. Filament width at different points in a 1.50% SP mix design

Filament Width (cm)	Nozzle Speed (mm/sec)		
	100 (V_1)	116.67 (V_2)	133.34 (V_3)
FW_I	4.1	3.5	3.2
FW_L	3.3	2.7	1.9
FW_F	3.5	3.1	2.4

An addition of 0.05% to the previous mix proportions with a sum of 1.55% superplasticizer shifted the behavior of the mix to a traditional behavior, starting with maximum workability at the beginning of the test and with the lowest workability at the end. This was reflected in the filament width variation where it recorded an initial filament width of 5cm, 4.7cm, and 5.1cm for speeds V_1, V_2, and V_3 simultaneously. The final filament widths obtained were 3.8cm. 3.5cm, and 3.3cm for speeds V_1, V_2, and V_3 simultaneously. Two additional points will be recorded which are the filament width at t = 2min 12sec (FW_1) and t = 4min, 37sec (FW_2). FW_1 and FW_2 represent the filament width at the finish point of printing each of the first and the second specimen in phases two and three of the experiment. FW_1 recorded 4.4cm, 4.1cm, and 4.0cm while FW_2 recorded 4.3cm, 3.8cm, and 3.4cm for speeds V_1, V_2, and V_3 simultaneously. Graphical plots of the previous results are shown in figure 46.

The results of the third mix design with 1.60% superplasticizer showed a similar behavior to the second mix with 1.55% SP. The initial filament widths were the highest at 5.3cm, 4.7cm and 4.5cm for speeds V_1, V_2, and V_3 simultaneously. The final filament widths recorded were 4.1cm, 3.8cm, and 3.5cm for speeds V_1, V_2, and V_3 simultaneously. FW_1 recorded 4.7cm, 4.1cm, and 3.7cm while FW_2 recorded 4.2cm, 3.8cm, and 3.5cm for

speeds V_1, V_2, and V_3 simultaneously. Graphical results of a mix containing 1.60% SP are shown in figure 47. Tabulated results of mixes with 1.55% and 1.60% of SP are shown in table 10.

Table 10. Filament width at different points in a 1.55% and 1.6% SP mix design

SP%	1.55%			1.60%		
Filament Width (cm)	Nozzle Speed (mm/sec)			Nozzle Speed (mm/sec)		
	100	116.67	133.34	100	116.67	133.34
FW_I	5.0	4.7	5.1	5.3	4.7	4.5
FW_1	4.4	4.1	4.0	4.7	4.1	3.7
FW_2	4.3	3.8	3.4	4.2	3.8	3.5
FW_F	3.8	3.5	3.3	4.1	3.8	3.5

Filament width variation when using retarder was compared to a mix without retarder. Both SP% and nozzle speed were fixed at 1.60% and speed V_1. The initial filament widths obtained are 5.5cm and 5.3cm, and the final filament widths are 4.7cm and 4.1cm for 0.2% and 0% retarder percentage simultaneously. FW1 recorded 5.0cm and 4.7cm, while FW_2 recorded 4.7cm and 4.2cm for speeds V_1, V_2, and V_3 simultaneously. Results of this test are shown in figure 48 and table 11.

Table 11. Filament width at different points in a 0.2% and 0% retarder mix design

Retarder %	0.2%	0%
Filament Width (cm)	Nozzle Speed (mm/sec)	Nozzle Speed (mm/sec)
	100	100
FW_I	5.5	5.3
FW_1	5.0	4.7
FW_2	4.7	4.2
FW_F	4.7	4.1

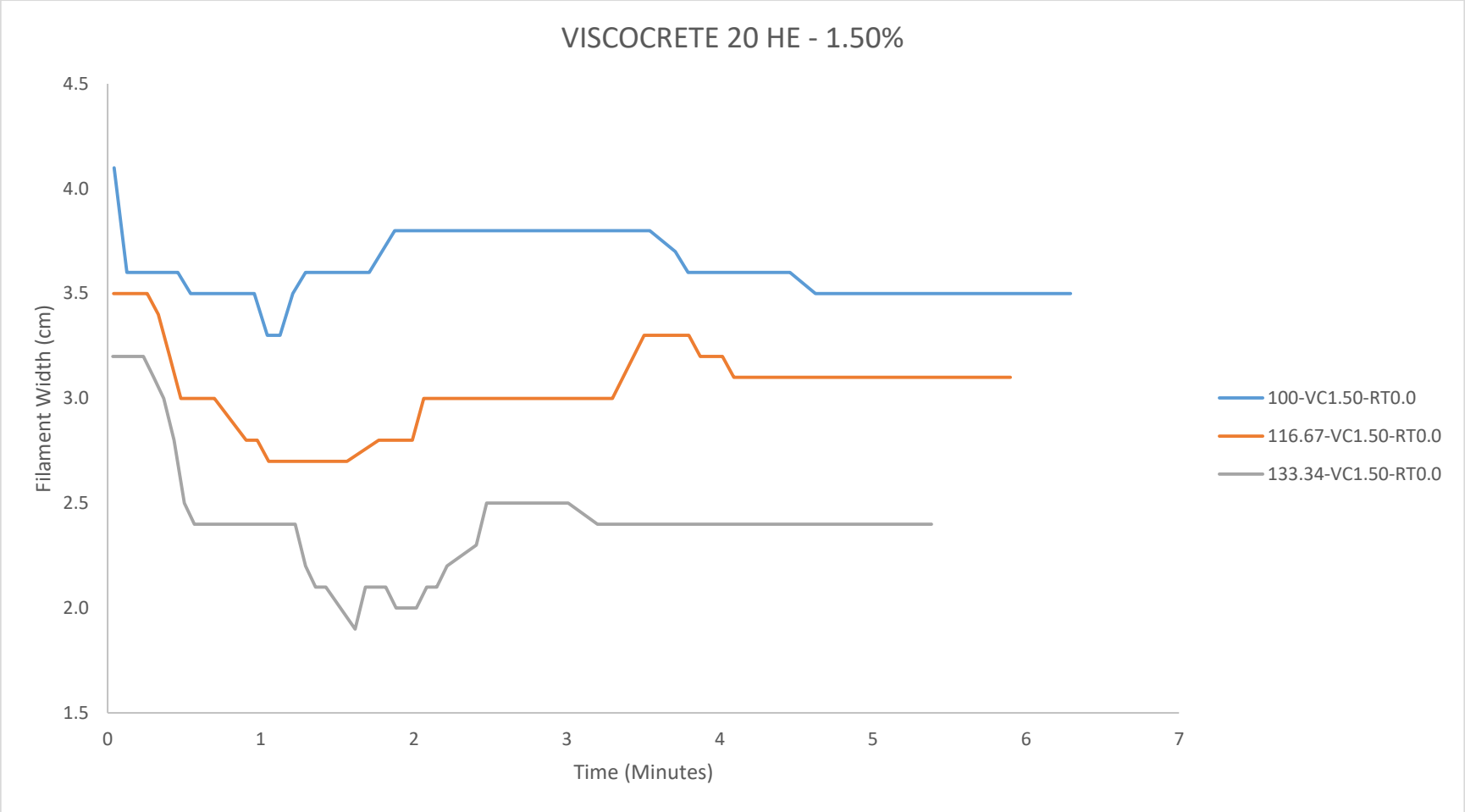

Figure 45. Filament width versus time for a 1.5% HRWR and variable speeds

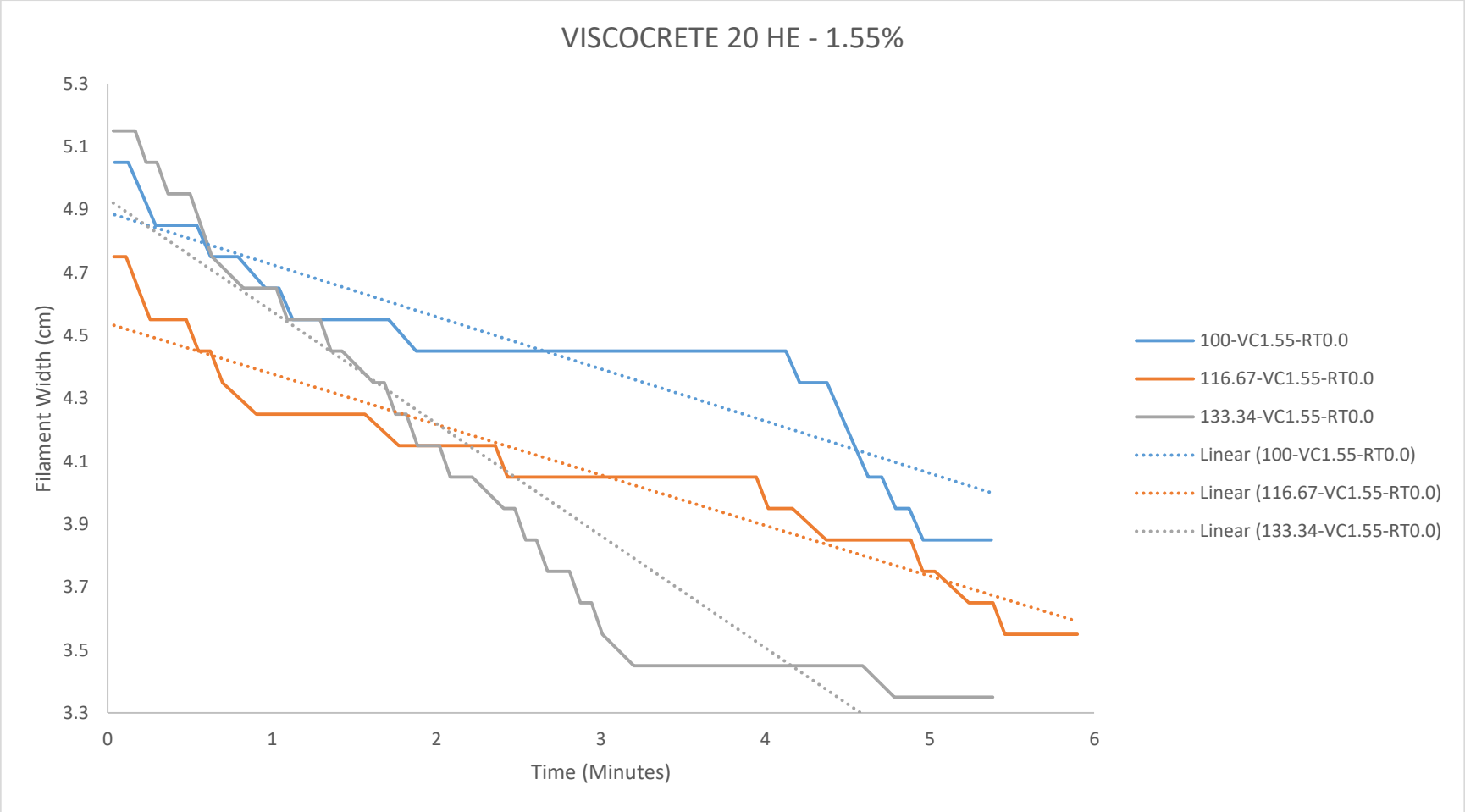

Figure 46. Filament width versus time for a 1.55% HRWR and variable speeds

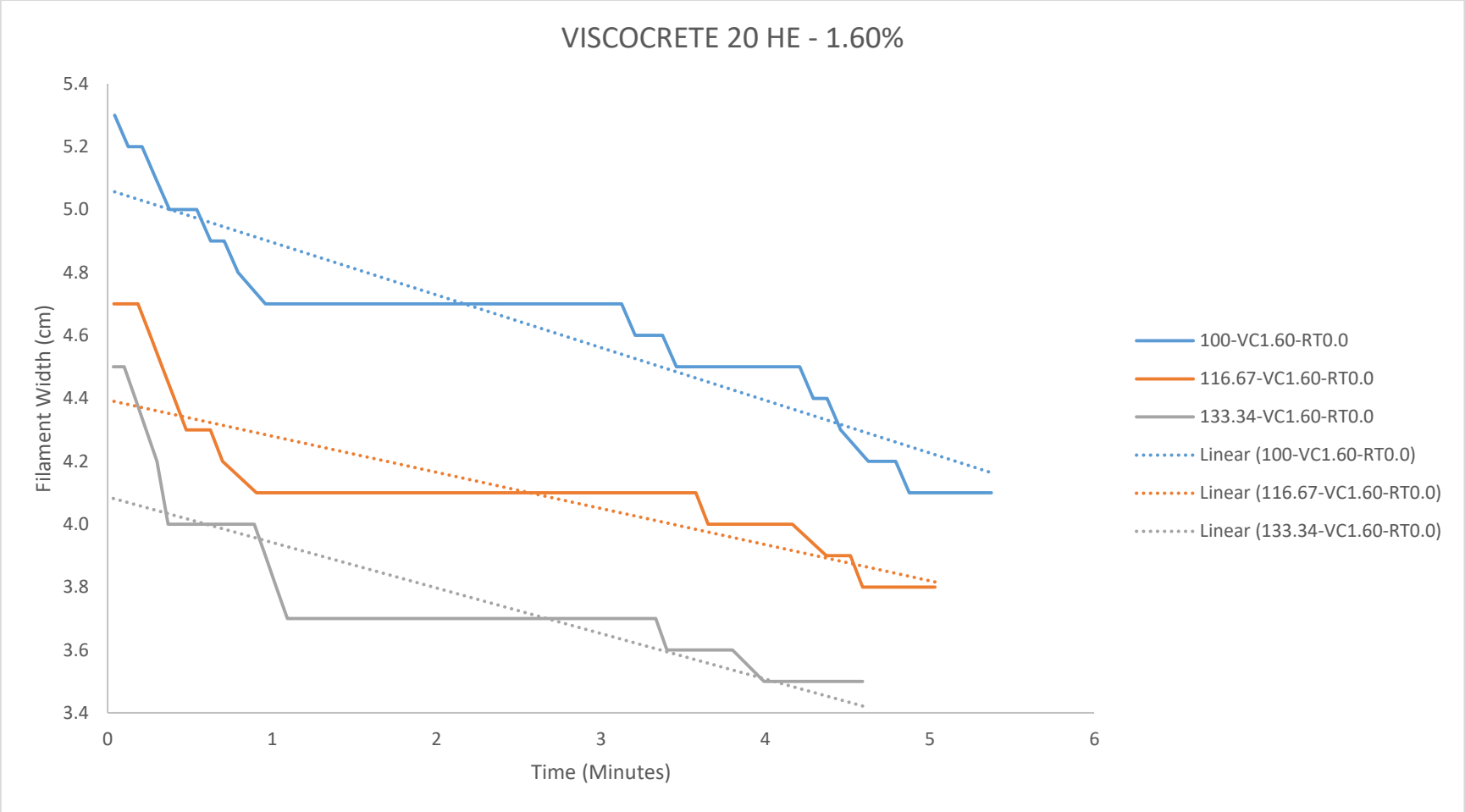

Figure 47. Filament width versus time for a 1.6% HRWR and variable speeds

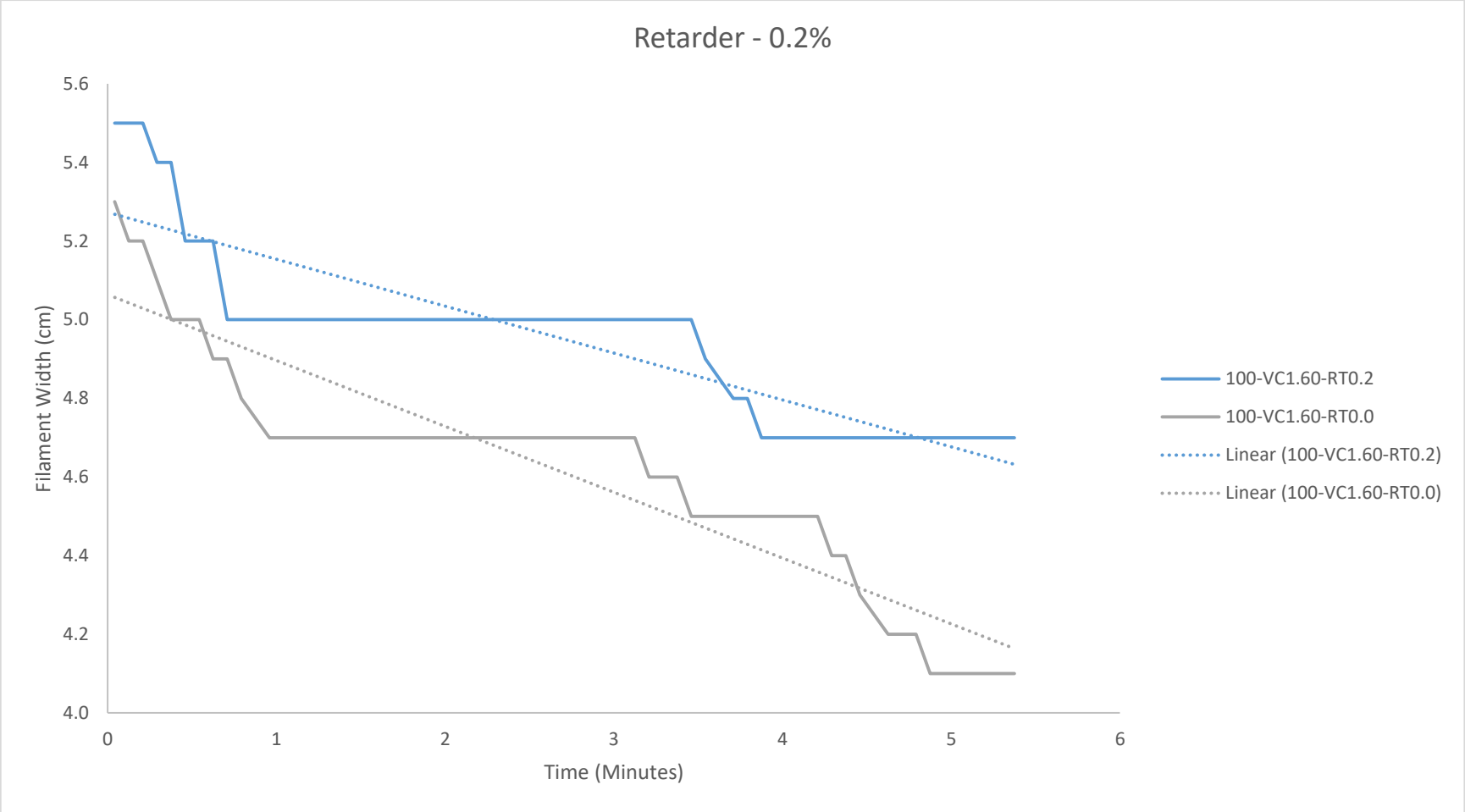

Figure 48. Filament width versus time for a 0.2% added retarder and a 0% added retarder mixes

.

5.2. Discussion of Phase 1 Results

From the results obtained in the first phase of the experiment, a better understanding of the mix behavior is achieved. The understanding of these results and discussions based upon them are tackled in this section.

5.2.1. Effect of Superplasticizer

Using 1.50% SP leads to an undesirable mix behavior. The mix exhibits early reduction in workably but then the workability increases after a while. Delayed action of the HRWR because of the small quantity and the mixing process may be the reason for this behavior. Hence, using a 1.50% SP is not advisable in this mix.

When using either 1.55% or 1.60% SP, the mix exhibited a normal behavior, starting with a high initial workability; reflected by a wide filament width, and decreasing gradually as time passes reaching its minimum when the experiment ends. However, as the SP dosage increases from 1.55% to 1.6%, three main observations were made. First, as the SP dosage increased, the filament width increased for the same speed. This is due to the workability gained by the mix due to the added amount of SP. Second, as the dosage increased from 1.55 % to 1.6%, the rate of drop in filament width decreased. This is shown in figures 46 and 47 where the rate of drop in a 1.55% mix is 0.166cm/min for speeds V_1 and V_2, and 0.35cm/min for speed V_3, whereas the rate of drop in a 1.6% mix is 0.142cm/min, 0.12cm/min, and 0.185cm/min for speeds V_1, V_2, and V_3 simultaneously. The third observation is that as the SP% increases, the time at which the filament width remains constant increases. This is shown in figures 41 and 42 were the average time at which the filament width is constant is 1.75min for a 1.55% SP and 2.46min for a 1.6% SP.

5.2.2. Effect of nozzle speed

Regardless of the SP% used, an increase in the nozzle speed would always lead to a decrease in the filament diameter. This is due to the fact that at a constant SP% and a constant pumping rate (constant flow rate), the same volume is extruded in a given amount of time regardless of the nozzle speed. Hence, to compensate for the added speed, the volume of concrete per unit length of a filament decreases. This is explained better in the following discussion.

Flow rate Q is defined to be the volume of fluid passing by some location through an area during a period of time.

$$Q = \frac{V}{t} \qquad \text{Equation 1}$$

Where V is the volume and t is the elapsed time.

The volume of concrete per unit time flowing from one point to another is the cross sectional area of the concrete filament multiplied by the distance crossed. Hence, equation 1 can be written in the following form:

$$Q = \frac{Ad}{t} \qquad \text{Equation 2}$$

Where A is the cross sectional area and d is the distance crossed.

The distance crossed divided by the time taken to cross that distance is the velocity at that segment. Hence, equation 2 can be written as:

$$Q = Av \qquad \text{Equation 3}$$

Where $\boldsymbol{\upsilon}$ is the velocity in that segment.

From equation 3, A and $\boldsymbol{\upsilon}$ are shown to be inversely proportional, which explains the decrease in filament width as nozzle speed increases.

5.2.3. Effect of retarder

Using a minimum dosage of retarder to the mix alters the mix behavior in two main ways, both of which imply that the retarder is providing added workability to the mix. First, the initial filament width when adding retarder was higher than that of without retarder. This can be due to the initial workability right after mixing having a higher workability when using retarder. Second, the rate of drop in filament width decreased when using retarder from 0.166cm/min to 0.11cm/min which implies that the rate at which workability is lost decreases.

5.2.4. Parameters used in phases 2 and 3

In the upcoming experimental phases, samples of aspects ratios 1:1, 1:2, and 1:4 will be manufactured. However, regardless of the aspect ratio, samples of aspect ratio 1:1 will always be printed separately, then joined together later as described in the methodology. Thus, and to speed up the printing process, all samples other than aspect ratios 1:1 had two 1:1 samples manufactured using the same mix. Hence, the time required to print the two specimens exceeds 4min 30sec if set on speed V_2. As time of printing extends, the variability in filament width also increases, which would yield samples with wide material inhomogeneity, and inconsistency of filament width, within the same sample and between two separate samples. In order to overcome this issue, parameters that control the material and process properties (SP% and nozzle speed) should be carefully chosen based on the different results plotted earlier.

Among the three SP% tested, the mix containing 1.50% SP was opted out due to its undesirable behavior and its low filament width results. The acceptable filament width set, ranges between 4.1cm and 4.6cm. Although pattern are designed based on a 4cm filament width, trials have shown that a wider filament width would ensure better bonding

in the horizontal directions. However, a wider filament width would mean a narrower void diameter, hence difficulty in placing rebar and grouting. Both mixes containing 1.55% and 1.60% print with filament widths that fall within the acceptable range, however the 1.60% mix was less buildable than the 1.55% mix. In addition, at speed V_1 and a SP% of 1.60, the filament width was near the upper bound of the defined range. Although this is acceptable, it is preferable to keep the filament width closer to the lower bound to obtain wider void diameters for easier placement of bars and grouting later. For all the reasons above, a SP% of 1.55% was chosen as the most adequate HRWR dosage.

After fixing the SP%, the second issue regarding the variation in filament width as time passes is addressed. At a 1.55% SP and at speed V_2, the filament width decreases from an initial value of 4.7cm at t = 0.0min to 4.1cm at t = 2.0 min. Then from that point on and up to t = 4min 30sec, the filament width decreases below 4.1cm to reach 3.8cm. To avoid a drop in the filament width below the lower bound of the acceptable range, the nozzle speed is changed from V_2 to V_1 right before printing the second specimen; at t = 2min 12sec. This drop in speed allows the filament width to increase to an acceptable value of 4.4cm at t = 2min 12sec and 4.1cm at t = 4min 37sec (time at which second sample is done).

Throughout the discussion above, only speeds V_1 and V_2 were considered, whereas speed V_3 was opted out. The main reason for excluding speed V_3 is due to the geometric mismatch between the corner filament width sizes and the straight segments filament width sizes. This occurs when the machine shifts direction 90 degrees, it would decelerate at the point of rotation. This deceleration results in an excessive accumulation of concrete at the corners more than that of on the edges where speed is constant. Hence, speed V_3 was altogether discarded.

5.3. Phase 2 results

5.3.1. Compression test experimental results:

Three cylinders were cast and tested as per ASTM C39 at 28 days. Results of the cylindrical samples will be a benchmark for comparison with other samples casted or printed using the same mix and will be used for theoretical calculations. Table 12 summarizes the results obtained for the cylindrical compression tests.

Table 12. Compressive strength test results for cylindrical samples

Casting date	Cylinder age (days)	Average compressive strength (MPA)
October 9	28	47.8

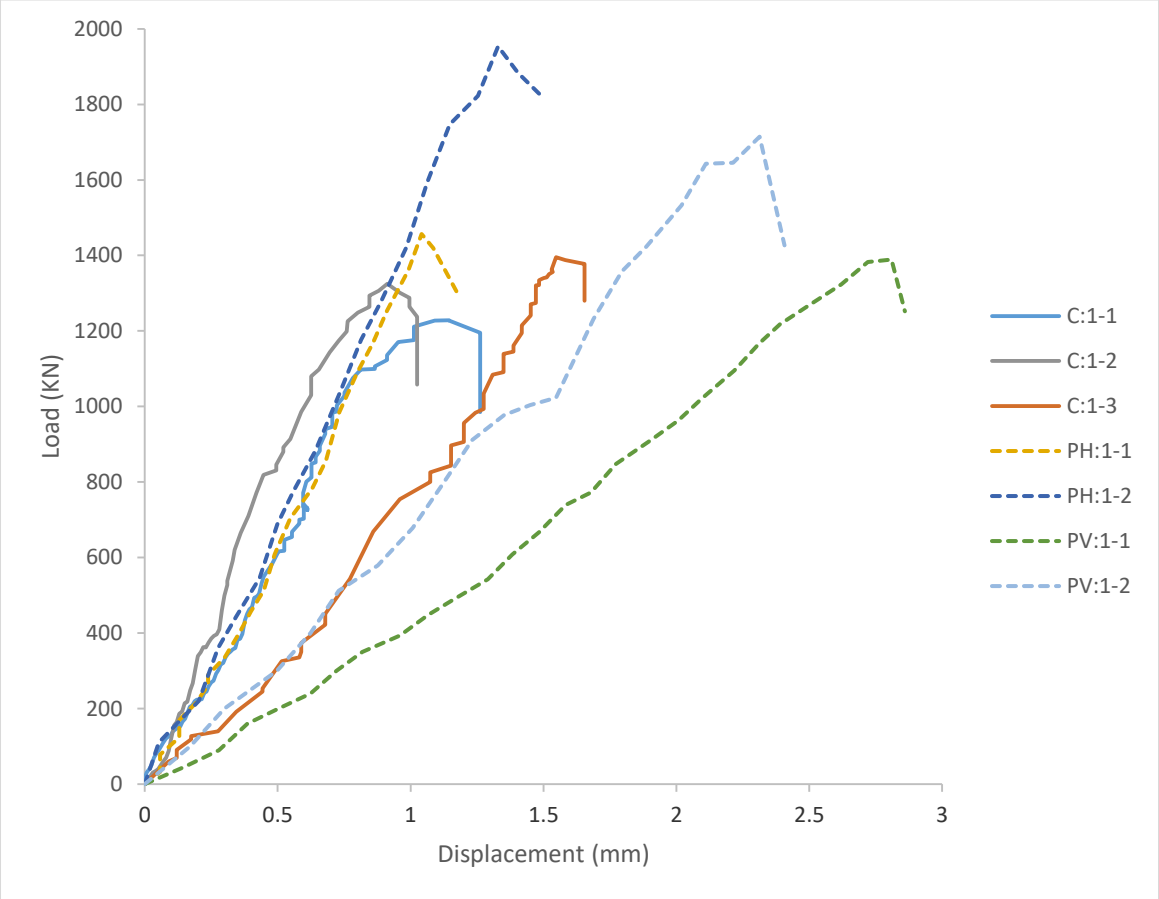

Figure 49. Load deformation curves for specimens tested in compression

Specimens of aspect ratio 1:1 were tested until failure and the load deformation graphs were plotted. Plots are shown in figure 49 and the failure loads are given in table 13 along with the average failure load and the average compressive stress.

Table 13. Failure loads of different samples tested for compression

Specimen Code Name	Compressive Strength Test Loads (KN)	Average Load (KN)	Average f'_c (60 days) (MPa)
C:1-1	1228.3		
C:1-2	1324.7	1313.67	26.5
C:1-3	1388		
PH:1-1	1468	1715.95	27.5
PH:1-2	1963.9		
PV:1-1	1385.4	1561.4	25.0
PV:1-2	1737.4		

5.3.2. Flexural test theoretical and experimental results:

The theoretical modulus of rupture is calculated based on equation 19.2.3.1 in ACI 318RM-14. The equation is provided below:

$$fr = 0.62\sqrt{f'c}$$

Where:

f_r = Theoretical modulus of rupture (MPa)

f'_c = Compressive strength of concrete (MPa)

In the prediction of the experimental cracking load of the reinforced concrete beams studied in chapter 5, a different lower bound equation that was specified by MacGregor & Weight (2005) will be adopted for more realistic results. The expression is defined by equation 3:

$$fr = 0.48\sqrt{f'c}$$

Where f'_c and f_r are in MPa.

The load at failure obtained from the experimental procedure was used to calculate the experimental modulus of rupture using equation 4:

$$R = \frac{FL}{bd^2} \qquad \text{Equation 4}$$

Where:

R = Experimental modulus of rupture (in MPA or psi)

F = Maximum applied load indicated by the testing machine (in N or lbs)

L = Span length of the specimen

b = Average width of the specimen (in mm or inch)

d = Average depth of the specimen (in mm or inch)

Table 14. Flexural test results and modulus of rupture calculations

Sample name	Failure load (KN)	R (MPa)	$R_{average}$ (MPa)	F_r (MPa)
C:2-1	16.77	1.94		
C:2-2	17.02	1.97	1.95	
C:2-3	16.83	1.95		3.32
P:1-1	26.05	3.02		
P:1-2	23.72	2.74	2.88	
P:1-3	-	-		

Results of the flexural test of the control samples and the 3D printed samples obtained from four point bending test were plotted and their values are shown in figure 50. The ultimate loads are extracted and used in the calculation of the modulus of rupture in each sample. Table 14 shows a comparison in the moduli of rupture of different tested samples.

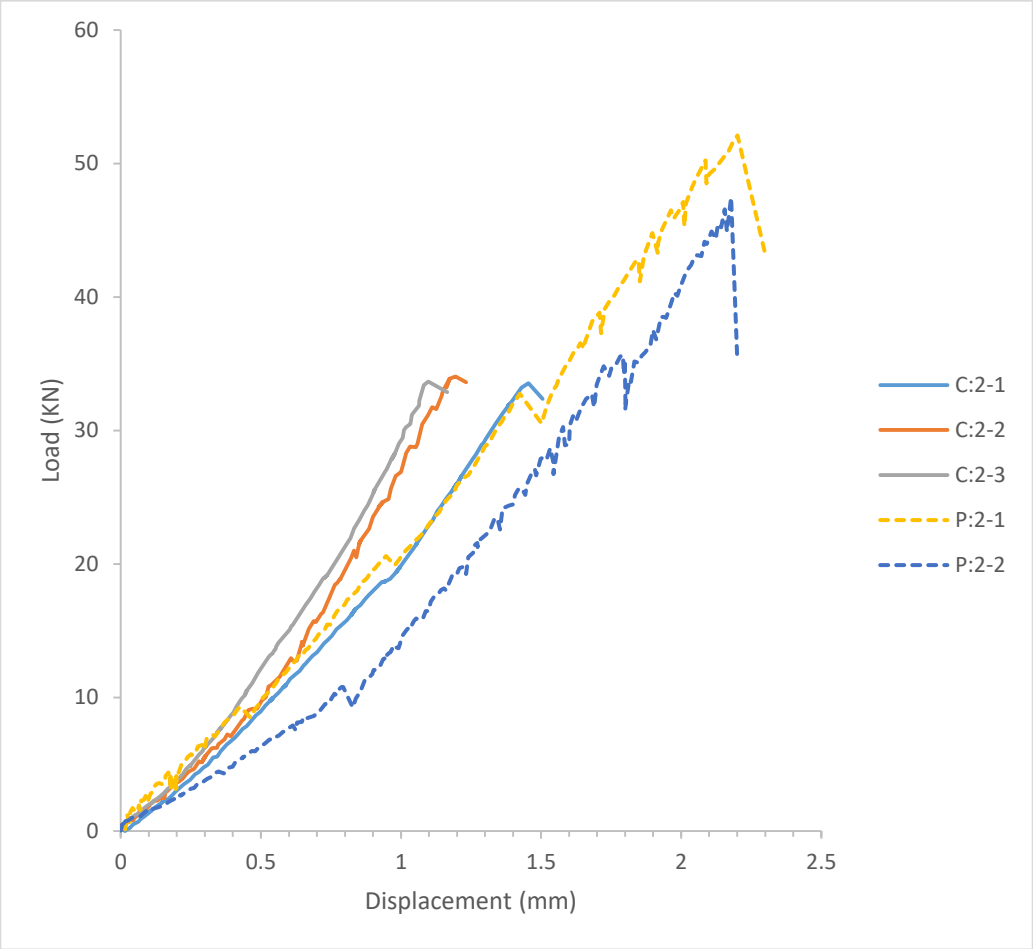

Figure 50. Load deformation curves of 1:2 samples tested for flexure

5.4. Analysis and discussions of phase 2 results:

5.4.1. Compression test results analysis and discussions:

5.4.1.1. Crack pattern and fracture plane:

Compressive tests on the cast and printed samples showed a clear difference in the cracking pattern between the four different sample types.

Cylindrical cast specimen developed an inclined fracture surface, after which a steep decrease in the load carried is witnessed, whereas cubical cast specimen failed gradually by first the spalling of the lateral sides, then crushing of the inner core. Cracking patterns for the cast specimen are shown in figure 51.

Figure 51. Cracking patterns of cast specimens

Crack propagation and fracture planes in 3D printed specimens were shown to be dependent on two factors: the loading direction, and the grout position. Both PH:1 specimens tested showed a similar fracture plane, spalling at the interface crossing the grout on the cube corner. This does not necessarily mean that the grout is a weak point, since in cube specimen, stress is first concentrated on the edges, and when edge spalling occurs, stress is redirected into the middle portion. Fracture plane in PH:1 samples is shown in figure 52.

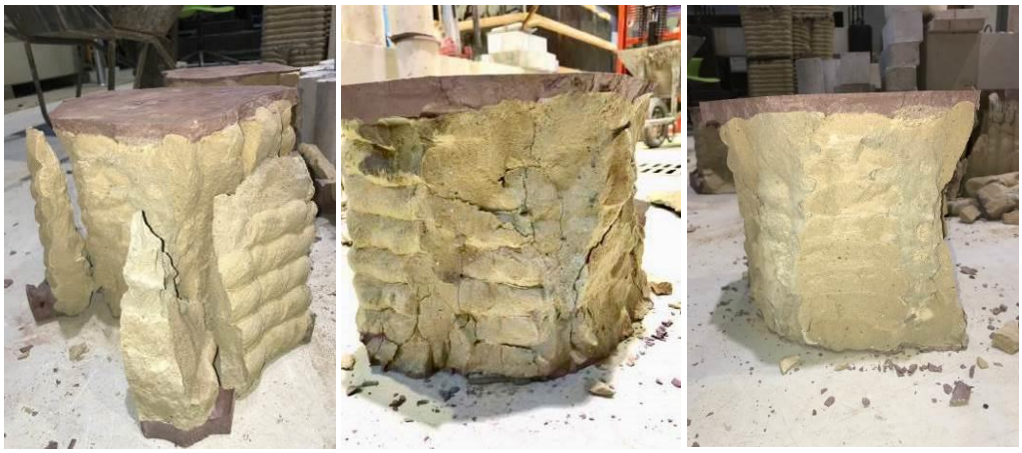

Figure 52. Concrete edge spalling and fracture plane in PH:1 samples

Specimens PV:1 having the loading direction parallel to the print plane showed a rather predictable cracking pattern. Cracks first initiated in the interfaces between 3D printed layers, which lead to their detachment from each other. Layer crushing followed by edge spalling then occurred. The latter is shown in figure 53.

Figure 53. Concrete interlayer fracture and failure in PV:1 samples

5.4.1.2. Compressive strength:

A considerable difference is noticed between the cylindrical specimens of dimensions 150mm x 300mm and the cube specimen of dimensions 240mm x 240mm x 240mm, both tested after 28 days from casting. The former recorder an average of 47.8

MPa while the latter recorder an average of 22.8 MPa. Specimen size and shape affects the compressive strength of concrete as shown in many research papers (Del Viso, Carmona, & Ruiz, 2008; Sim, Yang, Kim, & Choi, 2013; Yi, Yang, & Choi, 2006). Findings in these papers proved that the cube compressive strength is higher than the cylinder compressive strength for any given shape, and that as the size of the specimen increases, the compressive strength decreases. Each of these papers proposed model equations to predict the change in compressive strength as the size and shape of samples vary. However, none of the suggested model equations or results can explain the low ratio of $F_{cube\ (d=240mm)} / F_{cylinder\ (d=150mm,\ h=300mm)} = 0.47$.

A possible explanation for the low value of compressive strength in control specimen is that when the specimen is loaded, stress concentration at the edges would cause spalling of concrete from edges of the specimen, this in turn would decrease the gross area of the specimen. The load that would lead to crushing of the concrete cube then, would be the failure load and the total area minus the area of the spalled concrete would be the effective area at failure load.

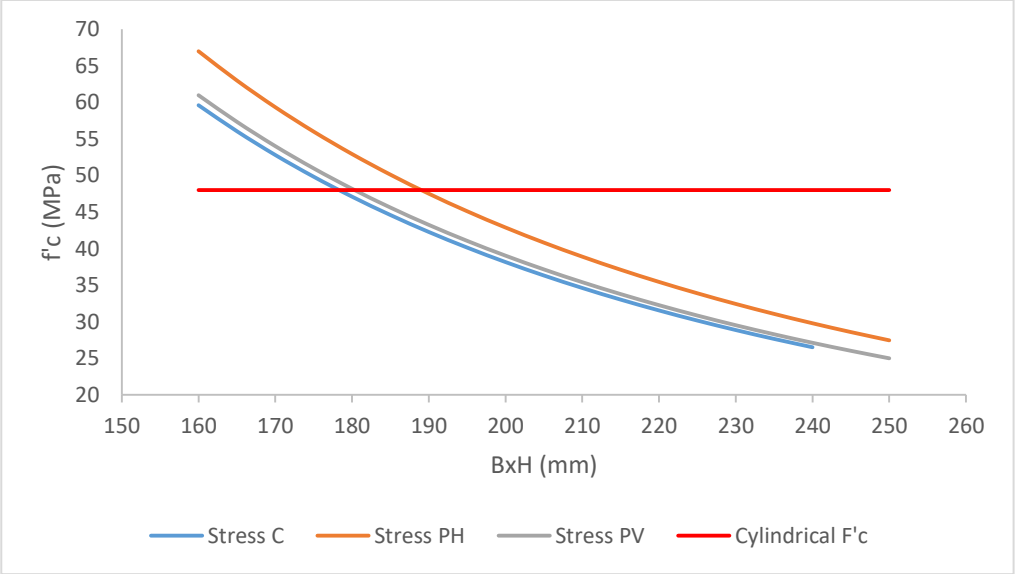

Figure 54. Relationship between compressive strength (MPa) and the specimen gross area

Figure 54 shows the variation between the specimen gross area and the compressive strength. Assuming the area of the specimen remains constant throughout the experiment (no edge spalling), the compressive strength obtained are 26.5 MPa, 27 MPa, and 25 MPa for samples C, PH, and PV simultaneously. However, if edge spalling occurs while loading and the sides are reduced to 180mm, the compressive strength of the specimen would be relatively equal to the compressive strength of the standard cylindrical specimen. Since only the load and displacement were tracked in the experiment, not enough data were recorded to track the exact time and amount of spalling occurring.

Despite this drop, and since our main objective is to compare cast in place cubes with 3D printed cubes, the value of the cylindrical compressive strength will not affect the comparison.

Printed samples PH:1 and PV:1 tested 60 days after casting recorded a compressive strength higher than that of the control samples. This is attributed to the strength gained after 28 days in the printed samples. In order to predict the compressive strength value of the control samples C:1 at 60 days, a calculation model proposed by (AbdElaty, 2014) is used. The relationship between compressive strength at age (t) and the 28 days cylindrical compressive strength is given as following:

$f_t = A \ln(t) + B$

Where:

f_t = compressive strength of concrete at time t (MPa)

t = time at which f'c value is calculated (days)

B = level of strength constant (grade constant)

A = rate of strength gain constant (rate constant)

$B = 0.005(f'_c)^{2.20}$

A = 1.4035 ln (B) + 2.9956

Where:

f'_c = compressive strength of standard cylinder at 28 days (MPa)

The value of $f'c_{t=60}$ equals to 26.46 MPa which is slightly less than the PH:1 samples average value of 27.5MPa (3.9% less) and slightly higher than that of the PV:1 value of 25MPa (5.5%). PH:1 compressive strength values were higher than PV:1 compressive strength values by a total of 9.1% on average. Results of the difference in compressive strength in different samples are shown in figure 55.

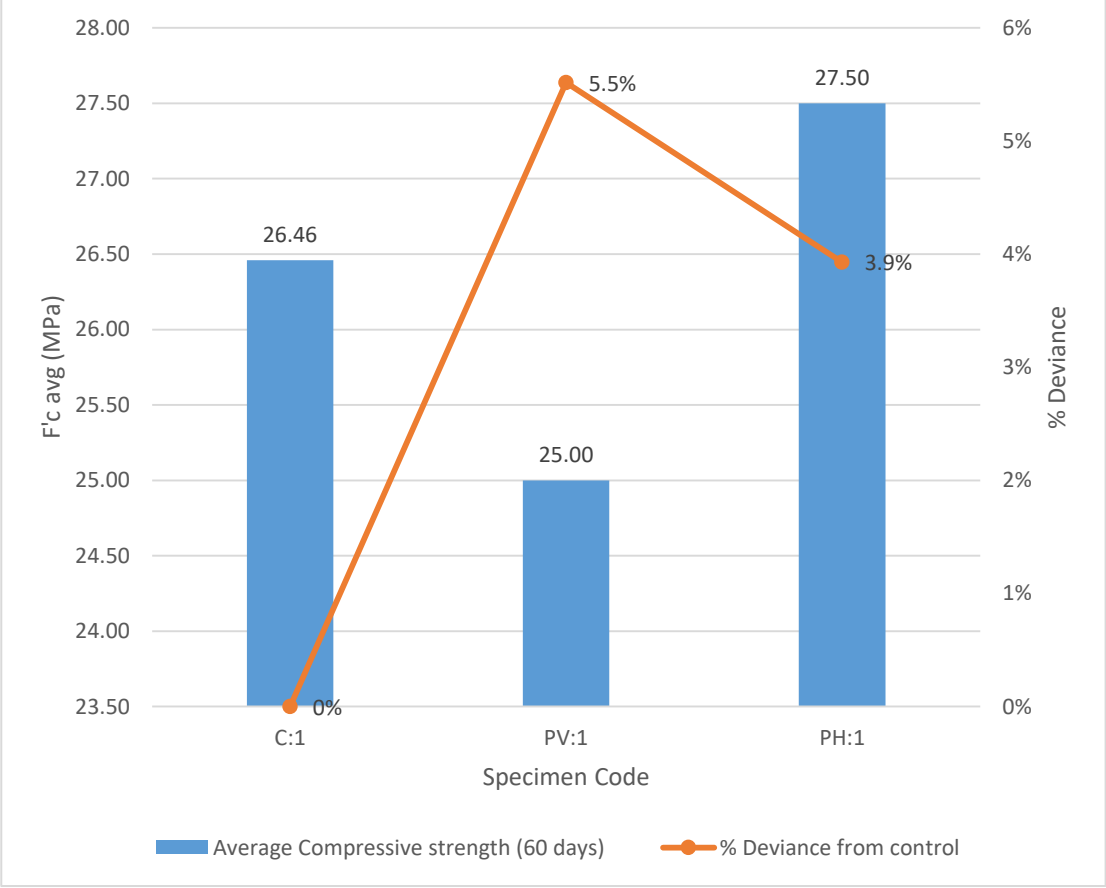

Figure 55. Average compressive strength of different cube specimens

The results obtained are aligned with results of a similar study by (Paul, Tay, Panda, & Tan, 2018) where the compressive strength of 3D printed concrete cube

specimens were either equal or higher than that of the cast specimens. The higher strength in PH:1 specimens may be due to the formation of denser, well compacted concrete filaments extruded with a pressure applied on each adjacent filament when concrete is still in its fresh state, which would help reduce the voids and subsequently, achieve higher strength (figure 56). The slightly lower strength obtained in PV:1 specimens is due to loading in the direction parallel to the filaments plane which caused several simultaneous pre-defined shear failure planes that lead to a sudden drop in strength as soon as the cracks appeared. However, these slight differences are negligible, and it could be concluded that if a specimen is properly 3D printed, only minor differences between cast specimen and 3D printed specimen are obtained.

Figure 56. Difference in void sizes between extruded concrete and regularly mixed concrete

The averaged stress strain curves were plotted for all three sample types to compare the behavior of the 3D printed specimen in different loading schemes with the cast specimens. Figure 57 shows that when the load applied is perpendicular to the printing plane, a linear relationship between stress and strain is shown. The linear graph remains linear until failure occurs. PH:1 samples showed to have the same slope as that of the control specimen. However, control specimen showed a loss of linearity before reaching the peak load, which indicates the initiation of the fracture process. On average, PH:1 samples recorded higher peak failure load than C:1 samples. Comparing the latter

with PV:1 samples, a peak value slightly less than the control was recorded with a linear ramp-up till failure. However, the slope of PV:1 samples, unlike PH:1 samples and C:1 samples showed a shallower slope indicating more ductility before failure. The slope of the obtained stress-strain curve is usually characterized as the modulus of elasticity of the section. This seems to be true for C:1 samples and PH:1 samples where for a concrete compressive strength of 26.46 MPa, the theoretical modulus of elasticity would equal to 24.67 GPa whereas the experimentally calculated value from the stress strain diagram would equal to 22.4 GPa. The experimental slope in PV:1 curve gives a value of 8.61 GPa. An explanation for the difference in the curve slopes is possibly due to the anisotropy in the 3D printed concrete specimen depending on the direction of loading.

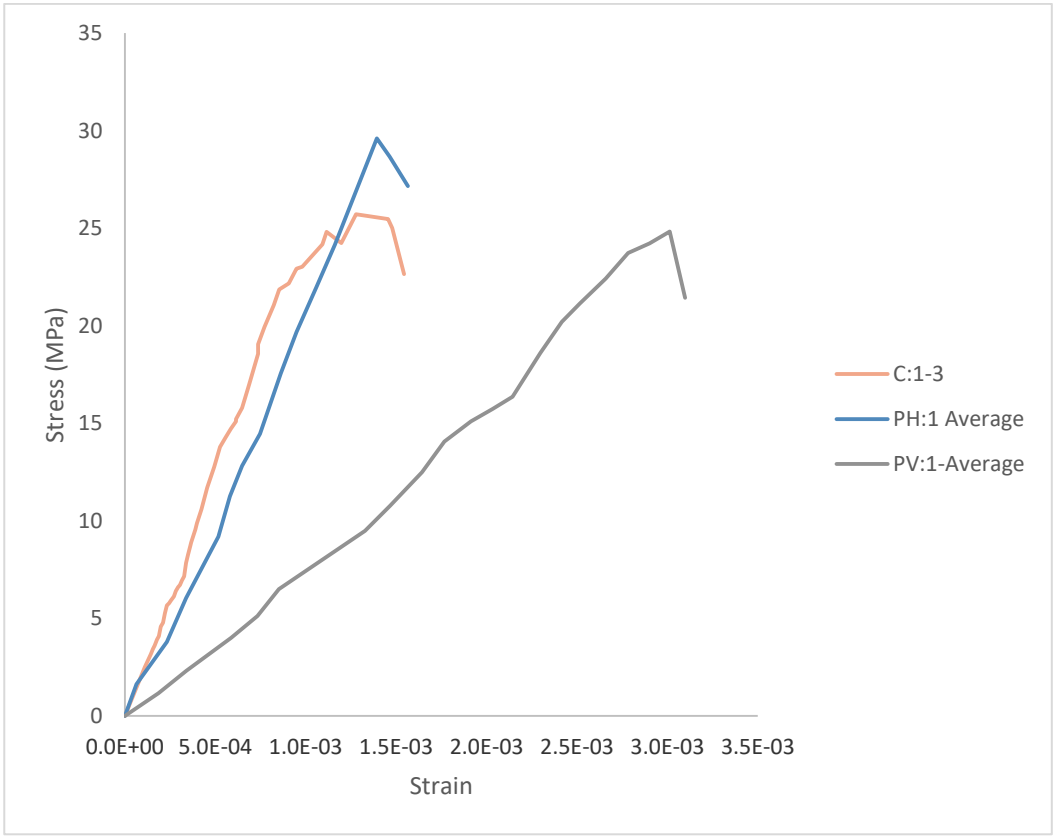

Figure 57. Stress strain curves of specimens tested in compression

5.4.2. Flexural test results analysis and discussions:

The average flexural strength of the control specimen C:2 was 1.95 MPa which is fairly lower than calculated theoretical value of 3.32 MPa. The flexural strength of the 3D printed concrete with tensile load occurring in the direction parallel to filament plane recorded a flexural strength of 2.88 MPa which is 13.2% lower than the theoretical value of the flexural strength and 32.22% higher than the control specimen value. Failure occurred 5cm away from the center of the specimen, initiating at the interface between filaments and within the constant moment region. The failure caused a clear separation between the two overlaying filaments slightly propagating within adjacent planes randomly (figure 58). This shows that the bond between layers is sufficiently developed and that the two interfaces are acting as if they were a homogenous mix since the value of f_r was higher than the control.

Figure 58. Interface separation in P:2 samples due to flexural failure

Although failure occurred in the constant moment middle region in both 3D printed and control specimens, the control specimens failed exactly at mid-span (figure 59), while P:2 samples failed at the second interface after the mid-span interface (figure 60).

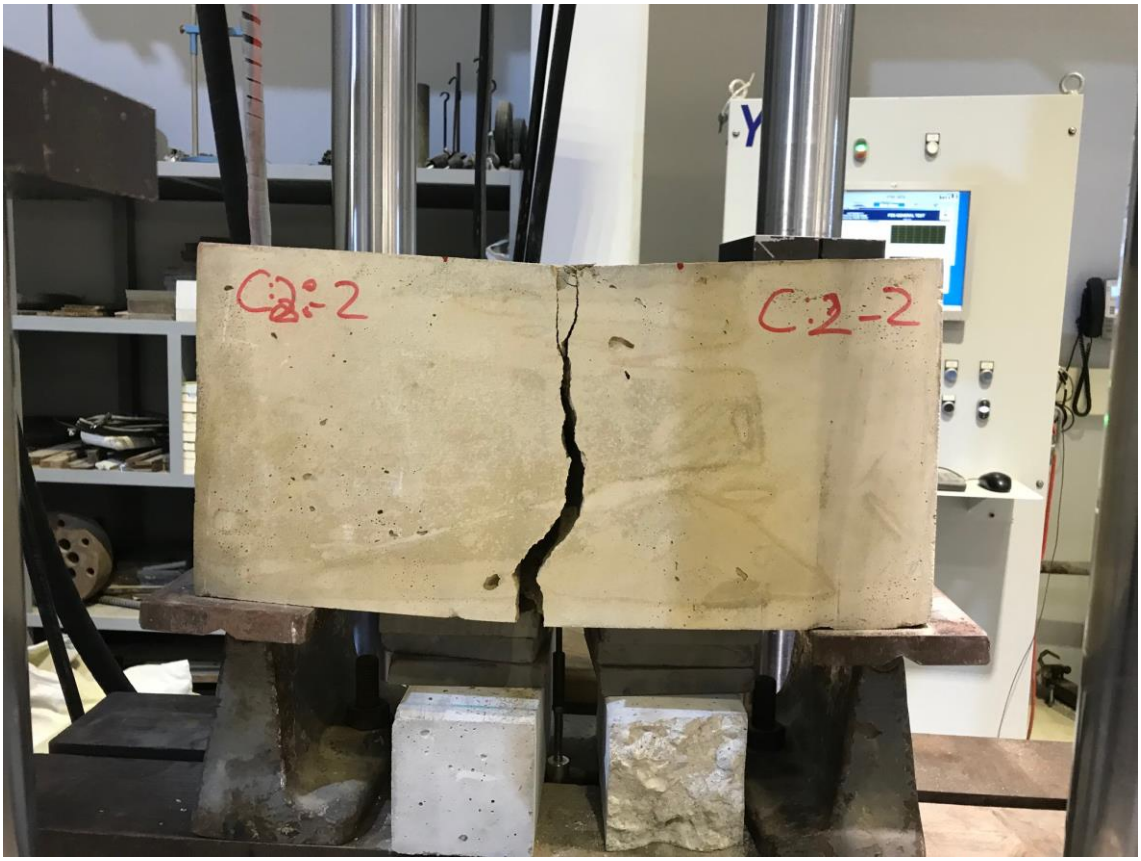

Figure 59. C:2 samples in flexure failure crack

Figure 60. P:2 samples in flexure failure crack

To explain the cause of this behavior, a sketch that illustrates the test setup is shown in figure 61. Control specimens all failed at mid-span where maximum stresses occur. This behavior would've been expected as well in the 3D printed specimen if they were not bonded with epoxy. Due to the higher tensile strength of epoxy, the failure did not occur in epoxy or between concrete and epoxy interface. This shows that the epoxy-concrete bond is well developed. Since moment is presumably constant between the two points loads, flexural stresses are constant in that region. Hence, failure should occur at a random location between layers L_r1, L_r2, and L_r3. However, failure occurred in all specimen at the interface between L_r2 and L_r3. This might be due to two reasons: The increase in bond strength due to the built up stresses from the upper added layers, and the imbalance in loads distribution due to skewing of the load distributing plate.

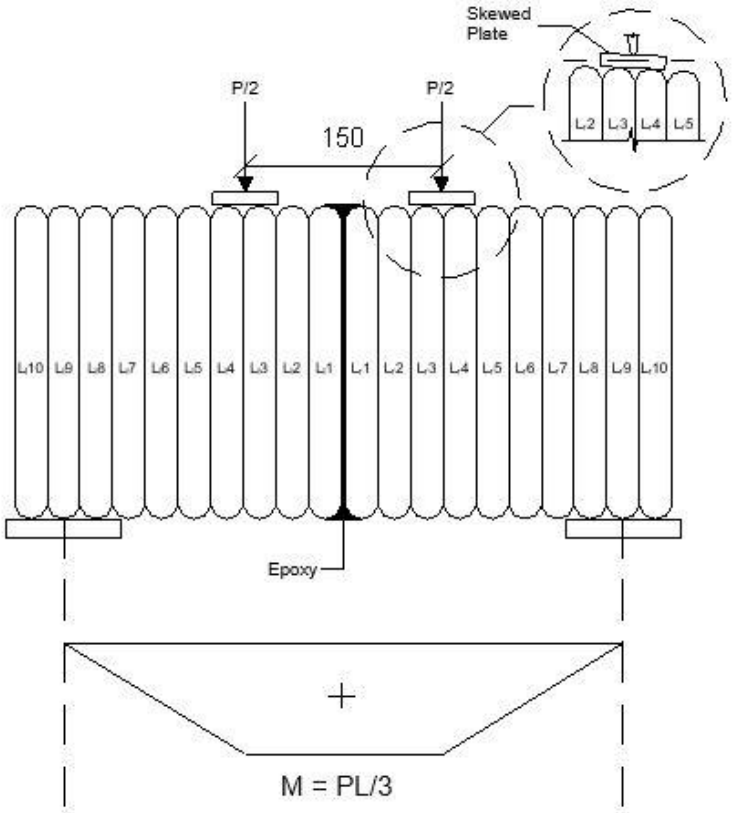

Figure 61. Test setup for P:2 samples

Bond strength is affected by many factors, such as the pressure applied on two overlaying concrete interfaces. With this being a major factor that affects bond strength, it can be said that the bond strength between L_r1 and L_r2 (L_r1-2) is greater than that between L_r2 and L_r3 since the pressure applied at the lower interfaces are subjected to a total pressure from all layers above. Hence $L_r1\text{-}2 > L_r2\text{-}3 > L_rn\text{-}m \ldots > L_rn\text{-}10$. This would explain why, although the moment is constant in that certain section, failure did not occur in L_r1-2.

While 3D printing fresh concrete, each added layer would cause a lateral strain in the subsequent fresh base layer. This strain can be seen as a gradual bulking of the section with its wider dimension being at the bottom and the narrowest being on top. This caused a skew when placing the bearing plate that would distribute the applied load. The skew caused the plate to exert more pressure on the filament with L_r3 which shifted the theoretical moment diagram to the left (figure 61). Hence the interface between filaments L_r3 and L_r4 fell into a region of decreasing moment capacity. This might have caused the failure to shift from L_r3-4 to L_r2-3. In addition, the increase in the section size as the section bulks at bottom layers would mean an increase in the inertia, hence and increase in the flexural capacity as we are nearer to the bottom.

An additional factor that might have affected the flexural strength of the sections P:2 is the effect of epoxy's flexural strength and effective bond area to the total section strength. However, epoxy might have minimal effect due to its relatively small width (ranging between 1mm and 3mm). Figure 61 shows the filament width of the epoxy in a P:2 sample after failure.

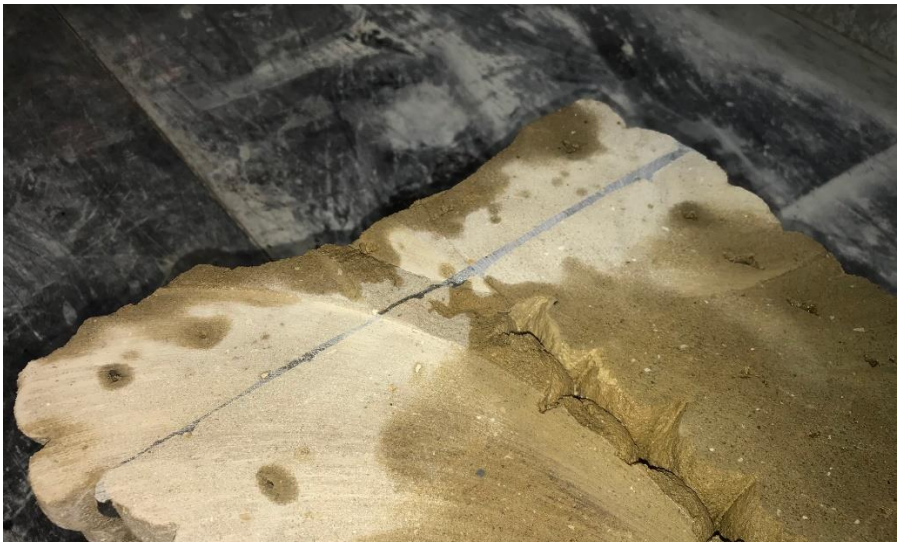

Figure 62. Epoxy layer showing after sawing a P:2 sample

These results however are different from the results obtained by (Le et al., 2012) where flexural loading in the direction perpendicular to the filament plane caused a decrease in the flexural capacity up to 36.3%. This decrease was attributed to the anisotropy resulting from the printing process, which would decrease the interlayer bond adhesion. However and as explained, many factors affect the bond strength and these factors would differ from one study to another.

It should be noted that although the designed section is 240mm x 240mm in cross section, due to the bulking effect, the section might vary from 250mm x 250mm to 240mm x 240 mm depending on the location along height. Hence, calculations performed assuming that the section is a 240mm x 240mm might be slightly inaccurate yet can be ignored.

5.5. Phase 3 Results

5.5.1. Theoretical analysis of the RC beam:

The structural behavior of the control beams were studied using the equations of ACI 318RM-14 code. This was undertaken to predict the failure mode and load before experimental testing. This section presents the procedure followed to find the nominal capacity of the beams used.

Since this is a comparative study, section dimensions, clear cover to reinforcement, and the choice of reinforcement used in the control specimen were mainly governed by values used in the 3D printed specimen. Hence, a sub-ideal configuration of steel, cover requirements and section dimensions are observed.

A four point bending test was adopted in this study to assess the behavior of the reinforced concrete beams. Two points were placed at a distance L/3 from the supports on each side to ensure a constant moment region in the middle. A constant moment in the middle is desired to prevent any possibility of failure at the epoxy interface due to maximum moment only at mid-span (where epoxy interface is).

The hardened properties of concrete and steel were taken from the compressive tests on cylindrical samples and tensile tests on steel bars. The latter were used to calculate the moment and shear capacities of the available reinforced concrete section.

5.5.1.1. Flexural analysis:

An iterative process was used to estimate the depth of the neutral axis by first assuming that the neutral axis is at a distance d’ (distance to center of top steel) from the top face of the compression zone and substituting the assumed value in the equilibrium equation of summation of F_x in the section; the compression force in concrete block should be equal to the tension force in the steel bars at yield. If the equation are not in

equilibrium, the value of the neutral axis is either increased or decreased based on the results. The calculation procedure are shown below.

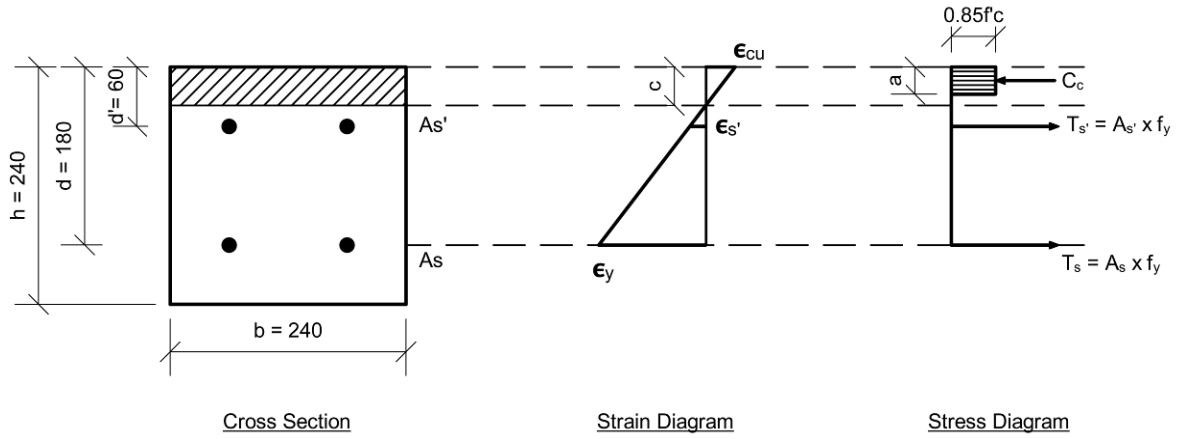

Figure 63. Section analysis using strain and stress diagrams

From strain diagram:

$$\epsilon s' = \left(\frac{d'-c}{c}\right) * \epsilon cu$$

$$\epsilon s = \left(\frac{d-c}{c}\right) * \epsilon cu$$

Where:

ϵs’ = Stain in top steel

ϵs = Strain in bottom steel

ϵcu = ultimate strain in concrete

d’ = distance from the top of the compression zone to the centroid of the top steel (mm)

d = distance from the top of the compression zone to the centroid of the bottom steel (mm)

c = distance from the top of the compression zone to the neutral axis (mm)

From stress diagram:

$\sum Fx = 0 \quad \Rightarrow T_{s'} + T_s = C_c$

$$\Rightarrow A_{s'} \times f_{s'} + A_s \times f_s = 0.85 \times f'_c \times b \times a$$

Where:

$T_{s'}$ = Tension force in top steel (N)

T_s = Tension force in bottom steel (N)

C_c = Compression force in concrete (N)

$A_{s'}$ = Area of top steel (mm^2)

A_s = Area of bottom steel (mm^2)

$f_{s'}$ = Stress in top steel (MPa)

f_s = Stress in bottom steel (MPa)

f'_c = Compressive strength of concrete (MPa)

b = section width (mm)

$a = \beta_1 \times c$

β_1 = stress block depth factor determines based on equation 22.2.2.4.1 in ACI 318-14

c = distance from the top of the compression zone to the neutral axis (mm)

A value of c = 60mm is first assumed, and from which the strains are calculated, then the stresses in the top and bottom steel are determined. Finally, both sides of the equation are calculated; ($T_{s'} + T_s$) & C_c. If the latter are not equal, another value of c is assumed and calculations are iterated again until the values match. When a final value of c is reached, the stresses in top and bottom steel are calculated and the strain value in the concrete compression block is checked. A sample of the following iterations is shown in table 15.

Table 15. Iterations to determine the neutral axis of the beam section

Parameter	Iteration 1	Iteration 2	Iteration 3
	Value	Value	Value
c	60.0	38.0	38.9
a	42.53	26.94	27.6
ϵ's	0.0000	0.0017	0.0016
ϵs	0.0060	0.0112	0.0109
f's	0.0	347.4	325.4
fs	550.0	550.0	550.0
Cc+Cs	414383	262442	268658
T	169246	276138	269393
Decision	DECREASE C	INCREASE C	INCREASE C

When the value of c is determined, and the stresses in steel are known, the moment capacity of the section can be calculated by:

$$\sum Mts = 0 \quad \Rightarrow M_n = C_c \left(d - \frac{a}{2}\right) - T_{s'} (d\text{-}d')$$

$$\Rightarrow M_n = 0.85 \times f'_c \times b \times a \left(d - \frac{a}{2}\right) - A_{s'} \times f_{s'} (d\text{-}d')$$

Where:

M_n = Nominal section flexural capacity (N.mm)

$T_{s'}$ = Tension force in top steel (N)

C_c = Compression force in concrete (N)

$A_{s'}$ = Area of top steel (mm^2)

$f_{s'}$ = Stress in top steel (MPa)

f'_c = Compressive strength of concrete (MPa)

d = distance from the top of the compression zone to the centroid of the bottom steel (mm)

b = section width (mm)

$a = \beta_1 \times c$

β_1 = stress block depth factor determines based on equation 22.2.2.4.1 in ACI 318-14

c = distance from the top of the compression zone to the neutral axis (mm)

From the value of the nominal capacity, the theoretical failure load in flexure can be calculated from equation 5, assuming the loads are placed at L/3 from the supports.

$$P = 3 \times \frac{Mn}{L} \qquad \text{Equation 5}$$

Where:

P = Theoretical failure load (N)

L = Beam length (mm)

M_n = Nominal section flexural capacity (N.mm)

Input parameters to calculate the theoretical flexural capacity of the section and subsequently the theoretical failure load in flexure are listed in table 16.

Table 16. Input parameters used in calculating the nominal moment capacity

Input Parameter	Parameter value
f'_c (MPa)	47.76
F_{yt} (MPa)	550
E_s (MPa)	200000
b_w (mm)	240
d (mm)	180
d'(mm)	60
$A_{s\ bottom}$ (mm^2)	307.72
As'_{top}(mm^2)	307.72
L (mm)	850
L between loads (mm)	287
β1	0.709

The calculated values of the nominal moment and its corresponding failure load are shown in table 17.

Table 17. Theoretical moment capacity and its corresponding failure load

Sample Code	Theoretical M_n (KN.m)	Theoretical P_u (KN)
C:4	32.64	115.19

5.5.1.2. Shear analysis:

ACI 318RM-14 specifies two equations to calculate the maximum shear that can be carried by concrete at a specific section of the beam. The first equation (equation 22.5.5.1) is an approximate equation that is in function of the compressive strength of concrete and the shear resistance factor $\boldsymbol{\lambda}$. The second equation (second equation of table 22.5.5.1) is used in a section subject to an applied moment and shear as a function of concrete compressive strength and the supplied reinforcement ratio.

Approximate shear capacity equation:

$$V_c = \boldsymbol{\lambda} \frac{\sqrt{f'c}}{6} \times b \times d$$

Where:

$\boldsymbol{\lambda}$ = Shear strength resistance factor (Table 19.2.4.2 in ACI 318RM-14)

d = distance from the top of the compression zone to the centroid of the bottom steel (mm)

b = section width (mm)

Exact shear capacity equation:

$$V_c = \boldsymbol{\lambda} \frac{\sqrt{f'c}}{6} \times b \times d + 17 \times A_s$$

Where:

A_s = Area of bottom steel (mm^2)

Maximum shear applied is also resisted by the transverse reinforcement that intersects the failure plane extending from the face of the support at an angle of 45°.

Equation 22.5.10.5.3 in ACI 318RM-14 presents the portion of the shear carried by shear reinforcement. The equation is:

$$Vs = \frac{As \times fy \times d}{S}$$

Where:

S = spacing of stirrups.

In the latter equation, d/s is intended to calculate the number of stirrups crossing a shear plane. Hence, d/s will be substituted by n to give the equation:

$$Vs = As \times Fy \times n$$

Where:

n = number of stirrups crossing the shear plane.

Input parameters to calculate the theoretical shear capacity of the section and subsequently the theoretical failure load in shear are listed in table 18.

Table 18. Input parameters used in calculating the nominal shear capacity

Input Parameter	Parameter Value
f'c (MPa)	47.76
Fyv (MPa)	550
d (mm)	180
Tension As (mm2)	307.72
Shear As (mm2)	100.48
n bars crossing shear plane	1
$\boldsymbol{\lambda}$	0.75

The calculated values of the nominal shear capacity using both the exact and the approximate equations are shown in table 19.

Table 19. Nominal shear capacity values

Sample Code	Parameter	Value (KN)
C:4	V_c approximate equation	37.32
	V_c exact equation	41.06
	V_s	55.26
	V_t approximate equation	92.58
	V_t exact equation	96.32

5.6. Experimental Results:

The loads at ultimate shear failure are listed in table 20 for each of the control and the 3D printed specimen. The load deformation curves for the tested samples are shown in figure 64. The load showing are those read by the MTS machine, whereas the failure load in table 20 is the load read by the machine divided among both load application points. Results from samples P:4-1 were discarded due to an experimental setup error which lead to undesirable results.

Table 20. Ultimate shear failure loads and % deviance from the theoretical values

Sample name	Failure load (KN)	Average failure load/point load (KN)	Theoretical failure load (KN)	$(V_{u\ theo} - V_{u\ exp})/V_{u\ theo}$ (%)
C:4-1	91.05			
C:4-2	107.13	96.28	96.32	0.04%
C:4-3	90.67			
P:4-1	-			
P:4-2	77.83	75.64	-	21.47%
P:4-3	73.45			

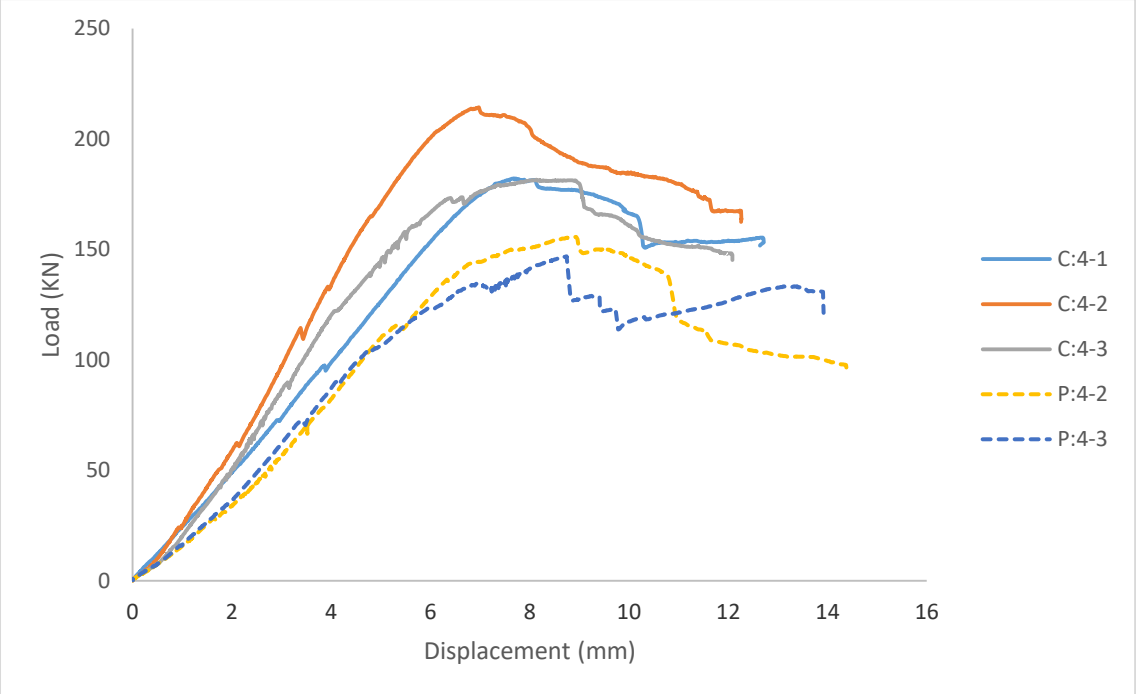

Figure 64. Load deformation curves of C:4 and P:4 specimens

5.7. Analysis and Discussions of Phase 3 Results:

View of the cracked beams of type C:4 are shown in figures 66, 67, and 68 whereas figures 69 and 70 show the crack at the failing support of the 3D printed beams. Test results considering crack appearance in different sections are shown in table 21. The results include the experimental results of the occurrence of the first flexural crack, first diagonal crack, shear failure load, number of cracks, maximum flexural crack width, and maximum shear crack width.

Table 21. View of test results for C:4 and P:4 beams

Specimen Name	C:4-1	C:4-2	C:4-3	P:4-1	P:4-2	P:4-3
P at first flexural crack	10.43	11.46	11.38	-	46.36	44.20
P at first diagonal crack	59.61	52.44	54.6	-	52.21	50.31
P at ultimate shear failure	91.04	107.13	90.67	-	77.83	73.45
Number of cracks	6	7	8	-	6	6
Max flexural crack width	0.2	0.15	0.1	-	0.1	0.1
Max shear crack width	2.4	4.6	2.1	-	3	3

Although the cracking pattern for both C:4 and P:4 samples are similar, the first visible flexural crack occurred at an average load of 11.09 KN in samples C:4 as compared to 45.28 KN in samples P:4. The cracking moment of C:4 samples is 3.14 KN.m which is 58% less than the theoretical value of the cracking moment equal to 7.64 KN.m, while the cracking moment of P:4 samples is 12.82 KN.m which is 40.4% higher than the theoretical cracking moment. Although the results show a big gap between the theoretical and experimental values in flexural strength of the given concrete mix, it is clear that the flexural capacity of 3D printed concrete is better than that of ordinary cast concrete, even when tensile stresses are perpendicular to the plane of filaments. These results are aligned with those of the previous part of the study where plain concrete strength was found to be higher that the normally cast concrete. It should be noted that flexural cracks in the 3D printed samples might have occurred earlier than recorded in

small voids resulting from the circular nature of the nozzle used. However, these cracks were not visible and only the visible crack results were recorded.

The first diagonal crack showed similar results for both cast and printed specimens averaging at 55.5 KN for C:4 specimens and 51.26 KN for P:4 specimens. The difference between the two is comparably small, hence 3D printed and cast specimens might not have any variation in shear strength.

The ultimate failure load in C:4 specimen recorded an average value of 96.28 KN which is aligned to the theoretical value of 96.32 KN calculated previously taking into consideration the concrete strength, the effect of the longitudinal reinforcement and the applied moment on shear resistance, and the capacity given by one T8 stirrup having two legs resisting shear. It should be noted here that a 25% reduction factor was applied when calculating the shear strength of concrete due to the reduction of the aggregate interlock effect as described in table 19.2.4.2 of ACI 318RM-14. The ultimate failure load decreased by a percentage of 21.4% recording an average value of 75.64 KN in P:4 samples. To investigate the causation of this drop in shear strength, a better understanding of the factors that contribute to the overall shear strength of the section is necessary. A study investigating the forces carried across cracks in reinforced concrete beams in shear by interlock of aggregates in 1970 deduced that 25 percent of the shear was transferred by the compression zone, about 25 percent by Dowling effect of flexural reinforcement, and about 50 percent by the aggregate interlock along the cracks (Taylor, 1970). An investigation of the failed specimen did not show any debonding in flexural reinforcement nor premature crushing in the compression zone. Hence, the lost shear strength is attributed to a loss in the aggregate interlock effect. Considering that the shear strength of the section is provided by the cumulative addition of shear flow across the developing

shear plane, a crack that propagates in a direction which its principle axis is parallel to the tension force in the section, would theoretically have zero contribution to the shear strength since the tension force component would be maximum and the compression force would be zero.

A close inspection of the crack propagation revealed that the inclined crack that later caused shear failure was initially propagating at an angle of 45°, then at a given interface between two layers, the crack propagated along the given interface (figure 65). A likely explanation to why the shear propagated along the interface and did not pursue its original path is that the horizontal component of the flowing shear force (component perpendicular to the principle axis) reached a point where the tensile capacity between the interface layers was less than both, the applied force and the shear capacity within the adjacent filament.

Figure 65. Diagonal crack propagating along the interface between two 3D printed filaments

This would conceptually explain the drop in shear strength in P:4 samples. If we were to roughly quantify the effect of this vertical crack along the interface, substituting the depth in which the crack propagated in a diagonal manner ($d_{diagonal}$) with the effect depth (d) in the concrete capacity equation should give an approximate theoretical value as the experimental value. Taking $d_{diagonal}$ equal to 120mm from lab measures gives a total shear capacity value of 78.41 KN, which is close to the experimental value equal to 75.64 KN.

Figure 66. Cracked beam C:4-1

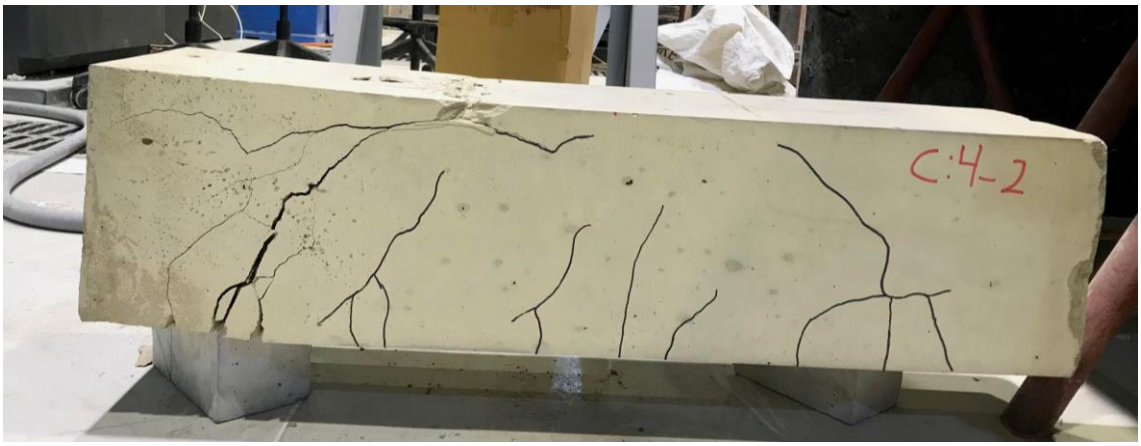

Figure 67. Cracked beam C:4-2

Figure 68. Cracked beam C:4-3

Figure 69. Cracked beam P:4-2

Figure 70. Cracked beam P:4-3

CHAPTER 6

CONCLUSIONS AND RECOMMENDATIONS

Concrete 3D printing promises to automate construction works and is rapidly growing in industrial and academic fields. The new technology offers a solution for problems that have plagued the construction industry in the last decades such as productivity loss, material waste, process inefficiencies, limitations on geometric complexity due to the rigidity of tools used, and low innovation levels. However, this technology is still in its infancy and suffers from many shortcomings itself. Due to the complex nature of the interdependencies within a 3D printing system, research effort has not been able to grasp the whole system yet. Shortcomings are inherent in each individual component of a 3D system whether it is the process used, material properties, technologies used to assemble and operate a 3D printing system, or the structural integrity of the final product. In addition, and since all components are interdependent, several dimensions of complexity are added to the whole picture.

Research efforts have been addressing the uncertainties in both, the individual components and the interdependent components. Some studies focused on the fresh and hard properties of materials used in concrete 3D printing while using different binding materials and admixture content. Others have incorporated fibers into the mix, while some have used sustainable materials. Some studies also explored the effect of different software or hardware on the efficiency and quality of the final product. Frequently, studies of new processes emerge, each time solving an issue inherent in the previous processes. Although seldom found, but slowly emerging as well, studies on procedures to provide structural integrity for the printed concrete elements are surfing up (Abou Yassin,

Hamzeh, & EL Sakka, 2019). However, none of these studies have yet proposed a practical procedure that can make use of robotics to automate the construction of structurally sound reinforced concrete printed elements that are comparably similar to the conventional manufactured elements and that fit to the existing design codes.

Given the inherent deficiencies in the existing system, and the lack of a suitable procedure to reinforce 3D printed concrete, a new procedure is proposed in this study that makes use of a predetermined behavior of fresh material properties to optimized the nozzle speed (process parameter) as the machine prints, to manufacture concrete 3D printed samples that can be reinforced with traditional steel bars. The hardened properties and structural response of the samples is analyzed and compared with traditionally cast samples to validate the viability of the proposed procedure. Results show that the proposed procedure yields plain concrete elements with better compressive and flexural strengths that the normally cast concrete, while then 3D printed RC beams showed a slightly lower shear capacity due to filament orientation.

This chapter summarizes the research methodology developed and highlights the key findings of this study. Recommendations and suggestions for practice and research based on the resulting outcomes of this study are also presented in this chapter, and the contributions are also highlighted. Finally, further plans and ideas for to extend this research are suggested for future research.

6.1. Summary and Conclusions

6.1.1. Summary of the study

6.1.1.1. Summary of methodology

The aim of this study is to contribute to the evolution of the concrete 3D printing industry by proposing a method to manufacture structurally sound 3D printed concrete

elements. The methodology used included three phases. The first phase aimed at providing a clear understanding of the mix behavior with time, as the chemical admixture percentages are varied with the speed of the nozzle. Experimental tests on the 3D printed were carried out to measure the extruded filament width as a measure of workability, and the results were compared to decide which would be an optimum mix depending on the target filament width. From this phase, the effect of the chemical admixtures and the nozzle speed were conceived, and parameters that were used in later phases were selected.

The second phase of the experiment made use of the parameters deduced from the first phase to generate a pre-designed print pattern that would manufacture 3D printed concrete square samples with four voids inside. Voids were filled with grout in this phase but are originally intended to be a pathway for reinforcement insertion as done in the third phase of the experiment. Two aspect ratios were manufactured, 1:1 and 1:2 samples. The former tested for compression and the latter tested for flexure. Both 3D printed samples were compared to regularly cast samples to assess their performance with a control sample.

The third and final phase of the experiment aimed to assess the shear strength of 3D printed beams of aspect ratio 1:4. Four separate 1:1 3D printed samples were joined together with epoxy to form the 1:4 3D printed beams. One reinforcement bar was inserted in each void and grouted to provide the reinforcement layout of the printed beam, while stirrups were inserted between layers when the printer is operating to provide transversal reinforcement that would resist the shear force. Four point bending test was carried out and the results were compared to the regularly cast and reinforced beams.

6.1.1.2. Summary of results

Filament width readings from the first phase of the experimental procedure measured for different mixes shows that, for the same amount of cement and sand used, a superplasticizer percent of 1.55 by weight of cement would be ideal for our set filament width target range. It was also found that starting with a nozzle speed of 116.67mm/sec and decreasing to 100mm/sec after around two minutes would produce best results in terms of filament width consistency.

As for the compressive strength of the printed samples, results showed high degree of similarity between samples loaded perpendicular to the direction of the printing plane (PH), samples loaded parallel to the direction of the printing plane (PV), and between the control samples (C). Cracking in PH and C specimen showed similar patterns, whereas cracking in PV samples was aligned with the filament to filament interface. In addition, both PH and C samples showed a similar modulus of elasticity whereas the modulus of elasticity in PV samples showed much lower values.

Flexural strength in plain concrete elements of aspect ratio 1:2 gave on average higher results from the control samples. The cracking initiated on the interface joining two filaments and not the epoxy that glues two separate samples. Both control and 3D printed samples however recorded results that are lower than the theoretical value of flexural strength for the given compressive strength.

Reinforced concrete 3D printed beams showed a cracking pattern similar to that of the control samples, and failure modes were as expected. Both control and 3D printed beams failed in shear. However, the ultimate shear capacity of the 3D printed beams is around 22% lower than that of the control samples. The value at which the first flexural

crack appeared 3D printed samples was almost four times higher than that of the regularly cast samples. Finally, both 3D printed and control samples showed a similar ductility.

6.2. Key Findings of the study:

6.2.1. Structural integrity of 3D printed concrete

In alignment to other research studies, it was found that the compressive strength of 3D printed elements would yield higher or similar results to the regularly cast samples if correctly executed. This is mainly attributed to the denser concrete mix obtained when hose pumping and pressure placing filaments on top of each other with a low void ratio and with minimal gap time between two consecutive horizontal or vertical layers.

In contrary to several research studies, the flexural strength of 3D printed concrete samples recorded a higher values than regularly cast concrete samples when loaded in the direction causing tension perpendicular to the interface between two layers. This is attributed to two factors which are the exerted pressure when adding a new filament on top of an old filament, and the dense structure of the concrete mix due to the extrusion process.

The proposed method proved to be an efficient way, from a structural engineer's point of view, to manufacture reinforced concrete framing elements. This study investigated the shear behavior of reinforced concrete 3D printed beams and it showed results that are comparably similar to the regularly cast beams with a drop of 20% in shear capacity of the studied beam section. This percentage would be even lower if a longer beam with a denser stirrup distribution is used. Either ways, it is shown that when designing for shear in 3D printed reinforced concrete beams, the possibility of losing strength due to a failure in the filament interface should be taken into account, which would necessitate a reduction in the section's concrete shear capacity.

6.2.2. Answer to research questions

This section summarizes the answers to the posed research questions stated in chapter three of this report.

Q1: How much superplasticizer and retarder should be used to ensure a printable, workable and buildable concrete mix?

A1: If using Viscocrete 20HE as a high range water reducer, a value of 1.55% and above is found to ensure the minimum workability required to print a sample with filament widths of 4cm. an added dosage of retarder would further increase the filament width. Sika Retarder, which has no super-plasticizing effect would slightly increase the workability of the mix but would more importantly maintain this workability as time passes by. A dosage of 0.2% is found to have a suitable retarding effect. However, adding retarder would negatively affect buildability.

Q2: What are the ideal speed and nozzle offset to ensure a uniformly printed filament?

A2: Nozzle speed values of 100mm/sec and 116.67mm./sec were found to be ideal depending on the workability of the mix. As the mix loses workability, a lower speed is recommended. As for the nozzle offset, both values of 3cm and 2.5cm were found to be ideal. However, using a 2.5cm offset would reduce the risk of filament distortion at higher level layers and might yield a better bond between filaments.

Q3: Will the 3D printed concrete samples have the same axial and flexural strength as the normally cast samples?

A3: 3D printed samples loaded in the direction perpendicular to the printing plane showed a slightly higher compressive strength whereas those loaded in the direction parallel to the printing plane showed a slightly lower compressive strength. However,

samples tested for flexure and loaded in the weakest direction, with flexure causing tension perpendicular to the printing plane showed higher flexural strengths than the regularly cast specimen.

Q4: How will the shear capacity and failure mode of the 3D printed beams with rebar and grout be affected if compared to regularly cast beams with regular reinforcement?

A4: The response of the 3D printed and the regularly cast concrete beams showed similar results in terms of ductility and crack initiation. However, crack propagation through the interfaces between the printed layers caused a drop in the concrete shear capacity leading to a total drop in the shear capacity of the designed section.

6.3. Contributions and Recommendations:

From this study, a systematic experimental methodology to manufacture 3D printed concrete elements at the laboratory of the AUB is derived. Detailed steps for executing a concrete 3D printed job are described in the methodology chapter. After which, process and material parameters that would give results suitable for printing were deduced from a set of trial mixes with different variables.

A firm understanding of the experimental procedure and the mix behavior paved the way for manufacturing voided 3D printed cubical samples. With voids grouted, samples had their compressive and flexural strengths evaluated and a better understanding of their mechanical properties is achieved. This manufacturing procedure could be extended in use to manufacture reinforced concrete beams and columns by inserting steel bars inside voids and grouting. An experimental analysis proved the viability of the proposed procedure in providing structural integrity for 3D printed concrete elements.

From the limitations described in the methodology, and from the results obtained, several recommendations are suggested to further enhance concrete 3D printing system at the American university of Beirut. Recommendations are listed below:

1. A machine that would continuously feed ready mixed concrete into the mixer-pump drum would enable the delivery of fresh concrete in larger capacities, then the drum size would not be a limitation and more print volume can be achieved.

2. With the ongoing collaboration between the mechanical engineering and the civil engineering department, research on the best size and shape for the printing nozzle should be carried out for better mechanical properties of the printed samples.

3. Investment in a nozzle blocking mechanism would give more flexibility in designing the g-code and subsequently the intended print patterns.

4. Using the Sika Superplasticizer 10 would probably lead to a slower drop in the mix workability, hence reducing variability. Yet further research is needed to assess its accurate dosage.

5. Testing procedures need to be enhanced to take into account the imperfections in the 3D printed surfaces.

6. Densely distributed stirrups in the location of the diagonal shear crack are recommended to accommodate for the loss in the strength due to crack slipping into the interface plane.

6.4. Future Research

In addition to the direct contributions listed above, this study can be seen as the foundation stone for further research on this expanding topics. The methodology and results can be expanded and extended to study a plethora of topic, some of which are listed below:

1. Using the same methods adopted in this study, concrete columns of different aspect ratios can be constructed and tested for different loading schemes. Studies can start by investigating the structural response of columns loaded in pure compression, then expand to eccentrically loaded columns and laterally loaded columns.

2. Although the shear behavior in beams has been studied, further research is needed to better understand the behavior of 3D printed RC beams for different depth to span ratios in shear and flexure, with different reinforcement detailing layouts.

3. Due to the voided design of the 3D printed design, it is possible to study the behavior of post-tensioned RC beams and columns as well.

4. The bond strength between grout and 3D printed concrete and between grout and rebar should be studied to understand its effect on the different failure modes.

5. The effect of print path design on the mechanical properties of 3D printed concrete elements could be assessed. A better understanding of the in-plane filament distribution will decide on many important parameters especially the nozzle diameter.

6. To reduce the experimental effort exerted in understanding the wide spectrum of possible behaviors of 3D printed concrete elements, an understanding of the fresh and hard material properties must be developed to use as input in finite element analysis models. The models can predict numerically the behavior of 3D printed concrete, and lab tests would be used to verify the thoroughly simulated models. Numerical models can be developed for studying the fresh properties of concrete and the accumulating stresses of bottom layers to predict the collapse load using either a drucker-prager cap model a mohr circle material model. Hardened properties of 3D printed concrete such as the inter-layer bond adhesion using linear and nonlinear cohesive zone modeling.

7. A more in-depth research into a wide range of binder and sand types and ratios constituting a 3D printing mix should be done. The mix design should target both the fresh and hard properties of concrete such as buildability and bond strength.

8. A study of the nozzle offset on the bond strength would provide data on the optimum nozzle offset for a desired filament width and a strength bond between layers.

9. Hose length effect on the structure of fresh concrete ought to be studied, since 3D printed concrete proved to be more compacted due to the extrusion process. An optimum length and material could be decided upon based on the friction of the inner surface of the hose.

10. Further studies are required to figure out a way to assemble an entire structure using the proposed methodology. When this idea comes to age, the current method will evolve to a new more refined method that would further automate the printing process.

11. Construction process simulations could be performed to study the on-site and off-site applicability of the proposed procedure. Data related to time and cost of implementation and comparison with traditional, precast and modular construction would validate the applicability of the procedure.

12. Interdependencies between all components of the 3D printing system are hard to grasp (figure 71 and figure 72). Big data and machine learning could be used, when enough data is available, to build a decision making platform that would provide the best process and system parameters for the intended target.

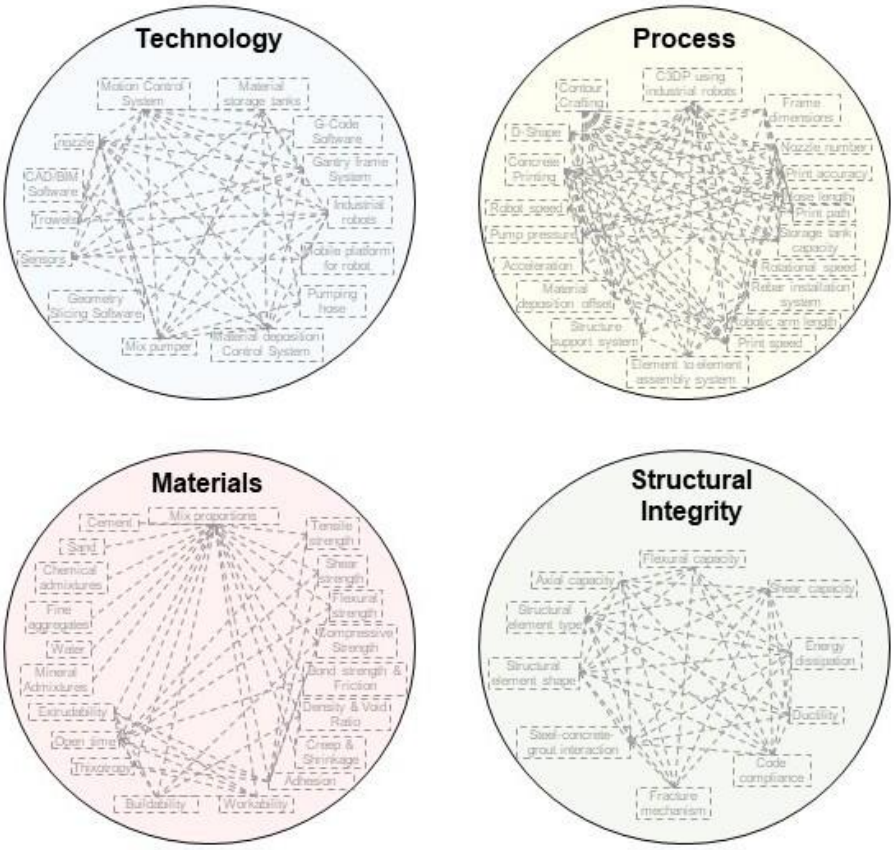

Figure 71. Interdependencies of parameters within each 3D printing component

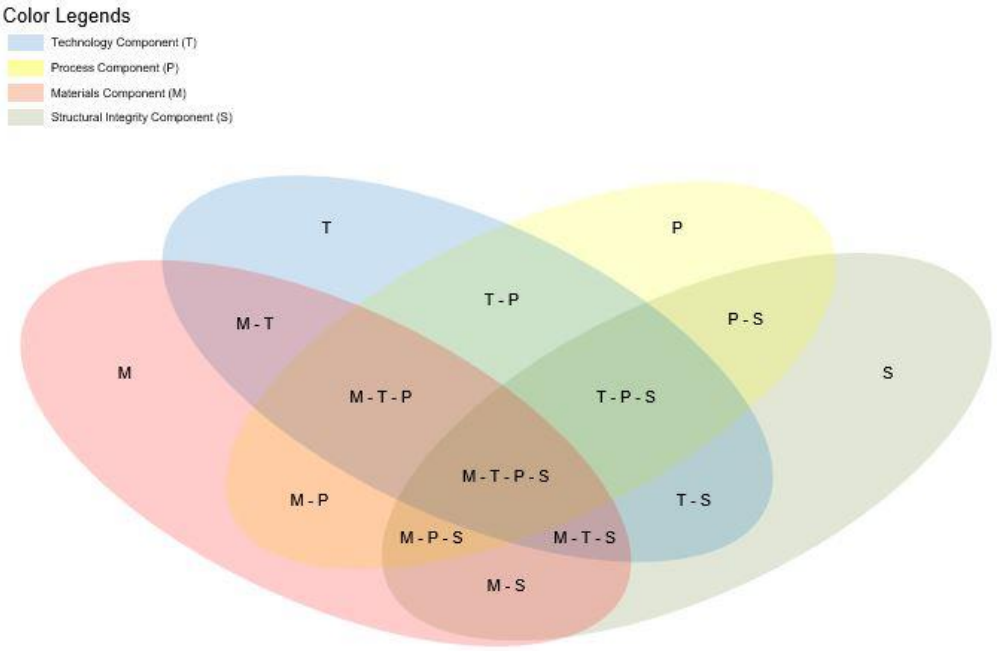

Figure 72. Four-circles Venn diagram showing the interdependence between different components of a 3D printing system

APPENDIX A

Construction

Sika® ViscoCrete®-20 HE

High Performance Superplasticizer

Product Description	**Sika® ViscoCrete®-20 HE** is a third generation superplasticizer for concrete and mortar. The product is suitable for tropical and hot climatic conditions
Uses	**Sika® ViscoCrete®-20 HE** is especially suitable for the production of concrete mixes which require high early strength development, powerful water reduction and excellent flowability. **Sika® ViscoCrete®-20 HE** is mainly used for the following applications: ▪ Pre-cast concrete ▪ Fast track concrete ▪ In situ concrete requiring fast stripping time ▪ Self-Compacting Concrete (SCC)
Advantages	**Sika® ViscoCrete®-20 HE** as a powerful superplasticizer acts by different mechanisms. Through surface adsorption and sterical effects separating the binder particles the following properties are achieved: ▪ Pronounced increase in the early strength development, resulting in very economic stripping times for pre-cast and in situ concrete ▪ Extremely powerful water reduction, resulting in high density, high strengths and reduced water permeability etc. ▪ Excellent plasticizing effect, resulting in improved flowability, placing and compacting behavior ▪ Reduced energy cost for steam cured pre-cast elements ▪ Especially suitable for the production of Self-Compacting Concrete (SCC) ▪ Improved shrinkage and creep behavior ▪ Reduced closure times for repairs of roads and runways **Sika® ViscoCrete®-20 HE** does not contain chlorides or other ingredients which promote the corrosion of steel reinforcement. It is therefore suitable for reinforced and pre-stressed steel.

Tests

Approval / Standards	**Sika® ViscoCrete®-20 HE** complies with the requirements for superplasticisers according to ASTM C494-86; SIA 262 (2003) and EN 934-2.

Product Data

Form	Liquid
Appearance / Colour	Light brownish, clear to slightly cloudy
Packaging	1000 lt. flow bins

Storage

Storage Conditions	Store in a dry area between 5ºC and 35ºC. Protect from direct sunlight and frost.
Shelf Life	12 months minimum from date of production if stored properly in original unopened packaging.

Technical Data

Chemical Base	Aqueous solution of modified polycarboxylates
Density (at 25°C)	Approximately 1.08 kg/lt
pH value	Approximately 4.3
Chloride content	Nil (EN 934-2)
Effect on setting	Non-retarding
Effect of overdosing	Bleeding may occur

Application Details

Dosage	Recommended dosage: ▪ For medium workability: 0.2-0.8% by weight of cement ▪ For concrete of high workability, very low water/cement ratio and for Self Compacting Concrete: 1.0 – 2.0% by weight of cement. It is advisable to carry out trial mixes to establish the correct dosage.
Compatibility	**Sika® ViscoCrete®-20 HE** may by combined with the following Sika Products among others: ▪ SikaPump® ▪ Sika® Ferrogard®-901 ▪ Sika® Fume ▪ SikaRapid® ▪ Sika Retarder® and Sika® Retardol 25 Pre-trials are always recommended before combining products. Please consult our Technical Services Department for further advice and information.
Dispensing	**Sika® ViscoCrete®-20 HE** is added to the gauging water or added with it into the concrete mixer. For optimum utilization of the high water reduction property we recommend thorough mixing at a minimal wet mixing time of 60 seconds.
Concrete Placing	The standard rules of good concreting practice, concerning production as well as placing, are to be followed. Refer to relevant standards.
Curing	Fresh concrete must be cured properly, especially at high temperatures in order to prevent plastic and drying shrinkage. Use Sika Antisol® products as a curing agent or apply wet hessian.
Cleaning	Clean all equipment and tools with water immediately after use.
Notes on Application/Limitations	When accidental overdosing occurs (within reason), apart from retardation of the initial set and increased bleeding, no detrimental effect will take place. When using **Sika® ViscoCrete®-20 HE** to produce Self-Compacting Concrete, a suitable mix design must be selected and local material sources should be trialled. Before pouring, suitability tests on the fresh concrete must be carried out.

Value Base	All technical data stated in this Product Data Sheet are based on laboratory tests. Actual measured data may vary due to circumstances beyond our control.
Local Restrictions	Please note that as a result of specific local regulations the performance of this product may vary from country to country. Please consult the local Product Data Sheet for the exact description of the product uses.
Health and Safety Information	For information and advice on the safe handling, storage and disposal of chemical products, users shall refer to the most recent Material Safety Data Sheet containing physical, ecological, toxicological and other safety related data.
Legal Notes	The information, and, in particular, the recommendations relating to the application and end-use of Sika products, are given in good faith based on Sika's current knowledge and experience of the products when properly stored, handled and applied under normal conditions in accordance with Sika's recommendations. In practice, the differences in materials, substrates and actual site conditions are such that no warranty in respect of merchantability or of fitness for a particular purpose, nor any liability arising out of any legal relationship whatsoever, can be inferred either from this information, or from any written recommendations, or from any other advice offered. The user of the product must test the product's suitability for the intended application and purpose. Sika reserves the right to change the properties of its products. The proprietary rights of third parties must be observed. All orders are accepted subject to our current terms of sale and delivery. Users must always refer to the most recent issue of the local Product Data Sheet for the product concerned, copies of which will be supplied on request.

All products are manufactured under a management system certified to conform to the requirements of the quality, environmental and occupational health & safety standards ISO 9001, ISO 14001 and OHSAS 18001.

Sika Pakistan (Pvt) Limited
141-CCA, Phase IV, DHA
Lahore
Pakistan
Phone: +92 42 35694266/7
Fax: +92 42 35694268
information@pk.sika.com
www.pak.sika.com

APPENDIX B

Construction

Sika® Retarder

Set-retarding concrete admixture

Product Description	Sika® Retarder is a highly efficient set-retarding admixture for structural and mass concrete where a controlled extension of setting time is required.
Uses	■ Large volume pours ■ Avoidance of cold joints ■ Construction joints without formwork ■ Long hauls ■ Difficult placing conditions ■ Elevated temperatures ■ Revibrated concrete
Characteristics / Advantages	■ Controlled setting time ■ Chloride free – does not attack reinforcement
Tests	
Approval / Standards	Complies with ASTM C 494-81 type B

Product Data

Form		
Appearance / Colours	liquid	Yellowish
Packaging	25 Litre and 200 Litre containers	
Storage		
Storage Conditions / Shelf Life	12 months from date of production if stored properly in undamaged containers, in dry conditions at temperatures between +5°C and +30°C. Protect from direct sunlight and frost.	

Technical Data

Chemical Base	Modified Phosphates
Density	Specific density, ±1.14 (at +25°C)
pH Value	±8.00

System Information

Application Details

Dosage	0.2 – 2.0% by weight of cement. The retardation rate achieved is directly dependant on the dosage rate which in turn is influenced by quality of cement and aggregates, water: cement ratio and temperatures. In many cases it is advisable to carry out trial mixes to establish the exact dosage rate required.

Application Conditions / Limitations

Compatibility	Sika® Retarder is compatible with all types of Portland Cement including S.R.C.

Application Instructions

Dispensing	Sika® Retarder should be added with the mixing water or introduced at the end of the mixing process.
Application Method / Tools	The standard rules of good concreting practice, concerning production as well as placing, are to be followed. Fresh concrete must be cured properly.
Cleaning of Tools	Sika® Retarder must NOT be used with anti-freeze agents
Notes on Application / Limitations	Clean all tools and application equipment with fresh water immediately after use.
Notes	All technical data stated in this Product Data Sheet are based on laboratory tests. Actual measured data may vary due to circumstances beyond our control.
Local Restrictions	Please note that as a result of specific local regulations the performance of this product may vary from country to country. Please consult the local Product Data Sheet for the exact description of the application fields.

Health and Safety Information

Protective Measures	To avoid rare allergic reactions, wear protective gloves. Change soiled work clothes and wash hands before eating and after finishing work. Local regulations as well as Health and Safety advice on packaging labels must be observed.
Ecology	
Transportation Class	

Important Notes	Uncured of material must be removed according to local regulations. Fully cured material can be disposed of as household waste under agreement with the responsible local authorities. Detailed health and safety information as well as detailed precautionary measures e.g. physical, toxicological and ecological data can be obtained from the Safety Data Sheet.
Toxicity	
Legal Notes	The information, and, in particular, the recommendations relating to the application and end-use of Sika® products, are given in good faith based on Sika's current knowledge and experience of the products when properly stored, handled and applied under normal conditions. In practice, the differences in materials, substrates and actual site conditions are such that no warranty in respect of merchantability or of fitness for a particular purpose, nor any liability arising out of any legal relationship whatsoever, can be inferred either from this information, or from any written recommendations, or from any other advice offered. The proprietary rights of third parties must be observed. All orders are accepted subject to our current terms of sale and delivery. Users should always refer to the most recent issue of the Product Data Sheet for the product concerned, copies of which will be supplied on request or access on the internet under www.sika.co.za.

Construction

Sika South Africa (Pty) Ltd
9 Hocking Place,
Westmead, 3608
South Africa

E-mail: headoffice@za.sika.com
Phone +27 31 792 6500
Telefax +27 31 700 1760
www.sika.co.za

APPENDIX C

TITLE NO. 75-46

Proposed ACI Standard 503.1: Standard Specification for Bonding Hardened Concrete, Steel, Wood, Brick, and Other Materials to Hardened Concrete with a Multi-Component Epoxy Adhesive

Reported by ACI Committee 503

R. W. GAUL
Chairman

GEORGE SELDEN
Secretary

RUSSELL H. BRINK
GEORGE HORECZKO
HAROLD C. KLASSEN
JOSEPH A. McELROY
LEONARD J. MITCHELL
MYLES A. MURRAY
LEONARD PEPPER
G. M. SCALES
RAYMOND J. SCHUTZ
GEORGE W. WHITESIDES

This specification describes the work of bonding hardened concrete, steel, wood, brick, and other materials to hardened concrete with a multi-component epoxy adhesive such as defined for this purpose in ASTM C 881. It includes controls for adhesive labeling, storage, handling, mixing and application, surface evaluation and preparation, as well as inspection and quality control.

Keywords: adhesives; aluminum; bond (concrete to concrete); bonding; bricks; concrete construction; copper; epoxy resins; hardened concrete; quality control; safety; specifications; standards; steels; wood.

FOREWORD

This foreword is included for explanatory purposes only; it does not form a part of Standard Specification ACI 503.1.

This specification is a reference standard which the architect/engineer may cite in the project specifications, together with the supplemental requirements for the specific project. It is written in terse, imperative language, and is divided into two sections: general requirements and materials and applications, including a section on the all-important surface preparation.

This document covers materials and methods for bonding concrete, steel, wood, brick, aluminum, copper, and other materials to hardened concrete.

This specification is written in the section and three-part format of the Construction Specifications Institute, but with the numbering system modified to ACI requirements.

A specification guide and checklist are included as a preface to, but not forming a part of, Standard Specification ACI 503.1. The purpose of this guide and checklist is to assist the Architect/Engineers' designer(s) and specifier(s) to properly choose and specify the necessary supplementary requirements for the project specification(s).

Offered as a standard of the American Concrete Institute in accordance with the Institute's standardization procedure. Approved for discussion by the membership; discussion closes Dec. 1, 1978.

CONTENTS

SPECIFICATION GUIDE

SG1—Standard Specification ACI 503.1 is intended to be used essentially in its entirety, by citation in the project specification, to cover all usual requirements for bonding hardened concrete, steel, wood, brick, and other materials to hardened concrete with a multi-component epoxy adhesive. Individual sections, parts, or articles should not be copied into project specifications since taking them out of context may change their meanings.

SG2—However, adjustments to the needs of a particular project shall be made by the Architect/Engineer's designers and specifiers by reviewing each of the items indicated in this specification guide and checklist and then including their decisions on each as mandatory requirements in the project specification.

SG3—These mandatory requirements shall designate specific qualities, procedures, materials, and performance criteria for which alternatives are permitted or for which provision is not made in Standard Specification ACI 503.1. Or exceptions shall be taken to Standard Specification ACI 503.1 if required.

SG4—A statement such as the following will serve to make Standard Specification ACI 503.1 an official part of the contract requirements:

> The use of an epoxy adhesive for bonding hardened concrete, steel, wood, brick, and other materials to hardened concrete shall conform to all requirements of "Standard Specification for Bonding Hardened Concrete, Steel, Wood, Brick, and Other Materials to Hardened Concrete with a Multi-Component Epoxy Adhesive (ACI 503.1-79)," published by the American Concrete Institute, Detroit, Mich., except as modified by the requirements of this project specification.

SG5—The specification checklist that follows is addressed to each item of ACI 503.1 that requires the designer/specifier to make a choice where alternates are indicated, or to add provisions where they are not indicated in ACI 503.1, or to take exceptions to ACI 503.1. The checklist consists of one column identifying sections, parts, and articles of ACI 503.1, and a second column of notes to the designers/specifiers to indicate the action required of them.

SPECIFICATION CHECKLIST

Section/Part/Article of ACI 503.1	Notes to the Designer/Specifier
Section 1—General requirements	
1.1 Scope	Indicate specific scope.
1.4 Reference standards	Review applicability of cited references and take exceptions if required.
Section 2—Materials and application	
Part 2.1—General	
2.1.2 Submittals	To whom sent?
2.1.3.2 Application control	To whom sent?
2.1.5 Project conditions	Specify any which would specifically affect this work.
Part 2.2—Products	
2.2.1 Epoxy adhesive	Specify Class and Grade as indicated. Also specify additional performance requirements and/or approved suppliers, as advisable.
Part 2.3—Execution	
2.3.1 Preparation of concrete surfaces	Specify limitations, if any, on use of mechanical abrasion or acid etching, and on disposal of waste products, especially acid waste. Also check if hydrochloric acid use may damage stainless steel or other materials; if so, specify phosphoric, sulfamic, or other non-injurious acids or suitable etchants.
2.3.2 Preparation of carbon steel surfaces	If sand abrasive not suitable, specify grit or shot.
2.3.6.2 Moisture content of wood	A commercially available "probe" type moisture meter should be used except for plywood which will require a "flat plate" type with a depth of field suitable for plywood. For a durable adhesive bond to wood the wood should be sealed on all exposed sides to reduce absorption of moisture which will swell the wood and stress (to rupture) the wood fibers which are restrained by the cured adhesive.

SECTION 1—GENERAL REQUIREMENTS

1.1—Scope

1.1.1—This standard specification covers the bonding of hardened concrete, steel, wood, brick, and other materials to hardened concrete with a multi-component epoxy adhesive.

1.1.2—The provisions of this standard specification shall govern unless otherwise specified in the contract documents. In case of conflicting requirements, the contract documents shall govern.

1.2—Notation

1.2.1—ACI: American Concrete Institute
P. O. Box 19150
Detroit, Mich. 48219

1.2.2—ASTM: American Society for Testing and Materials
1916 Race Street
Philadelphia, Pa. 19103

1.2.3—SSPC: Steel Structures Painting Council
4400 Fifth Avenue
Pittsburgh, Pa. 15213

1.3—Specification wording

1.3.1—The language of this standard specification is generally imperative and terse, and may include incomplete sentences. Omissions of phrases and of words such as "the contractor shall," "in accordance with," "shall be," "as indicated," "a," "an," "the," "all," etc., are intentional. Omitted phrases and words shall be supplied by inference.

1.4—Reference standards

1.4.1—The standards referred to in this Standard Specification ACI 503.1 are listed in Articles 1.4.2 and 1.4.3 of this section, with their complete designation and title including the year of adoption or revision and are declared to be a part of this Standard Specification ACI 503.1 the same as if fully set forth herein, unless otherwise indicated in the contract documents.

1.4.2 *ASTM standard*

C 881-78 Standard Specification for Epoxy Resin Base Bonding Systems for Concrete

1.4.3 *SSPC standards*

Vis 1-67T Surface Preparation Standard No. 1—Pictorial Surface Preparation. Standards for Painting Steel Surfaces

SP1-63 Surface Preparation Specification No. 1, Solvent Cleaning

SP2-63 Surface Preparation Specification No. 2, Hand Tool Cleaning

SP3-63 Surface Preparation Specification No. 3, Power Tool Cleaning

SP6-63 Surface Preparation Specification No. 6, Commercial Blast Cleaning

SECTION 2—MATERIALS AND APPLICATION

PART 2.1—GENERAL

2.1.1 *Description*—This section covers the requirements for surface preparation of specified materials and for application of the multi-component epoxy adhesive.

2.1.2 *Submittals*

2.1.2.1 Contractor shall submit manufacturer's certification verifying conformance to material specifications specified in Part 2.2.

2.1.3 *Quality assurance*

2.1.3.1 *Labeling*: Clearly mark all containers with the following information:

a. Name of manufacturer

b. Manufacturer's product identification

c. Manufacturer's instructions for mixing

d. Warning for handling and toxicity

2.1.3.2 *Application control*: Submit mixing and application procedures for approval prior to use.

2.1.4 *Product delivery, storage, and handling*

2.1.4.1 *Delivery of materials*: Deliver all materials in sealed containers with labels legible and intact.

2.1.4.2 *Storage of materials*: Store all materials at temperatures between 40-100 F (5-38 C) unless otherwise recommended by manufacturer.

2.1.4.3 *Handling of materials*: Handle all materials in a safe manner and in a way to avoid breaking container seals.

2.1.5 *Project conditions*

2.1.5.1 *Environmental requirements*: Contractor shall comply with manufacturer's recommendations as to environmental conditions under which the epoxy compound may be applied.

PART 2.2—PRODUCTS

2.2.1 *Epoxy adhesive*—ASTM C 881-78 Type I. Curing temperature requirements (Class) shall be determined by supplier and contractor after project conditions have been established. Use Grade 2 (medium viscosity) for bonding mating surfaces. Use Grade 3 (nonsagging) for overhead, or vertical, or sloping, surfaces, and for nonmating surfaces.

PART 2.3—EXECUTION

2.3.1 *Preparation of concrete surfaces*

2.3.1.1 Concrete surfaces to which epoxies are to be applied shall be newly exposed parent concrete free of loose and unsound materials. Prepare surfaces by mechanical abrasion unless prohibited by environmental limitations, in which case acid etching may be used.

2.3.1.2 *Mechanical abrasion*: Use sandblasting, scarifying, waterblasting, or other approved means.

2.3.1.3 *Acid etching*: Etch surface with a commercial grade (22 deg Baumé) of hydrochloric acid diluted at a rate of 10:90 to 20:80. After this application, scrub surface with a stiff bristled broom, brush, or similar implement. Immediately after foaming action of acid has subsided, flush surface with water jets until all residue is removed. Repeat procedure until laitance is completely removed.

2.3.2 *Preparation of carbon steel surfaces*

2.3.2.1 Blast-clean carbon steel surfaces, using SSPC SP6, to give a surface condition corresponding to ASa2, BSa2, CSa2 of SSPC Vis 1, depending on the initial surface condition of the steel surface. Use sand abrasive.

2.3.2.2 Prior to blast-cleaning, clean surfaces with SSPC SP1, SP2, and SP3, as required.

2.3.2.3 Remove blast-cleaning residue with compressed air from an oil-and-water-free compressed air source.

2.3.3 *Preparation of galvanized steel surfaces*

2.3.3.1 Scrub galvanized steel surfaces thoroughly in accordance with SSPC SP1, wash well with lime water, and dry.

2.3.3.2 For galvanized steel surfaces showing signs of subsurface corrosion, blast-clean as specified in Article 2.3.2 for carbon steel.

2.3.4 *Preparation of aluminum surfaces*

2.3.4.1 Scrub aluminum surfaces thoroughly with a nonchlorinated cleaner and then etch with proprietary chromate treatment in strict compliance with manufacturer's application instructions and safety warnings.

2.3.4.2 After etching, wash surface with distilled water and then dry thoroughly.

2.3.5 *Preparation of copper and copper-alloy surfaces*

2.3.5.1 Blast-clean copper and copper-alloy surfaces as specified in Article 2.3.2 for carbon steel.

2.3.5.2 Where blast-cleaning is not practical, clean the copper or copper-alloy surfaces with aqueous household ammonia, wash surfaces with distilled water, and then dry thoroughly.

2.3.6 *Preparation of wood surfaces*

2.3.6.1 Clean wood surfaces of all visible loose or foreign particles or contaminants by sanding. Remove sanding or filling dust by wiping with an alcohol-soaked rag, or clean with oil-and-water-free compressed air.

2.3.6.2 For use with moisture-sensitive epoxy adhesives, reduce moisture content of wood to below 12 percent by weight, or the wood should appear dry to touch.

2.3.7 *Inspection of concrete surfaces prior to adhesive application*

2.3.7.1 Inspect all concrete surfaces prior to application of adhesive to insure that requirements of this Article 2.3.7 are met.

2.3.7.2 Surfaces shall be sound and have coarse aggregate exposed. Coarse aggregate requirement may be waived when preparation is in accordance with Article 2.3.1.3.

2.3.7.3 Surfaces shall be free of any deleterious materials such as laitance, curing compounds, dust, dirt, and oil. Materials resulting from surface preparation specified in Article 2.3.1 shall be removed.

2.3.7.4 All concrete surfaces shall be dry unless a water-insensitive adhesive is used. Surface temperature shall be at a proper level to permit wetting of concrete surface by epoxy adhesive.

2.3.7.5 Evaluate moisture content for concrete by determining if moisture will collect at bond lines between old concrete and epoxy adhesive before epoxy has cured. This may be accomplished by taping a 4 x 4 ft polyethylene sheet to concrete surface. If moisture collects on underside of polyethylene sheet before epoxy would cure, then allow concrete to dry sufficiently to prevent the possibility of a moisture barrier between old concrete and new epoxy.

2.3.8 *Adhesive mixes*

2.3.8.1 Mix epoxy components in a clean container free of harmful residue or foreign particles.

2.3.8.2 Condition epoxy compound components to be at a temperature between 60-100 F (16-38 C), unless otherwise recommended by manufacturer.

2.3.8.3 Thoroughly blend epoxy components with a mechanical mixer to a uniform and homogeneous mixture. Mix small batches (up to 1 qt) by use of spatulas, palette knives, or similar devices.

2.3.9 *Adhesive application and placing of elements to be bonded*

2.3.9.1 Apply epoxy adhesive to concrete surface by brush, roller, broom, squeegee, or spray equipment. Apply epoxy adhesive at a thickness sufficient to fill, with slight excess, the gap between substrate and the element to be bonded.

2.3.9.2 Position elements to be bonded within contact time of adhesive as recommended by manufacturer.

2.3.9.3 If movement of elements to be bonded may occur on sloping, vertical, or overhead positions, temporarily fasten or shore these elements.

2.3.9.4 If epoxy adhesive cures to extent of losing its tack before elements are in contact with adhesive, remove or slightly abrade first coat before placing second coat.

2.3.9.5 Do not disturb elements being bonded until the adhesive has attained required strength.

2.3.10 *Cleanup*

2.3.10.1 Protect concrete surfaces, beyond limits of surface receiving adhesive, against spillage.

2.3.10.2 Immediately remove any epoxy compound applied or spilled beyond desired areas. Perform cleanup with material designated by epoxy adhesive manufacturer. Avoid contamination of work area.

2.3.11 *Safety*—Epoxy materials may be skin irritants or sensitizers to many people. Accordingly, advise applicators to avoid contact with eyes and skin, inhalation of vapors, and ingestion. Make protective and safety equipment available on site. Heed all label warnings by manufacturer.

This report was submitted to letter ballot of the committee, which consists of 12 members; 8 members returned their ballots, all of whom voted affirmatively. It has been processed in accordance with the Institute standardization procedure and is approved for publication and discussion with a view to its being submitted to letter ballot of the membership for consideration as a standard of the Institute. Discussion closes Dec. 1, 1978, and will be published, with the committee closure, in March 1979.

APPENDIX D

Sika® AnchorFix-3001

High performance, 2 component adhesive anchor system use in cracked & uncracked concrete

Construction

Description	Sika AnchorFix-3001 adhesive anchor system has been specially formulated as a high performance, two component adhesive anchor system for threaded bars and reinforcing bars in both cracked and uncracked concrete.
Where to Use	■ Cracked & uncracked concrete ■ Hard natural stone ■ Solid rock ■ Solid masonry
Advantages	■ Fixing close to free edges ■ Versatile range of embedment depths ■ Anchoring without expansion forces
Packaging	20.2 fl. oz. (600 ml) or 50.7 fl. oz. (1500 ml) cartridges
Approvals	■ ESR to AC308 by ICC-ES (ESR-3608) ■ Certified to ANSI /NSF - 61 by IAPMO-R&T (file N-7858) ■ Sikadur AnchorFix-3001 has been tested according to ASTM C 881 Type I, IV, Class C, Grade 3

Typical Data

RESULTS MAY DIFFER BASED UPON STATISTICAL VARIATIONS DEPENDING UPON MIXING METHODS AND EQUIPMENT, TEMPERATURE, APPLICATION METHODS, TEST METHODS, ACTUAL SITE CONDITIONS AND CURING CONDITIONS.

Shelf Life When stored correctly, the shelf life will be for 24 months from the date of manufacture.

Storage Conditions Cartridges should be stored in their original packaging, the correct way up, in cool conditions (+50°F to +77°F) out of direct sunlight.

Working & Loading Times

Cartridge Temperature	T Work (minutes)	Base Material Temperature	T Load (hours)
+50°F to +59°F	20	+40°F to +49°F	24
		+50°F to +59°F	12
+59°F to +72°F	15	+59°F to +72°F	8
+72°F to +77°F	11	+72°F to +77°F	7
+77°F to +86°F	8	+77°F to +86°F	6
+86°F to +95°F	6	+86°F to +95°F	5
+95°F to +104°F	4	+95°F to +104°F	4
+104°F	3	+104°F	3

T Work is the typical time to gel at the highest temperature in the range
T Load is the typical time to reach full capacity

*The design professional on the job is ultimately responsible for the interpretation of the data provided above.

Physical Properties		
Property	Result	Method
Consistency	Pass	ASTM C 881
Gel Time	10 minutes**	ASTM C 881
Bond Strength (2 day cure)	2,500 psi	ASTM C 882
Bond Strength (14 day cure)	2,700 psi	ASTM C 882
Compressive Strength (7 day)	>13,000 psi	ASTM D 695
Compressive Modulus (7 days)	420,000 psi	ASTM D 695
Water Absorption	0.08%	ASTM D 570
Heat Deflection Temperature	122°F	ASTM D 468
Linear Coefficient of Shrinkage	0.0003 in/in	ASTM D 2566

*The design professional on the job is ultimately responsible for the interpretation of the data provided above.
**Note: Per section 5.2 "The purchaser may specify a minimum gel time of 5 minutes for Types I and IV when automatic proportioning, mixing and dispensing equipment are used."

Installation Specification									
Property	Symbol	Unit							
Threaded Rod Diameter	d_a	in	3/8	1/2	5/8	3/4	7/8	1	1-1/4
Drill Bit Diameter	d_o	in	1/2	9/16	3/4	7/8	1	1-1/8	1-3/8
Cleaning Brush Size	d_b	-	S14H/F	S16H/F	S22H/F	S24H/F	S27H/F	S31H/F	S38H/F
Nozzle Type	-	-	Q	Q	Q /QH	QH	QH	QH	QH
Extension Tube Required?	-	-	Y1 > 3.5" h_{ef}	Y1 > 3.5" h_{ef}	Y2 > 10" h_{ef}	Y2 > 10" h_{ef}	Y2 > 10" h_{ef}	Y2 > 10" h_{ef}	Y2 > 10" h_{ef}
Resin Stopper Required?	-	-	NO	NO	RS18 > 10" h_{ef}	RS18 > 10" h_{ef}	RS22 > 10" h_{ef}	RS22 > 10" h_{ef}	RS30 > 10" h_{ef}
Rebar Size	d_a	in	#3	#4	#5	#6	#7	#8	#10
Drill Bit Diameter	d_o	in	9/16	5/8	3/4	7/8	1	1-1/8	1-3/8
Cleaning Brush Size	d_b	-	S16H/F	S18H/F	S22H/F	S27H/F	S31H/F	S35H/F	S43H/F
Nozzle Type	-	-	Q	Q	Q /QH	QH	QH	QH	QH
Extension Tube Required?	-	-	Y1 > 3.5" h_{ef}	Y1 > 3.5" h_{ef}	Y2 > 10" h_{ef}	Y2 > 10" h_{ef}	Y2 > 10" h_{ef}	Y2 > 10" h_{ef}	Y2 > 10" h_{ef}
Resin Stopper Required?	-	-	NO	NO	RS18 > 10" h_{ef}	RS18 > 10" h_{ef}	RS22 > 10" h_{ef}	RS22 > 10" h_{ef}	RS30 > 10" h_{ef}
Maximum Tightening Torque	T_{inst}	ft.lb	15	30	60	100	125	150	200

Y1 - requires 3/8" diameter extension tube fitted to Q nozzle
Y2 requires 9/16" diameter extension tube fitted to QH nozzle
RS22 - use 22mm diameter resin stopper
RS30 - use 30mm diameter resin stopper
***The design professional on the job is ultimately responsible for the interpretation of the data provided above.**

BIBLOGRAPHY

AbdElaty, M. (2014). *Compressive strength prediction of portland cement concrete with age using a new model*

Abou Yassin, A., Hamzeh, F., & EL Sakka, F. (2019). *Agent based modelling to optimize the construction workflow of steel and concrete 3D printers*

Amirikian, A. (1946). *Precast concrete structures*

apis cor. (2017). *FAQ/ construction technology * (http://apis-cor.com/en/faq/texnologiya-stroitelstva/ ed.)

Asprone, D., Auricchio, F., Menna, C., & Mercuri, V. (2018). *3D printing of reinforced concrete elements: Technology and design approach* Elsevier.

Bos, F., Wolfs, R., Ahmed, Z., & Salet, T. (2016). *Additive manufacturing of concrete in construction: Potentials and challenges of 3D concrete printing* Taylor & Francis.

Bosscher, P., Williams, R. L., Bryson, L. S., & Castro-Lacouture, D. (2007). *Cable-suspended robotic contour crafting system* Elsevier.

Canessa, E., Fonda, C., Zennaro, M., & Deadline, N. (2013). *Low--cost 3D printing for science, education and sustainable development* Citeseer.

Clarke, C. (2017). *Royal BAM group use 3D printer to make concrete bicycle bridge with TU eindhoven*. Amman: SyndiGate Media Inc. Retrieved from https://search.proquest.com/docview/1911503358

Concrete Construction Staff. (1980). *The many methods of concrete construction* (http://www.concreteconstruction.net/how-to/construction/the-many-methods-of-concrete-construction_o ed.)

Conner, B. P., Manogharan, G. P., Martof, A. N., Rodomsky, L. M., Rodomsky, C. M., Jordan, D. C., & Limperos, J. W. (2014). *Making sense of 3-D printing: Creating a map of additive manufacturing products and services* Elsevier.

Davtalab, O., Kazemian, A., & Khoshnevis, B. (2018). *Perspectives on a BIM-integrated software platform for robotic construction through contour crafting* Elsevier.

Del Viso, J. R., Carmona, J. R., & Ruiz, G. (2008). *Shape and size effects on the compressive strength of high-strength concrete* Elsevier.

Di Carlo, T., Khoshnevis, B., & Chen, Y. (2013). *Manufacturing additively, with fresh concrete* American Society of Mechanical Engineers.

Dini, E. (2010). *Archives* (https://d-shape.com/portfolio-item/ ed.)

Dini, E., Chiarugi, M., & Nannini, R. (2008). *No title* Google Patents.

Duballet, R., Baverel, O., & Dirrenberger, J. (2017). *Classification of building systems for concrete 3D printing* Elsevier.

Duballet, R., Gosselin, C., & Roux, P. (2015). *Additive manufacturing and multi-objective optimization of graded polystyrene aggregate concrete structures* Springer.

Farina, I., Fabbrocino, F., Carpentieri, G., Modano, M., Amendola, A., Goodall, R., . . . Fraternali, F. (2016). *On the reinforcement of cement mortars through 3D printed polymeric and metallic fibers* Elsevier.

Garfield, L. (2017). *A startup invented this $10,000 house that can be built in one day* (http://www.businessinsider.com/house-built-one-day-apis-cor-2017-3 ed.)

Gosselin, C., Duballet, R., Roux, P., Gaudillière, N., Dirrenberger, J., & Morel, P. (2016). *Large-scale 3D printing of ultra-high performance concrete–a new processing route for architects and builders* Elsevier.

Gramazio Kohler Research, ETH Zurich. (2017). *Mesh mould metal ,2015-2018* (http://gramaziokohler.arch.ethz.ch/web/e/forschung/316.html ed.)

Hack, N., Lauer, W., Gramazio, F., & Kohler, M. (2015). *Mesh mould: Robotically fabricated metal meshes as concrete formwork and reinforcement*

Hambach, M., & Volkmer, D. (2017). *Properties of 3D-printed fiber-reinforced portland cement paste* Elsevier.

Hassoun, M. N., & Al-Manaseer, A. (2012). *Structural concrete: Theory and design* John wiley & sons.

Hollis, N. C. (1925). *No title* Google Patents.

Howard, H. C., Levitt, R., Paulson, B. C., Pohl, J. G., & Tatum, C. B. (1989). *Computer integration: Reducing fragmentation in AEC industry* American Society of Civil Engineers.

Huang, S. H., Liu, P., Mokasdar, A., & Hou, L. (2013). *Additive manufacturing and its societal impact: A literature review* Springer.

HuaShang Luhai. (2016). *Demonstrating the whole process of 3D field application of reinforced concrete * (http://www.hstdgm.com/plus/list.php?tid=6 ed.)

Hunt, G., Mitzalis, F., Alhinai, T., Hooper, P. A., & Kovac, M. (2014). *3D printing with flying robots* IEEE.

Irving, M. (2017). *3D printed reinforced concrete bridge opens in the netherlands* (https://newatlas.com/3d-printed-concrete-bridge/51796/ ed.)

Jakupovic, A. (2016). *D-shape - report* 3D Printhuset A/S.

Joshi, S. C., & Sheikh, A. A. (2015). *3D printing in aerospace and its long-term sustainability* Taylor & Francis.

Khaled, S. A., Burley, J. C., Alexander, M. R., & Roberts, C. J. (2014). *Desktop 3D printing of controlled release pharmaceutical bilayer tablets* Elsevier.

Khoshnevis, B. (2004). *Automated construction by contour crafting—related robotics and information technologies* Elsevier.

Khoshnevis, B., Bodiford, M., Burks, K., Ethridge, E., Tucker, D., Kim, W., . . . Fiske, M. (2005). *Lunar contour crafting-a novel technique for ISRU-based habitat development*

Khoshnevis, B., & Dutton, R. (1998). *Innovative rapid prototyping process makes large sized, smooth surfaced complex shapes in a wide variety of materials* Taylor & Francis.

Khoshnevis, B., Hwang, D., Yao, K., & Yeh, Z. (2006). *Mega-scale fabrication by contour crafting* Inderscience Publishers.

Krassenstein, B. (2015). *Exclusive: How winsun stole IP from contour crafting and is "faking" their 3D printed homes & apartments* (https://3dprint.com/57764/winsun-3d-print-fake/ ed.)

Kwon, H., Bukkapatnam, S., Khoshnevis, B., & Saito, J. (2002). *Effects of orifice shape in contour crafting of ceramic materials* MCB UP Ltd.

Labonnote, N., Rønnquist, A., Manum, B., & Rüther, P. (2016). *Additive construction: State-of-the-art, challenges and opportunities* Elsevier.

Langenberg, E. (2015). *Mapping 20 years of 3D printing in architecture* (http://www.3dprintingarchitecture.net/?p=601 ed.)

Lawson, M., Ogden, R., & Goodier, C. (2014). *Design in modular construction* CRC Press.

Le, T. T., Austin, S. A., Lim, S., Buswell, R. A., Gibb, A. G., & Thorpe, T. (2012). *Mix design and fresh properties for high-performance printing concrete* Springer.

Le, T. T., Austin, S. A., Lim, S., Buswell, R. A., Law, R., Gibb, A. G., & Thorpe, T. (2012). *Hardened properties of high-performance printing concrete* Elsevier.

Lim, S., Buswell, R. A., Le, T. T., Austin, S. A., Gibb, A. G., & Thorpe, T. (2012). *Developments in construction-scale additive manufacturing processes* Elsevier.

Lim, S., Le, T., Webster, J., Buswell, R., Austin, A., Gibb, A., & Thorpe, T. (2009). *Fabricating construction components using layered manufacturing technology*

Lipson, H., & Kurman, M. (2013). *Fabricated: The new world of 3D printing* John Wiley & Sons.

Ma, G., & Wang, L. (2017). *A critical review of preparation design and workability measurement of concrete material for largescale 3D printing* Springer.

Ma, G., Wang, L., & Ju, Y. (2017). *State-of-the-art of 3D printing technology of cementitious material—An emerging technique for construction* Springer.

Malaeb, Z., Hachem, H., Tourbah, A., Maalouf, T., Zarwin, N. E., & Hamzeh, F. (2015). *3D concrete printing: Machine and mix design*

Marchment, T., Xia, M., Dodd, E., Sanjayan, J., & Nematollahi, B. (2017). *Effect of delay time on the mechanical properties of extrusion-based 3D printed concrete* Vilnius Gediminas Technical University, Department of Construction Economics & Property.

Molitch-Hou, M. (2016). *Dubai unveils first 3D-printed office building* (https://www.engineering.com/3DPrinting/3DPrintingArticles/ArticleID/12225/Dubai-Unveils-First-3D-Printed-Office-Building.aspx ed.)

Molitch-Hou, M. (2015). *House 3D printing fortified with WASP's reinfirved concrete beams* (https://3dprintingindustry.com/news/house-3d-printing-fortified-with-wasps-reinforced-concrete-beams-55345/ ed.)

Murphy, S. V., & Atala, A. (2014). *3D bioprinting of tissues and organs* Nature Publishing Group.

Narayanan, V. K. (2001). *Managing technology and innovation for competitive advantage* Pearson Education India.

Nawy, E. G. (2011). *Prestressed concrete* Pearson Education.

Newman, J., & Choo, B. S. (2003). *Advanced concrete technology 3: Processes* Butterworth-Heinemann.

Oxman, N., Duro-Royo, J., Keating, S., Peters, B., & Tsai, E. (2014). *Towards robotic swarm printing* Wiley Online Library.

Panda, B., Paul, S. C., Mohamed, N. A. N., Tay, Y. W. D., & Tan, M. J. (2018). *Measurement of tensile bond strength of 3D printed geopolymer mortar* Elsevier.

Panda, B., Paul, S. C., & Tan, M. J. (2017). *Anisotropic mechanical performance of 3D printed fiber reinforced sustainable construction material* Elsevier.

Paul, S. C., Tay, Y. W. D., Panda, B., & Tan, M. J. (2018). *Fresh and hardened properties of 3D printable cementitious materials for building and construction* Elsevier.

Paulson Jr, B. C. (1985). *Automation and robotics for construction* American Society of Civil Engineers.

Pegna, J. (1997). *Exploratory investigation of solid freeform construction* Elsevier.

Rengier, F., Mehndiratta, A., Von Tengg-Kobligk, H., Zechmann, C. M., Unterhinninghofen, R., Kauczor, H., & Giesel, F. L. (2010). *3D printing based on imaging data: Review of medical applications* Springer.

Salet, T. A., Bos, F. P., Wolfs, R. J., & Ahmed, Z. Y. (2018). *3D concrete printing–a structural engineering perspective* Springer Cham.

Schick, K. D., & Toth, N. P. (1994). *Making silent stones speak: Human evolution and the dawn of technology* Simon and Schuster.

Scott, C. (2016). *Chinese construction company 3D prints an entire two-story house on-site in 45 days*

Sim, J., Yang, K., Kim, H., & Choi, B. (2013). *Size and shape effects on compressive strength of lightweight concrete* Elsevier.

Taylor, H. P. J. (1970). *No title*

Tess. (2016). *Our top 27 3D printed housing and construction projects* (http://www.3ders.org/articles/20160926-our-top-26-3d-printed-houses-construction-projects.html ed.)

van der Zee, A., de Ruiter, P., & Meijs, H. (2017). *Unleash the building bots: 3d printing structures with an autonomous robot swarm*

Wang, L. (2015). *World's first 3D-printed hotel suite pops up in less than 5 days* (https://inhabitat.com/worlds-first-3d-printed-hotel-suite-pops-up-in-less-than-5-days/ ed.)

Williams II, R. L., Xin, M., & Bosscher, P. (2008). *Contour-crafting-cartesian-cable robot system concepts: Workspace and stiffness comparisons* American Society of Mechanical Engineers Brooklyn, USA.

Wohlers, T., & Gornet, T. (2014). *History of additive manufacturing*

Wong, K. V., & Hernandez, A. (2012). *A review of additive manufacturing* Hindawi Publishing Corporation.

Wu, P., Wang, J., & Wang, X. (2016). *A critical review of the use of 3-D printing in the construction industry* Elsevier.

Yi, S., Yang, E., & Choi, J. (2006). *Effect of specimen sizes, specimen shapes, and placement directions on compressive strength of concrete* Elsevier.

Zareiyan, B., & Khoshnevis, B. (2017a). *Effects of interlocking on interlayer adhesion and strength of structures in 3D printing of concrete* Elsevier.

Zareiyan, B., & Khoshnevis, B. (2017b). *Interlayer adhesion and strength of structures in contour crafting-effects of aggregate size, extrusion rate, and layer thickness* Elsevier.

Zhang, J., & Khoshnevis, B. (2013). *Optimal machine operation planning for construction by contour crafting* Elsevier.